Amphiphilic Spin Crossover Complexes

DISSERTATION

Zur Erlangung des akademischen Grades eines

Doktors der Naturwissenschaften (Dr. rer. nat.) im Fach Chemie

an der Fakultät für Biologie, Chemie und Geowissenschaften der Universität

Bayreuth

vorgelegt von

M. Sc. Stephan Schlamp

geboren in Tegernsee

Bayreuth, 2014

Die vorliegende Arbeit wurde in der Zeit von August 2009 bis Juni 2010 an der Ludwig-Maximilians-Universität München am Lehrstuhl für Bioanorganische Chemie und von Juli 2010 bis April 2014 an der Universität Bayreuth am Lehrstuhl für Anorganische Chemie II unter Betreuung von Frau Prof. Dr. Birgit Weber angefertigt.

Vollständiger Abdruck der von der Fakultät für Biologie, Chemie und Geowissenschaften der Universität Bayreuth genehmigten Dissertation zur Erlangung des akademischen Grades eines Doktors der Naturwissenschaften (Dr. rer. nat.).

Dissertation eingereicht am: 16.04.2014
Zulassung durch die Promotionskommission: 30.04.2014
Wissenschaftliches Kolloquium: 22.07.2014

Amtierender Dekan: Prof. Dr. Rhett Kempe

Prüfungsausschuss:

Prof. Dr. Birgit Weber   (Erstgutachter)
Prof. Dr. Jürgen Senker   (Zweitgutachter)
Prof. Dr. Seema Agarwal   (Vorsitz)
Prof. Dr. Markus Retsch

MEINER FAMILIE GEWIDMET

Um klar sehen zu können reicht oft ein Wechsel der Blickrichtung

A<small>NTOINE DE</small> S<small>AINT</small>-E<small>XUPÉRY</small>

Abbreviations

apy	4-aminopyridine
bpea	1,2-bis(4-pyridyl)ethane
bpee	1,2-bis(4-pyridyl)ethene
bpey	1,2-bis(4-pyridyl)ethyne
dmap	4-(dimethylamino)pyridine
DSC	differential scanning calorimetry
TGA	thermogravimetric analysis
DEI	direct electron impulse ionization
δ	chemical shift (ppm)
EA	elemental analysis
eq./equiv.	equivalents
Et	ethyl
HS	high-spin
L_{ax}	axial ligand
L_{eq}	equatorial ligand
LS	low-spin
M	metal
Me	methyl
MS	mass spectrometry
NMR	nuclear magnetic resonance
Ph	phenyl
py	pyridine
RT	room temperature
SCO/ST	spin crossover/spin transition
SQUID	superconducting quantum interference device
UV-Vis	ultraviolet-visible spectroscopy
γ_{HS}	molar high-spin fraction
k_B	Boltzmann constant
S	spin (quantum number)
$T_{1/2}$	spin transition temperature ($\gamma_{HS} = 0.5$)
χ_M	molar susceptibility

Table of contents

1 Summary/Zusammenfassung

1.1 Summary

The aim of the present thesis was the synthesis and characterization of amphiphilic iron(II) spin crossover complexes. The prime attention was on the self-assembly ability of the synthesized compounds and the influence of the supramolecular arrangement in the solid on the SCO behaviour. The used ligand system is based on Schiff base-like *Jäger* ligands that are suitable to realize iron(II) SCO compounds. The ligands were modified such that alkyl chains with different lengths were attached to the outer periphery. The newly established eight-step synthesis of the complexes comprises alkylation of catechol, subsequent nitration in *para-* positions and reduction of the nitro functionalities resulting in the diamino compound. Further reactions with different keto-enol ethers gave the ready ligand that reacts with iron(II) acetate to iron(II) complexes with methanol in axial positions. In order to shift the iron centre into the right energy region to enable thermally induced SCO, in the last step the methanol was replaced by N-donor ligands like pyridine and its derivatives such as apy and dmap, or by bpea, bpee and bpey which are bridging the iron centres, to provide the aimed [N$_4$O$_2$] coordination sphere.

Structural investigations using single crystal X-ray structure analysis gave a detailed insight into structure-property relationship of the synthesized complexes. The mechanism of the SCO of [FeL*a*(C16)(py)$_2$], a complex with the chain length of 16 carbon atoms and pyridine in axial positions was elucidated. The molecules organize in lipid layer-like arrangement where the iron centres point to each other. By this, a hydrogen bonding network between the polar heads was formed with co-crystallized H$_2$O, what is partially responsible for the 47 K wide hysteresis. It was demonstrated that, despite of long alkyl chains, abrupt ST with hysteresis is possible and that the cooperativity of SCO depends on the self-assembly of the amphiphiles.

This concept was confirmed by comparison with complexes bearing short C8 alkyl chains. The self-assembly is unpredictable resulting in different coordination geometries and crystal packings without lipid layer-like arrangement. The STs of the octahedrally coordinated modifications of [FeL*c*(C8)(dmap)$_2$] in the solid were found to be almost identical to that of the same compound in solution what proved the absence of cooperative effects in the crystal.

Investigations on pyridine complexes with different chain lengths (8, 12 and 16 carbon atoms) and substituents at R^1 and R^2 showed that the substituents influence the ST temperature $T_{1/2}$

but not the different chain lengths. Temperature-dependent paramagnetic ^{1}H NMR investigations confirm that the SCO behaviour in the solid is dominated by packing effects.

Attempts to synthesize coordination polymers or to coordinate bigger axial ligands with a lipid layer-like structure resulted in crystallization of dinuclear, penta-coordinated or other SCO inactive complexes. Extensive investigations on the compounds using X-ray structure analysis led to a concept enabling the prediction of crystallization behaviour depending on the chain length and the dimensions of the polar head group, named **s**elf-**a**ssembly **p**arameter, $sap = (H+B)/L$. H and B denote the height and the broadness of the polar part and L the entire length of the complex. When $sap \approx 1$, lipid layer-like arrangement can be expected. This concept was also applied to other amphiphilic systems.

In order to coordinate sterical more demanding axial ligands, the chain length was elongated from 16 to 22 carbon atoms and the synthesis pathway of the complexes was adjusted. This resulted on the one hand in the crystallization of the complex [FeLd(C22)(dmap)$_2$] which crystallized despite of sterical demanding substituents octahedrally with dmap in the layered structure motif. On the other hand, coordination polymers with bpea, bpee and bpey were synthesized that show all abrupt SCOs above room temperature. It could be demonstrated that cooperativity as well as $T_{1/2}$ can be increased choosing more rigid axial ligands. The three compounds organize in spherulites after warming which can be observed between crossed polarizers.

1.2 Zusammenfassung

Ziel der vorliegenden Dissertation war die Synthese und Charakterisierung amphiphiler Eisen(II) Spin-Crossover-Komplexe. Das Hauptaugenmerk lag hierbei auf dem supramolekularen Selbstanordnungsvermögen der dargestellten Verbindungen und dem Einfluss der Anordnung im Festkörper auf das SCO-Verhalten. Das verwendete Ligandensystem basiert auf den Schiff'sche Base ähnlichen *Jäger*-Liganden, welche zur Realisierung von Eisen(II)-SCO-Verbindungen geeignet sind. Die Liganden wurden so modifiziert, dass Alkylketten unterschiedlicher Länge in die äußere Peripherie eingebracht wurden. Die neu etablierte achtstufige Synthese der Komplexe beinhaltet die Alkylierung von Catechol, anschließende Nitrierung in der jeweiligen *para*-Position und Reduktion der Nitro- zu Aminofunktionen. Weiterreaktion mit unterschiedlichen Keto-Enolethern resultierte in den fertigen Liganden, welche durch Umsetzung mit Eisen(II)-Acetat zu Eisen(II)-Komplexen mit Methanol in axialer Position reagieren. Um das Eisenzentrum in den richtigen Energiebereich für thermisch induzierten SCO zu bringen, wurden in einem letzten Schritt diese Methanol-Moleküle durch N-Donor-Liganden wie Pyridin und dessen Derivate apy oder dmap, oder die verbrückenden Liganden bpea, bpee und bpey ersetzt, um die angestrebte [N_4O_2]-Koordinationssphäre zur Verfügung zu stellen.

Strukturelle Aufklärung durch Einkristallröntgenstrukturanalyse verschaffte einen detaillierten Einblick in die Struktur-Eigenschaftsbeziehungen der so dargestellten Komplexe. So konnte der Mechanismus des SCO eines Komplexes mit der Alkylkettenlänge von 16 Kohlenstoffatomen und Pyridin in axialer Position, [FeL*a*(C16)(py)$_2$], aufgeklärt werden. Die Moleküle ordnen sich in lipidähnlichen Schichten an, wobei die Eisenzentren einander zugewandt sind und dadurch untereinander ein Wasserstoffbrückenbindungsnetzwerk mit cokristallisiertem H_2O ausbilden können, welches für die Hysteresebreite von 47 K mitverantwortlich gemacht wird. Es konnte gezeigt werden, dass trotz der langen Alkylkettenlänge abrupte Spinübergänge mit Hysterese möglich sind und die Kooperativität des SCO von der Selbstanordnung der Amphiphile abhängig ist.

Ein Vergleich mit Komplexen, welche eine relativ kurze Kettenlänge von 8 Kohlenstoffatomen aufweisen, bestätigte dieses Konzept. Diese kristallisierten in verschiedenen Koordinationsgeometrien und Modifikationen und ohne Lipidschichtstruktur. Eine Gegenüberstellung der Spinübergänge der Modifikationen von oktaedrisch koordiniertem [FeL*c*(C8)(dmap)$_2$] mit dem SCO derselben Verbindung in Lösung bewies die Abwesenheit kooperativer Effekte im Festkörper.

Untersuchungen an Pyridin-Addukten unterschiedlicher Kettenlänge (8, 12 und 16 Kohlenstoffatome) und unterschiedlicher Substituenten R^1 und R^2 zeigten auf, dass die Substituenten einen Einfluss auf $T_{1/2}$ haben, jedoch nicht die unterschiedliche Kettenlänge. Temperaturabhängige paramagnetische ^{1}H-NMR-Untersuchungen in Lösung bestätigten den dominierenden Einfluss von Packungseffekten auf das SCO-Verhalten.

Bei den Versuchen, Koordinationspolymere darzustellen oder größere axiale Liganden unter Beibehaltung der Lipidschichtstruktur zu verwenden, konnten nur dinukleare, pentakoordinierte und andere SCO inaktive Komplexe kristallisiert werden. Eingehende röntgenstrukturanalytische Untersuchungen der erhaltenen Verbindungen führten zu einem Konzept zur Beurteilung der Kristallisationsverhaltens in Abhängigkeit der Kettenlänge und der Dimensionen des polaren Teils, benannt als **s**elf-**a**ssembly **p**arameter, *sap* = (H+B)/L. Dabei bezeichnen H und B die Höhe und Breite des polaren Teils und L die Gesamtlänge des Komplexes. Wenn *sap* ≈ 1, können lipidschichtähnliche Strukturen erwartet werden. Dieses Konzept wurde auch auf andere amphiphile Systeme angewendet.

Folglich wurde, um sterisch anspruchsvollere axiale Liganden zu koordinieren, die Kettenlänge von 16 auf 22 Kohlenstoffatome erhöht, wobei die Synthese der Komplexe entsprechend modifiziert werden musste. Dies resultierte einerseits in der Kristallisation des Komplexes [FeL*d*(C22)(dmap)$_2$], welcher trotz sterisch anspruchvoller Reste oktaedrisch mit dmap in der Schichtstruktur kristallisierte. Andererseits konnten Koordinationspolymere mit bpea, bpee und bpey dargestellt werden, welche alle abrupte Spinübergänge oberhalb Raumtemperatur aufwiesen. Es konnte gezeigt werden, dass die Kooperativität und auch $T_{1/2}$ durch rigidere axiale Liganden erhöht werden kann. Alle drei Verbindungen ordnen sich nach dem Erwämen in sphärulitischen Strukturen an, was zwischen gekreuzten Polarisatoren beobachtet werden kann.

2 Introduction

Ongoing digitalization of media and increasing needs for telecommunication and internet applications causes huge amounts of data. Size reduction of data storage devices is necessary and could be considered to reach until the molecular scale.[1] The possibility to address single molecules or small clusters of molecules would lead to an increase of number of logical gates per cm^2 on a microchip by several orders of magnitude, and the response times of molecular devices could be in the range of femtoseconds instead of nanoseconds in present devices.[1] Consequently, attention is focused on molecules that can exhibit this fundamentally important "on-off" switching possibility, what is the basis of a bit-based calculation. In the early 1930s Cambi *et al.* discovered the phenomenon of spin crossover, the possibility for a molecule to exhibit two different spin states.[2] As these molecules can switch from the HS to the LS state by appliance of physical perturbations like temperature, pressure, light irradiation or pulsed magnetic fields,[3-6] they appear to be good candidates not only for the use in information technologies[7] but also in displays,[8] sensors,[9] cold channel control units in food and medical storage[10] or as MRT contrast agents.[11] With regard to data processing ability, the material does not solely have to fulfill characteristics like chemical stability when embedded in a matrix or deposited on a surface. It is also of paramount importance that a movement or reorganization of the molecules is inhibited to ensure correct addressing and reading.[1] In this frame, the self-assembly of SCO molecules plays a decisive role. A correct projectable and predictable ordering of moieties is a synthetic challenge that can be confronted by using crystal engineering[12] approaches during the ligand design.

Over the last decades, the synthesis of a vast amount of SCO compounds with different metal centres and ligands led to a better understanding how this phenomenon can be controlled and therefore to concepts for a purposeful design. Notwithstanding encouraging results in realizing highly cooperative ST comprising hysteresis, numerous fundamental aspects of SCO are still debated. Despite of this, the exploitation of useable materials is in a very busy process.[13, 14] Through combination of the SCO phenomenon with additional features like miniaturization of SCO compounds (nanostructuring),[15] creation of cages[16] and micro- or nanoporous materials[17] a new variety of multifunctional SCO materials can be envisioned. Additionally, softness as well as the thermochromism during the spin state change are of uttermost interest to pave the way for possible applications.

2.1   Theory of the spin crossover

SCO can occur within coordination compounds with mostly first transition row metals as central atom exhibiting a d^4-d^7 electron configuration and primarily octahedral coordination geometry around the metal centre. Fe^{2+} represents the vast majority of used metals. The coordinating ligands induce a splitting of the d-orbitals of the central metal ion into the e_g* and t_{2g} orbitals, the ligand field splitting Δ_O (10*Dq*). In general, for systems bearing more than three d-electrons, the electron-electron repulsion has to be considered, the total spin pairing energy *P*. When $P >> \Delta_O$, the d-electrons are distributed according to Hund's law. This results, for example in a system with 6 d-electrons like Fe^{2+} in a total spin state of *S*=2, a strongly paramagnetic HS system ($^5T_{2g}$) with the maximum of unpaired electrons (Figure 1). If the induced ligand field strength is high enough to surpass the total spin pairing energy ($P << \Delta_O$), the spin system will exhibit the maximum number of paired electrons. This corresponds to the diamagnetic LS state with *S*=0 in a d^6 electron system ($^1A_{1g}$). If *P* is in the same order of magnitude as Δ_O, a switching from HS to LS, the SCO, can take place.[18]
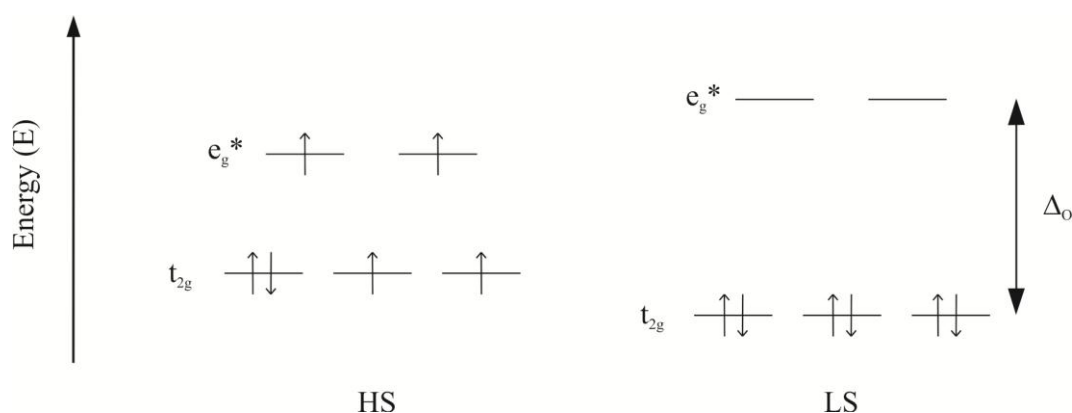
Figure 1. Schematic representation of the HS (left) and LS state (right) in an octahedral d^6 electron system.

The induced splitting is depending on the chosen ligand as well as on the metal ion. It is related to the position of the ligand in the spectrochemical row and inducing or withdrawing effects of functional groups at the coordinating ligands. Normally no metals in the 4d and 5d transition rows are found to be SCO active. The reason for this lies in an increased ligand field splitting. In complexes of metal ions of the same group and oxidation state and with identical ligand sphere, the ligand field strength increases by around 50 % on going from 3d

to 4d and from 4d to 5d elements, whereas the spin-pairing energy does not change much in this order.[19] Thus, the LS state is commonly adopted in 4d and 5d elements.

The states of d-orbital configuration for a given electron number under the influence of an octahedral ligand sphere involving the interplay of electron-electron repulsion and orbital momentum, can be calculated as functions of the so-called Racah parameters.[20] The results can be plotted in a Tanabe-Sugano diagram[21] (Figure 2), representing the relative energies of all the Russel-Saunders multiplet terms arising for a given d-electron configuration as a function of the crystal-field splitting parameter Δ_O and the electronic energies of the excited states relative to the ground state.
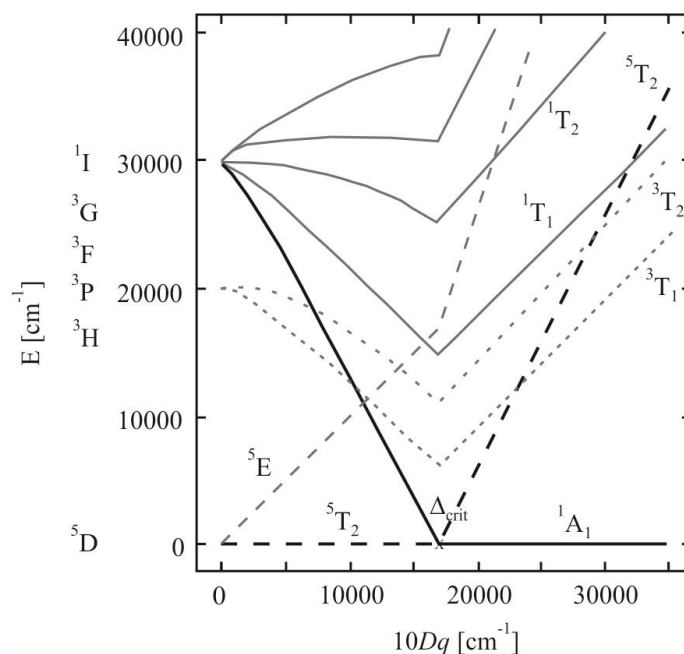
Figure 2. Tanabe-Sugano diagram[21] for octahedral d^6 complexes assuming a Racah parameter of B $\approx$ 1050 cm^{-1} for iron(II).

According to this, the $^5T_{2g}$ state is the ground state until a certain strength of ligand field (Δ_{crit}). Above this, the $^1A_{1g}$ state (the LS state) becomes the electronic ground state.

Due to the fact that two electrons are occupying the antibonding e_g* orbitals in the HS state, whereas in the LS state only non-bonding orbitals are occupied, bond lengths are elongated in relation to the LS state. For a given combination of ligands and metal ion, $10Dq$ depends on

the metal-ligand distance as r^{-n} (n=5-6). In iron(II) systems, the difference between the Fe–N or Fe–O bond lengths in the two states $\Delta r_{HL} = r_{HS} - r_{LS} \approx 0.2$ Å.[18]

Regarding thermally induced SCO, it is important in order to obtain thermally accessible SCO compounds that the energy differences between the two states are in the region of $k_B T$. This is illustrated in Figure 3, where a direct relation is shown between the metal to ligand radius and the energy difference:

$$\Delta E^0{}_{HL} = \Delta E^0{}_{HS} - \Delta E^0{}_{LS}$$

In general, the LS state remains the quantum mechanical ground state at all temperatures, but the HS state is the thermodynamically stable state at elevated temperatures.
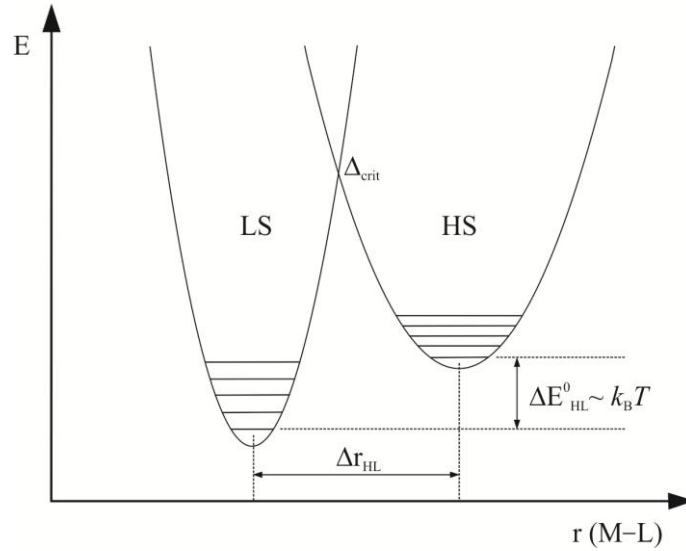
Figure 3. Potentials for the HS and the LS state along the metal-ligand stretch vibration $r_{(M–L)}$, M = Fe.

The energetic differences between HS and LS state are mainly determined by changes in the entropy ΔS comprising an electronic part due to spin degeneracy in the HS state and resulting higher degree of freedom for the electrons, and a vibrational part due to generally lower vibrational frequencies (weaker metal-ligand bonding) and the resulting higher density of vibrational states in the HS state.

$\Delta E^0{}_{HL}$ corresponds to the enthalpy term of the Gibbs-Helmholtz equation, in which the entropical favour of the HS state is also reflected:

$$\Delta G = \Delta H - T\Delta S$$

Switching from LS to HS gives a positive reaction enthalpy ΔH (heating up) but also a positive reaction entropy ΔS. At low temperatures, the enthalpy term is dominant and the LS state is favoured whereas the entropy term is outweighing at high temperatures leading to the HS state.[22] At the temperature where both spin states are in equilibrium, what corresponds to $T_{1/2}$, the free reaction energy is zero, $\Delta G = 0$:

$$0 = \Delta H - T_{1/2}\Delta S$$

Reordering of the Gibbs-Helmholtz equation shows then the temperature dependence of the ST given through entropy and enthalpy:

$$T_{1/2} = \Delta H/\Delta S$$

According to theoretical and empirical derivations following general assignments can be made in which energy region of ligand field splitting a complex will be present in the HS or LS state, and when it is possible for SCO to occur[18]:

For $10Dq^{HS} < 10{,}000$ cm^{-1} $\rightarrow$ HS complex

For $10Dq^{HS} \approx 11{,}000 - 12{,}500$ cm^{-1} and

          $10Dq^{LS} \approx 19{,}000 - 22{,}000$ cm^{-1} $\rightarrow$ SCO can occur

For $10Dq^{LS} > 23{,}000$ cm^{-1} $\rightarrow$ LS complex

2.2   Cooperativity in SCO systems

The temperature dependent SCO is usually plotted as a function of high spin fraction (γ_{HS}), or as a function of the product of the molar susceptibility with temperature ($\chi_M T$) versus temperature. This SCO curve can adopt different shapes, e. g. gradual, abrupt, with hysteresis, stepwise or also incomplete. Some examples are presented in Figure 4. The course of the curve is depending to a large extent on the forwarding of the ST information from one molecule to another through the crystal lattice through intermolecular interactions, what is synonymous with cooperative effects. These intermolecular interactions can be van der Waals

and π-π interactions as well as hydrogen bonding. They communicate the structural changes during ST, arised from the shortening or elongation of the metal-ligand distances to the neighboured molecules. In solution, cooperativity is almost vanished as no interactions between the molecules take place and the course of the SCO curve is gradual. Here, essentially a Boltzmann distribution of the molecular states is involved.[3b, 6] Stepwise STs can for example origin in different lattice sites for the complex molecules. The occurrence of hysteresis, where $T_{1/2}\downarrow$ is at lower temperatures than $T_{1/2}\uparrow$, depicts one of the most interesting phenomena associated with the SCO as this refers to a real bistability of a complex in a certain temperature range. It can occur at a very high degree of cooperativity that leads to internal pressure able to inhibit ST partially or completely. PTs can also be involved in the formation of hysteresis due to reversible order-reordering processes. The abruptness and completeness of ST curves is linked to the extent of cooperativity and therefore to the number and kind of intermolecular interactions between the molecules. Direct connection of the iron centres via multidentate bridging ligands resulting in coordination polymers can lead to higher cooperativity[7] as well as dramatically increased thermal stability and decreased air sensitivity. The covalent linking can moreover enhance the possibility for other elastic interactions to be formed in a more controlled way as the arrangement of the molecules in the crystal is more predictable than in mononuclear complexes.
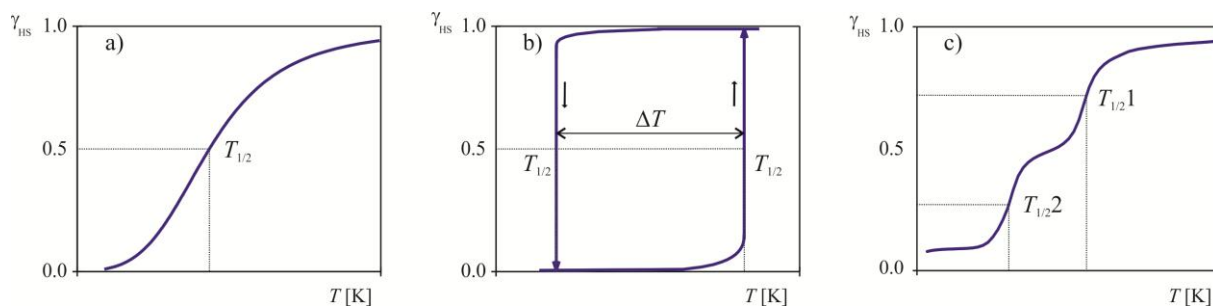

Figure 4. Representation of principle types of ST curves: a) gradual, b) with hysteresis, c) two-step. The HS fraction γ_{HS} is plotted against the temperature.

2.3 Amphiphilic complexes

Flexibility and softness are desirable physical properties for the construction of materials. Combined with the SCO phenomenon this can result in multifunctional SCO complexes. A common way to achieve this objective is to add long alkyl chains to already known SCO systems leading to amphiphilic SCO compounds, consisting of a polar head group containing the SCO active metal centre ("head") and the nonpolar "tail" group represented by the alkyl chains. This new class of molecules exhibits a wide variety for creating SCO materials due to the possibility to self-assemble in defined structures, e. g. micelles or inverse micelles, or flexible lipid double layer structures (Figure 5) as in case for mammalian cell walls. How amphiphiles with a defined shape will arrange in solution was mathematically determined and vividly implemented through the introduction of the critical packing parameter (cpp) by Israelachvili *et al.* in 1976.[23] Other possibilities for miniaturization and functionalization are the preparation of thin films,[24] respectively Langmuir-Blodgett films[25, 26, 27] (see Figure 5), gels,[28, 29, 30] and liquid crystals.[31]
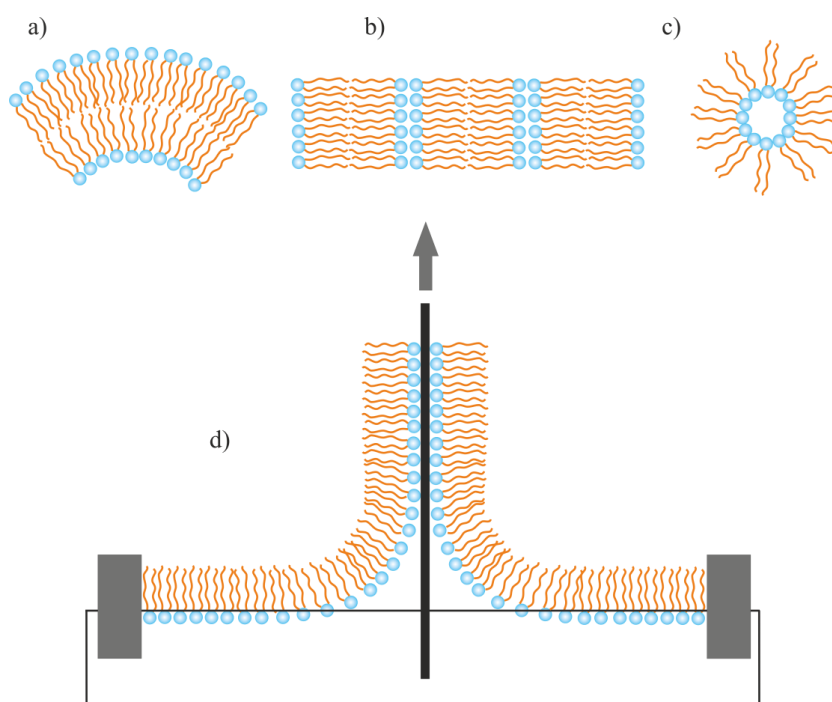

Figure 5. Schematic representation of possible arrangements of amphiphilic molecules in a) micelles, b) lipid double layers, c) inverse micelles. d) Schematic drawing of the formation of Langmuir-Blodgett films.

Next to the possibility of the formation of multifunctional materials in solution, also PTs of the bulk material showing a synchronicity between the metal complex and the long alkyl chains are very interesting to study. The SCO phenomenon is accompanied by significant structural changes mainly due to the changes in metal-ligand bond lengths and angles upon ST mentioned above, what leads to a change in the lattice parameters and the cell volume. Thus, it can be seen as intrinsic PT. The goal here is to examine in which way the nonpolar substituents influence the shape of the ST and $T_{1/2}$, or how strong the cell volume changes during ST. Further, the enhancement of cooperative effects through a well-defined ordering due to the self-assembly of the molecules driven by van der Waals interactions (London dispersion forces) can be envisioned and put to the test.

The bulk functionalized complexes are in general able to melt and the melting point can be tuned by variation of the alkyl chain length. During the melting, rather unpredictable extrinsic phase transitions (e. g., crystalline (Cr) ↔ liquid crystal (LC)) can occur. Metal containing liquid crystals are called metallomesogens. These extrinsic PTs can, on their part, influence the SCO as well. PTs accompanied by a spin state switching have been studied by Gaspar *et al.*[32] To synthesize materials that show a synchronism between ST and PT, first, a SCO system should be chosen that exhibits abrupt STs near or above room temperature in the unmodified matter. The reason for this is the fact that the Cr↔LC transition temperature lies in general at higher temperatures than room temperature. Second, the incorporation of a mesophase causing moiety into the SCO system should be conducted via attachment of e. g. an aromatic core with alkyl chain substituents to the ligands. The mesophase transition temperature should be adjusted to $T_{1/2}$ by changing the length or type of the alkyl chains.[33] It is possible to lower the mesophase transition temperature through adding branched alkyl chains as rests.[34]

In general, the functionalizing with alkyl chains strongly influences the magnetic behaviour of a compound. It appears that the longer the nonpolar rests are, the more the LS state of a complex is stabilized.[26] Electron density inducing effects as well as a fastener effect due to the dense packing caused by the hydrophobic interactions are possible explanations.

Established methods to detect the SCO are amongst others magnetic measurements[35] (e.g., with a SQUID magnetometer), Mössbauer spectroscopy,[36] paramagnetic temperature-dependent NMR spectroscopy (Evans method[37]) and temperature-dependent single crystal X-ray structure analysis. To detect Cr↔Cr or Cr↔LC PTs, additional methods are necessary. Differential scanning calorimetry (DSC)[38] provides insight into the changes of heat capacity

during PTs, and the enthalpy and entropy changes can be calculated by integration of the peak areas. Powder X-ray diffraction (PXRD), wide and small angle X-ray scattering (WAXS/SAXS) can illustrate the structural changes of a compound in defined temperature intervals. Finally, the detection of mesophases or spherulites can be made by investigations using polarizing optical microscopy (POM) as they exhibit typical textures viewed between crossed polarizers.[33, 39]
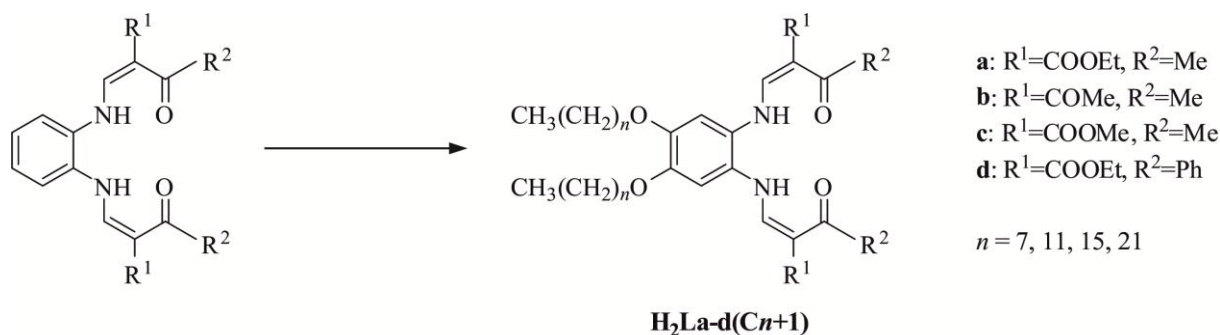
Several amphiphilic SCO systems have been reported for example with derivatives of the terpyridine ligand with cobalt(II)[40] and iron(II)[41] or modified tren (tren = tris[3-aza-4-(2-pyridyl)but-3-enyl]amine)[31b, 42] or triazole[28, 30, 43-45] ligands with iron(II) as well as with Schiff base ligands with iron(III)[31d] and salen ligands with manganese(III),[46] just to mention few examples. These compounds bear alkyl chains of varying lengths of 6 up to 20 carbon atoms and exhibit different interesting physical properties or specific supramolecular modes of aggregation (e. g., nanowires). All of them are ionic complexes and therefore contain different kinds of counterions. They can, of course, additionally influence the SCO behaviour. However, their presence reduces the intermolecular interactions between the SCO centres and by this the cooperativity.

As mentioned above, ST in solution is always gradual. Nevertheless, with the use of amphiphilic iron(III) compounds, an improvement of cooperativity in solution by self-assembly of the molecules could be observed.[47, 48]

As critical parameter for inducing self-assembly the alkyl chain length plays a crucial role. It will be very instructively to study the self-assembly of amphiphilic molecules in the solid as the arrangement in the solid can be seen as a result of the arrangement in solution after removing the solvent. Unfortunately, the yield of crystal structures of amphiphilic SCO compounds is quite rare so far. So far, it was possible to structurally characterize manganese(III)[46] and iron(II)[31b] complexes with C6 alkyl chains, iron(III) complexes with C8[47] and C12[49] alkyl chains and one cobalt(II) complex[40] with C16 alkyl chains, the crystal structure with the longest alkyl chains published up to now.

2.4   The ligand system

Schiff base-like ligands are a very powerful system to realize SCO. Originally established by Jäger *et al.*,[50] they are commonly used and developed further in our workgroup. They provide a square planar [N_2O_2] coordination sphere and the ligand field strength can be varied and fine-tuned through variation of the substituents at R^1 and R^2 (Scheme 1). Additionally, sterical modifications at these substituents may influence the crystallization behaviour. In contrary to classic Schiff base ligands like salen or salophen, the tautomeric equilibrium of the free ligand is shifted to the keto-enamin instead of the enol-imin structure.[51] Deprotonation of the ligand leads to a twofold negatively charged delocated π-system. Upon coordination to iron(II) this results in a neutral complex.

a: R^1=COOEt, R^2=Me
b: R^1=COMe, R^2=Me
c: R^1=COOMe, R^2=Me
d: R^1=COOEt, R^2=Ph

n = 7, 11, 15, 21

H₂La-d(C*n*+1)

Scheme 1. Functionalization of the Schiff base-like ligand with long alkyl chains and the used abbreviations.

Based on this ligand system, one goal in this work was to add long alkyl chains in the outer periphery to create new amphiphilic complexes. The second goal was to investigate the crystallization behaviour and the resulting SCO behaviour depending on the variation of the alkyl chain length, substituents and chosen axial ligands.

2.5 References

[1]   J.-F. Létard, P. Guionneau, L. Goux-Capes, *Topics in Current Chemistry*, *Vol. 235* (Eds.: P. Gütlich, H. A. Goodwin), Springer, Wien, New York, **2004**, 221–249.

[2]   a) L. Cambi, L. Szegö, *Ber. Dtsch. Chem. Ges. A* **1931**, *64*, 167; b) L. Cambi, L. Malatesta, *Ber. Dtsch. Chem. Ges. B* **1937**, *70*, 2067; c) L. Cambi, L. Malatasta, *Ber. Dtsch. Chem. Ges. (A and B series)* **1937**, *70*, 2067.

[3]   a) P. Gütlich, A. Hauser, H. Spiering, *Angew. Chem. Int. Ed. Engl.* **1994**, *33*, 2024–2054; b) O. Sato, J. Tao, Y.-Z. Zhang, *Angew. Chem.* **2007**, *119*, 2200; c) *Angew. Chem. Int. Ed.* **2007**, *46*, 2152–2187; d) J. A. Kitchen, S. Brooker, *Coord. Chem. Rev.* **2008**, *252*, 2072–2092; e) M. A. Halcrow, *Coord. Chem. Rev.* **2009**, *253*, 2493–2514.

[4]   B. Weber, *Coord. Chem. Rev.* **2009**, *253*(19-20), 2432–2449.

[5]   A. Gaspar, M. Seredyuk, P. Gütlich, *J. Mol. Struct.* **2009**, *924–926*, 9–19.

[6]   P. Gütlich, H. A. Goodwin, *Topics in Current Chemistry*, *Vol. 233* (Eds.: P. Gütlich, H. A. Goodwin), Springer, Wien, New York, **2004**, 1–39.

[7]   O. Kahn, C. J. Martinez, *Science* **1998**, 279, 44–48.

[8]   a) J.-F. Létard, O. Nguyen, N. Daro, Patent, FR05124762005; b) A. Galet, A. B. Gaspar, M. C. Munoz, G. V. Bukin, G. Levchenko and J. A. Real, *Adv. Mater.* **2005**, *17*, 2949–2957.

[9]   a) Y. Garcia, V. Ksenofontov, P. Gütlich, *Hyperfine Interact.* **2002**, *139–140*, 543; b) J. Linares, E. Codjovi, Y. Garcia, *Sensors* **2012**, *12*(4), 4479–4492.

[10]   Y. Garcia, V. Ksenofontov, S. Mentior, M. M. Dîrtu, C. Gieck, A. Bhatthacharjee, P. Gütlich, *Chem. Eur. J.* **2008**, *14*, 3745–3758.

[11]   a) R. N. Muller, L. V. Elst, S. Laurent, *J. Am. Chem. Soc.* **2003**, *125*(27), 8405–8407; b) C. Rajadurai, M. Ruben, D. Kruk, Patent, EP2072062B1.

[12]   a) P. Dandekar, Z. B. Kuvadia, M. F. Doherty, *Annu. Rev. Mater. Res.* **2013**, *43*, 359–386; b) G. R. Desiraju, *J. Am. Chem. Soc.* **2013**, *135*(27), 9952–9967; c) Y. Garcia, N. N. Adarsh, A. D. Naik, *Chimia* **2013**, *67*(6), 411–418.

[13]   T. G. Gopakumar, F. Matino, H. Naggert, A. Bannwarth, F. Tuczek, R. Berndt, *Angew. Chem. Int. Ed.* **2012**, *51*, 6262–6266.

[14]   S. Venkataramani, U. Jana, M. Dommaschk, F. D. Sönnichsen, F. Tuczek, R. Herges, *Science* **2011**, *331*, 445–447.

[15]   a) I. Boldog, A. B. Gaspar, V. Martinez, P. Pardo-Ibanez, V. Ksenofontov, A.

Bhattacharjee, P. Gütlich, J. A. Real, *Angew. Chem. Int. Ed.* **2008**, *47*, 6433–6437; b) S. Cobo, G. Molnar, J. A. Real, A. Bousseksou, *Angew. Chem. Int. Ed.* **2006**, *45*, 5786–5789; c) G. Molnar, S. Cobo, J. A. Real, F. Carcenac, E. Daran, C. Vieu, A. Bousseksou, *Adv. Mater.* **2007**, *19*, 2163; d) M. Cavallini, I. Bergenti, S. Milita, G. Ruani, I. Salitros, Z.-R. Qu, R. Chandrasekar, M. Ruben, *Angew. Chem. Int. Ed.* **2008**, *47*, 8596; e) A. D. Naik, L. Stappers, J. Snauwaert, J. Fransaer, Y. Garcia, *Small* **2010**, *6*, 2842; f) H. J. Shepherd, G. Molnár, W. Nicolazzi, L. Salmon, A. Bousseksou, *Eur. J. Inorg. Chem.* **2013**, 653–661.

[16]   S. Hayami, K. Hashigucchi, G. Juhasz, M. Ohba, H. Okawa, Y. Maeda, K. Kato, K. Osaka, M. Takata, K. Inoue, *Inorg. Chem.* **2009**, *43*, 4124–4126.

[17]   S. Horike, S. Shimomura, S. Kitagawa, *Nat. Chem.* **2009**, *1*, 695–704.

[18]   A. Hauser, *Topics in Current Chemistry*, *Vol. 233* (Eds.: P. Gütlich, H. A. Goodwin), Springer, Wien, New York, **2004**, 49–58.

[19]   P. Gütlich, *Eur. J. Inorg. Chem.* **2013**, 581–591.

[20]   a) G. Racah, *Phys. Rev.* **1943**, *63*, 367–382. b) G. Racah, *Phys. Rev.* **1949**, *76*, 1352–1365.

[21]   a) Y. Tanabe, S. Sugano, *J. Phys. Soc. Jpn.* **1954**, *9*(5), 753–766; b) Y. Tanabe, S. Sugano, *J. Phys. Soc. Jpn.* **1954**, *9*(5), 766–779; c) S. Sugano, Y. Tanabe, H. Kamimura, *Pure and Applied Physics*, *Vol. 33*, Academic Press, New York, **1970**, 82.

[22]   O. Kahn, *Molecular Magnetism*, VCH, New York, **1993**, 53–86.

[23]   J. N. Israelachvili, D. J. Mitchell, B. W. Ninham, *J. Chem. Soc., Faraday Trans. 2*, **1976**, *72*, 1525–1568.

[24]   a) S. Cobo, G. Molnar, J. A. Real, A. Bousseksou, *Angew. Chem. Int. Ed.* **2006**, *45*, 5786–5789; b) Y. Bodenthin, U. Pietsch, H. Möhwald, D. G. Kurth, *J. Am. Chem. Soc.* **2005**, *127*, 3110–3114.

[25]   a) C. Gandolfi, N. Miyashita, D. G. Kurth, P. N. Martinho, G. G. Morgan, M. Albrecht, *Dalton Trans.* **2010**, *39*, 4508–4516. b) M. Cavallini, *Phys. Chem. Chem. Phys.* **2012**, *14*, 11867–11876.

[26]   C. Gandolfi, T. Cotting, P. N. Martinho, O. Sereda, A. Neels, G. G. Morgan, M. Albrecht, *Dalton Trans.* **2011**, *40*, 1855–1865.

[27]   H. Soyer, C. Mingotaud, M.-L. Boillot, P. Delhaes, *Langmuir* **1998,** *14,* 5890–5895.

[28]   K. Kuroiwa, T. Shibata, S. Sasaki, M. Ohba, A. Takahara, T. Kunitake, N. Kimizuka, *J. Polym. Sci.: Part A: Polym. Chem.* **2006**, *44*, 5192–5202.

[29]   a) T. Fujigaya, D.-L. Jiang, T. Aida, *Chem. Asian J.* **2007**, *2*, 106–113; b) P. Grondin, O. Roubeau, M. Castro, H. Saadaoui, A. Colin, R. Clérac, *Langmuir* **2010**, *26*, 5184–5195; c) O. Roubeau, A. Colin, W. Schmitt, R. Clérac, *Angew. Chem. Int. Ed.* **2004**, *43*, 3283–3286.

[30]   C. Echeverria, M. Rubio, G. R. Mitchell, D. Lopez, *Eur. Polym. J.* **2014**, *53*, 238–245.

[31]   a) M. Seredyuk, A. B. Gaspar, V. Ksenofontov, Y. Galyametdinov, J. Kusz, P. Gütlich, *Adv. Funct. Mater.* **2008**, *18*, 2089–2101; b) M. Seredyuk, A. B. Gaspar, V. Ksenofontov, Y. Galyametdinov, J. Kusz, P. Gütlich, *J. Am. Chem. Soc.* **2008**, *130*, 1431–1439; c) S. Hayami, Y. Kojima, D. Urakami, K. Ohta, K. Inoue, *Polyhedron* **2009**, *28*, 2053–2057; d) Y. Galyametdinov, V. Ksenofontov, A. Prosvirin, I. Ovchinnikov, G. Ivanova, P. Gütlich, W. Haase, *Angew. Chem. Int. Ed.* **2001**, *40*(22), 4269–4271.

[32]   A.B. Gaspar, M. Seredyuk, P. Gütlich, *Coord. Chem. Rev.* **2009**, *253*, 2399–2413.

[33]   S. Hayami, *Spin Crossover Materials – Properties and Applications* (Ed.: M. A. Halcrow), Wiley, **2013**, 321–345.

[34]   S. Hayami, R. Moriyama, A. Shuto, Y. Maeda, K. Ohta, K. Inoue, *Inorg. Chem.* **2007**, *46*, 7692–7694.

[35]   H. Luecken, *Magnetochemie*, B. G. Teubner, Stuttgart, Leipzig, **1999**.

[36]   P. Gütlich, E. Bill, A. X. Trautwein, *Mössbauer Spectroscopy and Transition Metal Chemistry*, Springer, Berlin, Heidelberg, **2011**.

[37]   a) D. F. J. Evans, *J. Chem. Soc.* **1959**, 2003–2005; b) L. A. Yatsunyk, F. A. Walker, *Inorg. Chem.* **2004**, *43*, 757–777.

[38]   G. W. H. Höhne, W. F. Hemminger, H.-J. Flammersheim, *Differential Scanning Calorimetry*, Second Edition, Springer, **2003**.

[39]   H.-B. Duan, X.-M. Ren, L.-J. Shen, W.-Q. Jin, Q.-J. Meng, Z.-F. Tian, S.-M. Zhou, *Dalton Trans.* **2011**, *40*, 3622–3630.

[40]   a) S. Hayami, Y. Shigeyoshi, M. Akita, K. Inoue, K. Kato, K. Osaka, M. Takata, R. Kawajiri, T. Mitani, Y. Maeda, *Angew. Chem. Int. Ed.* **2005**, *44*(31), 4899–4903; b) S. Hayami, Y. Komatsu, T. Shimizu, H. Kamihata, Y. H. Lee, *Coord. Chem. Rev.* **2011**, *255*(17-18), 1981–1990.

[41]   S. Hayami, Y. Kojima, D. Urakami, K. Ohta, K. Inoue, *Monatsh. Chem.* **2009**, *140*, 829–838.

[42]   M. Seredyuk, M. C. Muñoz, M. Castro, T. Romero-Morcillo, A. B. Gaspar, J. A. Real,

Chem. Eur. J. **2013**, *19*, 6591–6596.

[43]   a) T. Fujigaya, D.-L. Jiang, T. Aida, *J. Am. Chem. Soc.* **2003**, *125*, 14690–14691; b) T. Fujigaya, D.-L. Jiang, T. Aida, *J. Am. Chem. Soc.* **2005**, *127*, 5484–5489.

[44]   M. Seredyuk, A. B. Gaspar, V. Ksenofontov, S. Reiman, Y. Galyametdinov, W. Haase, E. Rentschler, P. Gütlich, *Chem. Mater.* **2006**, *18*, 2513–2519.

[45]   S. Kume, K. Kuroiwa, N. Kimizuka, *Chem. Commun.* **2006**, 2442–2444.

[46]   C. Gandolfi, T. Cotting, P. N. Martinho, O. Sereda, A. Neels, G. G. Morgan, M. Albrecht, *Dalton Trans.* **2011**, *40*(9), 1855–1865.

[47]   C. Gandolfi, C. Moitzi, P. Schurtenberger, G. G. Morgan, M. Albrecht, *J. Am. Chem. Soc.* **2008**, *130*, 14434–14435.

[48]   P. N. Martinho, Y. Ortin, B. Gildea, C. Gandolfi, G. McKerr, B. O'Hagan, M. Albrecht, G. G. Morgan, *Dalton Trans.* **2012**, *41*, 7461–7463.

[49]   A. M. Ako, M. S. Alam, M. Rahman, J. P. Hill, N. M. Sanchez-Ballester, K. Ariga, G. Buth, C. E. Anson, A. K. Powell, *Chem. Eur. J.* **2012**, *18*(51), 16419–16425.

[50]   E.-G. Jäger, E. Häussler, M. Rudolph, A. Schneider, *Z. anorg. allg. Chem.* **1985**, *525*, 67–85.

[51]   W. Bauer, T. Ossiander, B. Weber, *Z. Naturforsch. B* **2010**, *65*, 323–328.

3 Overview of Thesis Results

This thesis comprises five publications, which are presented in Chapter 4-8. The individual contributions to joint publications are pointed out in Chapter 3.2.

3.1 Synopsis

This work deals with the synthesis and characterization of amphiphilic iron(II) SCO complexes, especially with regard to the self-assembly ability of the molecules and enhancement of cooperativity of SCO. The ligand system is derived from the already known Schiff base-like *Jäger* type, which has been proved to be an excellent ligand system for realizing thermally induced SCO. Additionally, it forms with iron(II), in contrast to commonly used ligands, a neutral complex without counter anions. These are excellent preconditions for realizing highly cooperative STs. The idea was to add long alkyl chains with different chain lengths at the outer periphery of the ligand. Together with the possibility to fine-tune the ligand field strength by variation of the different substituents at R^1 and R^2 and variation of axial ligands, this gives a large pool of possible new amphiphilic SCO compounds.

The preparation of the complexes was established and follows an eight-step synthesis including alkylation of catechol, nitration in *para*-positions, reduction of the dinitro derivative and condensation with the corresponding keto-enol ether. Conversion with iron(II) acetate gives the iron(II) complex [FeLa-d(Cn+1)(MeOH)$_{0-2}$] bearing methanol molecules as axial ligands. Exchange of the methanol molecules through N-donor ligands like pyridine and its derivatives shifts the crystal field strength into the right energy region for thermally induced SCO. Though preparation was partially leaned on previously published syntheses, for each chain length and substituents adjustments had to be made and the exact conditions (reaction time, solvent, excess, workup conditions) were optimized.

Chapter 4 describes one of the first results of this approach. An iron complex with an alkyl chain length of 16 carbon atoms, substituent *a* and pyridine as axial ligands was synthesized and due to X-ray structure analysis in the LS and HS state the molecular setup could be elucidated. It became clear that the molecules arrange in a lipid layer-like ordering, in which the head groups containing the metal centre point to each other and the alkyl chains, the

nonpolar tail groups, are interlocking. This complex shows, in contrast to the gradual SCO often observed for long alkyl chain compounds, a highly cooperative ST with hysteresis with a width up to 47 K, exhibiting small steps in the cooling as well as in the warming mode. This was also confirmed by DSC measurements. A hydrogen bonding network and structural changes regarding order-disorder transitions of the pyridine are made responsible for this behaviour. This compound provided deep insight into the spin switching mechanism and proved due to the low value of cell volume change ($\Delta V/V \approx 2.9$ %) arising from the sterical demand of the long alkyl chains that the hysteresis cannot solely be related to elastic interactions. It could be shown that the functionalization of the parent compounds without alkyl chains led to a highly ordered arrangement in the crystal controlled by the hydrophobic van der Waals interactions of the alkyl chains.

This promising outcome was a motivation to synthesize a series of complexes bearing pyridine as axial ligands, in order to investigate this new class of iron complexes in more detail. The results for different chain lengths ($n = 7, 11, 15$) and different substituents *a*, *b* and *c* for $n = 11$ are delineated in Chapter 5. Here, only two crystal structures of the precursors with C12 alkyl chains and methanol as axial ligands [FeL*a*(C12)(MeOH)$_2$] and [FeL*c*(C12)(MeOH)$_2$] could be obtained. They are again organized in the lipid layer-like arrangement in the crystal as observed before. All described pyridine complexes showed a broad variety of ST curves. [FeL*a*(C8)(py)$_2$] revealed a relatively abrupt SCO with a small 4 K hysteresis, and the compound with four more carbon atoms in the hydrophobic rests, [FeL*a*(C12)(py)$_2$] a gradual, stepwise and incomplete SCO. In this frame, the alkyl chain length appeared not to play a decisive role concerning $T_{1/2}$. For complexes with the same chain length but different substituents it differed quite strongly. Stepwise and also incomplete curves were observed and the transition temperatures $T_{1/2}$ were significantly different. To clarify the various ST curve shapes of complexes with the same substituents but different chain lengths in the solid, temperature-dependent paramagnetic NMR experiments in solution were conducted for [FeL*a*(C8)(py)$_2$], [FeL*a*(C12)(py)$_2$] and the compound discussed in Chapter 4, [FeL*a*(C16)(py)$_2$]. It turned out that the ST curve progression was nearly identical for all of the three compounds, the length of the alkyl chains did not influence the ST properties in solution. Thus, all the differences observed in the solid state were caused by packing effects.

So far, lipid layer-like structures were the only motif observed for the newly introduced amphiphilic complexes with chain lengths of 12 and 16 carbon atoms. Syntheses were also

carried out with compounds of the chain length of 8 carbon atoms to further investigate the dependency of the length of the alkyl chains on the arrangement in the crystal and the resulting SCO behaviour. As described in Chapter 6, X-ray structure analysis of crystals of two modifications of the hexa-coordinated complex [FeL*c*(C8)(dmap)$_2$] · x MeOH – one of them in the HS and LS state – and two modifications of the penta-coordinated analogue [FeL*c*(C8)(dmap)] was performed. Synthetic attempts with different amounts of the axial ligand dmap revealed that at a relatively high 30 fold excess, penta- and hexa-coordinated products could be obtained, depending on the exact reaction conditions. Less dmap led to penta-coordination and at higher excess the system could be forced to crystallize hexa-coordinated. None of the hexa-coordinated compounds exhibited the lipid layer-like arrangement. Moreover, both modifications showed a very diverse variety of crystallization modes which were quite unpredictable. Nevertheless, the hexa-coordinated products both presented a very similar gradual SCO between 125 and 325 K, which was almost identical to the transition curve obtained by the SQUID measurement of the compound in solution where all cooperative effects are switched off. The missing layered structure and the absence of other factors that are responsible for cooperative interactions was made responsible for this behaviour.

It was noticed that the layered arrangement is quite suitable for increasing the possibility of cooperative effects, for example hydrogen bonds between the opposed heads, through a well-defined ordering in the crystal. The C8 alkyl chains are too short to dominate the packing pattern in such way.
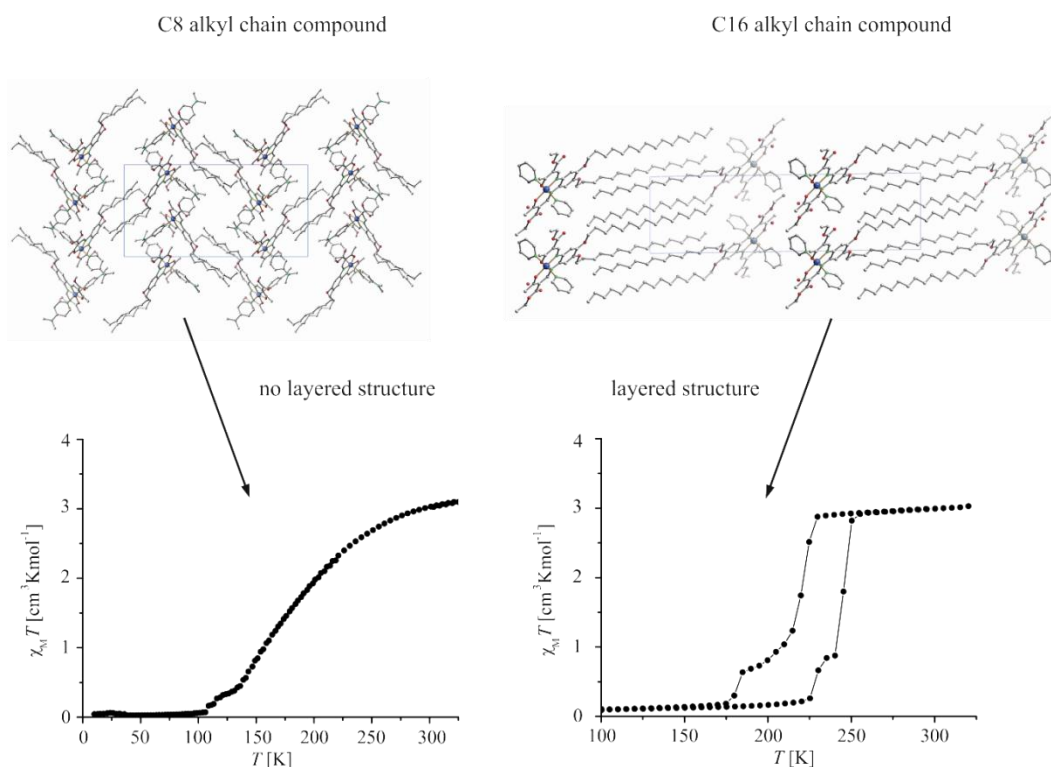
Figure 1. Comparison of short alkyl chain compound [FeL*c*(C8)(dmap)$_2$] without layered arrangement and gradual SCO (left) and long alkyl chain compound [FeL*a*(C16)(py)$_2$] · 0.25 H$_2$O exhibiting lipid layer-like structure and abrupt SCO with hysteresis (right).

Attempts to examine ST or PT behaviour at elevated temperatures were limited by the frequently observed decomposition of the mononuclear compounds, for example the loss of the axial ligand pyridine. In order to increase thermal stability and to decrease air sensitivity of the compounds, as well as to further enhance cooperativity, approaches were made to synthesize coordination polymers with bidentate ligands like bpea or bpee. In this frame, crystal structures of dinuclear complexes could be obtained. Attempts to add bigger axial ligands like dmap to compounds with C12 or C16 alkyl chains while keeping the lamellar structure motif resulted in the crystallization of SCO inactive penta-coordinated compounds or mixed ligand configurations. The question, with which Chapter 7 deals arised, how the crystallization mode could be controlled in a fashion in which octahedral complexes with [N$_4$O$_2$] coordination sphere and lipid layer-like arrangement can be obtained. For this, the complex size of all crystal structures gathered so far were measured out and a rather simple empirical rule for this system could be derived: when the added height and broadness of the

polar head group, divided through the entire length of the complex, is around 1, lipid layer-like arrangement in the crystal can be expected. The relation was named the **s**elf-**a**ssembly **p**arameter *sap*:

$$sap = \frac{(H+B)}{L}$$

H = height of the polar head group

B = broadness of the polar head group

L = entire length of the complex

This result explained vividly the relative conformation of the molecules discussed in this work and can, moreover, predict possible structure outcomes.

Following this crystal engineering tool, the alkyl chain length of the complexes had to be elongated to add more bulky ligands in axial position. The ligand synthesis was modified and alkyl chains with the length of 22 carbon atoms were attached to the outer sphere of the ligand. Adding the bulky axial ligand dmap to [FeLd(C22)(MeOH)$_2$] resulted, despite of the sterically demanding phenylene rests in substituent *d*, in the octahedrally coordinated [FeLd(C22)(dmap)$_2$], proved by X-ray structure analysis.

Iron(II) coordination polymers with C22 chain ligands and bpea, bpee and bpey were synthesized and the complex [FeLc(C22)(bpea)]$_n$ could be structurally characterized with good *R*-values. It showed a highly ordered lipid layer-like arrangement, while the [N$_4$O$_2$] coordination sphere was provided. Powder samples thereof precipitated in two modifications which revealed different magnetic behaviours (SCO above RT and SCO below RT with small hysteresis).
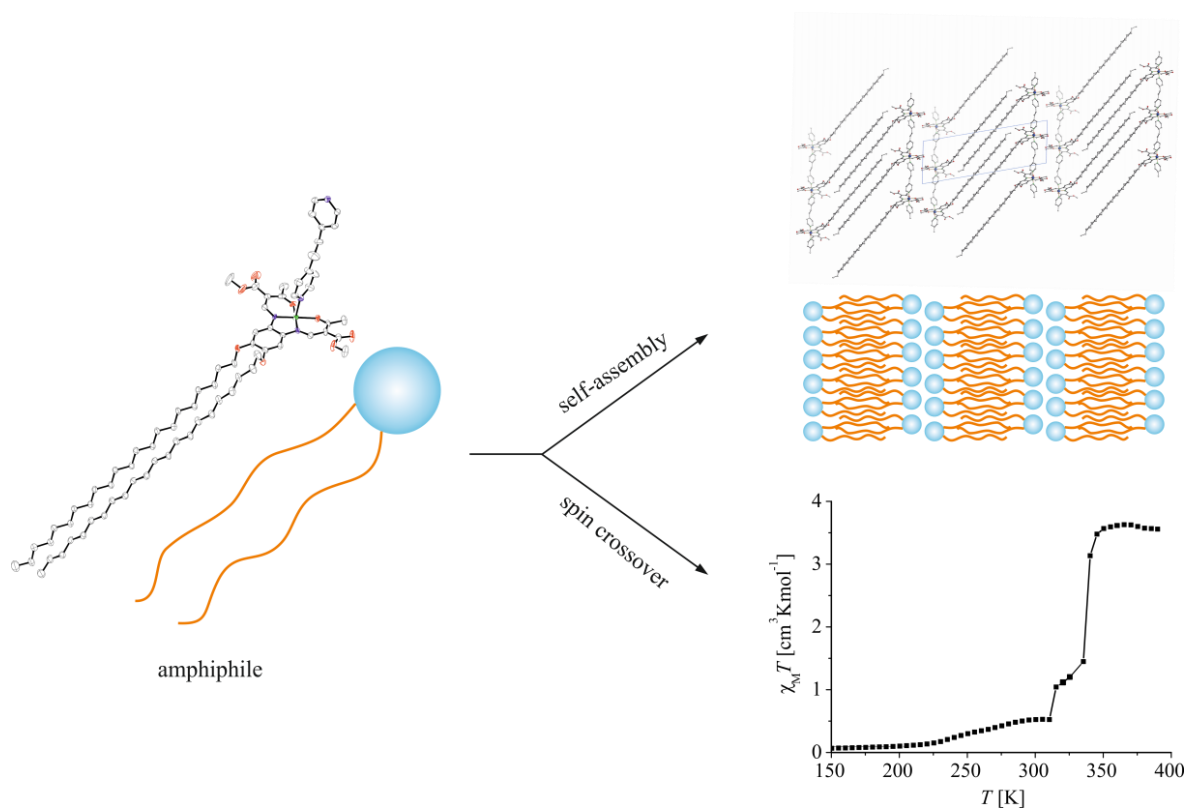
Figure 2. Crystal engineering and SCO of [FeL*c*(C22)(bpea)]$_n$.

Magnetic measurements revealed for all crystalline compounds discussed in Chapter 8 the LS state at room temperature and a very abrupt ST situated around 350 K. It could be demonstrated that the ST becomes more abrupt replacing bpea by bpee as more rigid bridging ligand with a C=C double bond instead of a single bond, and $T_{1/2}$ is shifted to higher temperatures. Replacing bpee for bpey as axial ligand led to even more abrupt SCO what showed the enhancement of cooperativity. All of the C22 alkyl chain compounds exhibit an ordering into spherulites after warming what could be observed through view between crossed polarizers.

3.2 Individual Contributions to Joint Publications

The results presented in this thesis were obtained in collaboration with others and are published, accepted, or are to be submitted as indicated below. In the following, the contributions of all co-authors to the publications are specified. The asterisk denotes the corresponding authors.

Chapter 4

This work was published in Chemical Communications (*Chem. Commun.* **2011**, *47*, 7152–7154) with the title

"Cooperative spin transition in a lipid layer like system".

Stephan Schlamp, Birgit Weber*, Anil D. Naik and Yann Garcia*

I synthesized and characterized all complexes and ligands presented in this work, carried out the magnetic measurements and wrote the experimental section, the conclusion and parts of the result section (X-ray structure analysis, magnetic measurements). Anil D. Naik and Yann Garcia carried out the DSC measurements at the Université Catholique de Louvain, interpreted the DSC data and wrote this part in the manuscript. Birgit Weber supervised this work, helped interpreting the magnetic and X-ray data, wrote the introduction and was involved in scientific discussions and correction of the manuscript.

Chapter 5

This work was published in European Journal of Inorganic Chemistry (*Eur. J. Inorg. Chem.* **2012**, 2759–2768) with the title

"New Octahedral, Head–Tail Iron(II) Complexes with Spin Crossover Properties".

Stephan Schlamp, Peter Thoma and Birgit Weber*

I synthesized and characterized all complexes and ligands presented in this work, carried out the magnetic measurements and wrote the publication. Peter Thoma carried out the paramagnetic ^{1}H NMR experiments and wrote this part in the article. Birgit Weber supervised this work and was involved in scientific discussions and the correction of the manuscript.

Chapter 6

This work was published in New Journal of Chemistry (*New J. Chem.* **2014**, *38*, 1965–1972) with the title

"Amphiphilic iron(II) complexes with short alkyl chains – crystal packing and spin transition properties".

Stephan Schlamp, Katja Dankhoff and Birgit Weber*

I established the ligand system, wrote the publication, carried out the magnetic measurements and synthesized and characterized parts of the ligands and complexes discussed in this work by myself or supported Katja Dankhoff as her supervising tutor. Birgit Weber supervised this work and was involved in scientific discussions and correction of the manuscript.

Chapter 7

This work was published in Chemistry – A European Journal (*Chem. Eur. J.* **2014**, *20*, 6462–6473) with the title

"Influence of the Alkyl Chain Length on the Self-Assembly of Amphiphilic Iron Complexes – An Analysis of X-Ray Structures".

Stephan Schlamp, Peter Thoma and Birgit Weber*

I synthesized and characterized all ligands and complexes discussed in this work, solved and

treated all crystal structure data and wrote the publication. Peter Thoma collected most of the crystallographic X-ray data and was involved in scientific discussions. Birgit Weber supervised this work and was involved in scientific discussions and correction of the manuscript.

Chapter 8

This work is to be submitted with the title

"Amphiphilic Spin Crossover Coordination Polymers with C22 Alkyl Chains"

Stephan Schlamp and Birgit Weber*

I synthesized and characterized the ligands and complexes discussed in this work, carried out the magnetic measurements and the polarizing optical microscopy measurements, solved the crystal structure and wrote the publication. Birgit Weber supervised this work and was involved in scientific discussions and correction of the manuscript.

4   Cooperative spin transition in a lipid layer-like system

Stephan Schlamp,[a] Birgit Weber,*[a] Anil D. Naik[b], Yann Garcia*[b]

[a] Lehrstuhl für Anorganische Chemie II, Universität Bayreuth, Universitätsstraße 30, NW 1, 95440 Bayreuth, Germany; Fax: +49-92155-2157; E-mail: weber@uni-bayreuth.de

[b] Institute of Condensed Matter and Nanosciences, MOST-Inorganic Chemistry, Université Catholique de Louvain, Place L. Pasteur 1, 1348 Louvain-la-Neuve, Belgium; Fax: +32 10472831; E-mail: yann.garcia@uclouvain.be

Abstract: A novel iron(II) mononuclear spin transition complex [FeL(py)$_2$] displays an abrupt spin transition around 225 K accompanied by a very wide thermal hysteresis loop (~ 50 K) that spreads out over 100 K. Crystal structure analysis in both low-spin and high-spin states reveal a lipid layer-like arrangement of the complex molecules and provides insights into the spin switching mechanism.

4.1   Introduction

Since the discovery of spin crossover (SCO) compounds in 1931 by Cambi et al.[1] the interest in this substance class never vanished,[2] as the thermochromism associated to the spin state change makes them potentially useful for various applications such as display and memory device units,[3] sensors[4] and cold channel control units in food and medical sectors.[5] In order to realise application it is important to explore different possibilities for the nanostructuration of SCO materials[6] and to investigate if additional properties can be combined (e.g. liquid crystal behaviour,[7] magnetic exchange interactions[8]) resulting in multifunctional SCO materials.[9] In this frame, we modified Schiff base-like ligands used for the synthesis of SCO complexes[10] by adding long alkyl chains in the outer periphery by pre-

paring [FeL(py)₂] (**1**) with L = (E,E)-[{diethyl-2,2'-[4,5-dihexadecyloxy-1,2-phenylenebis-(iminomethylidyne)]bis-3-oxobut-anato}]. We aimed to study the influence of this modification on the crystal packing as well as on the SCO behaviour and investigate if additional features could be achieved for **1**.

4.2   Results and Discussion

A complete description of the synthesis of H_2L and the iron complex (**1**), is given in the Supporting Information. Single crystals suitable for an X-ray analysis of **1**×0.25H₂O were obtained and the crystal structure was determined first at 250 K and then at 125 K (same crystal, in both cases space group *P* 1̄), corresponding to the high-spin (HS) and low-spin (LS) state of the complex as seen in the magnetic measurement (Fig. 3). The crystallographic data are summarized in the Supporting Information, Table S1. Fig. 1 displays an ORTEP drawing of the asymmetric unit of **1** in the HS and the LS state. An excerpt of the coordination environment is given in Fig. S1. Selected bond lengths and angles around the inner coordination sphere of the iron centre are summarized in Table 1.
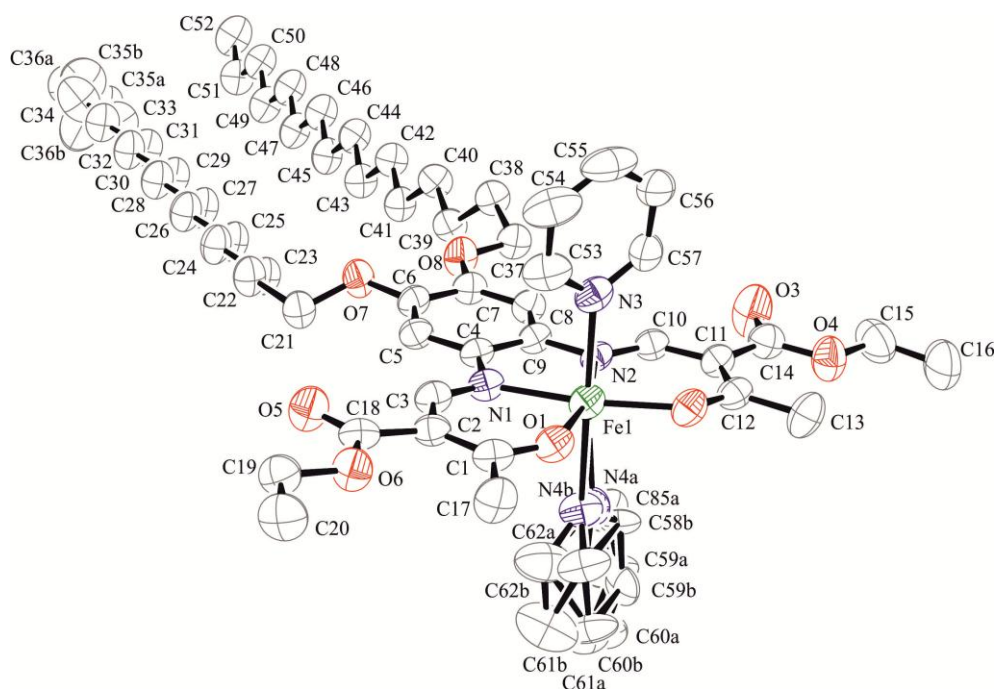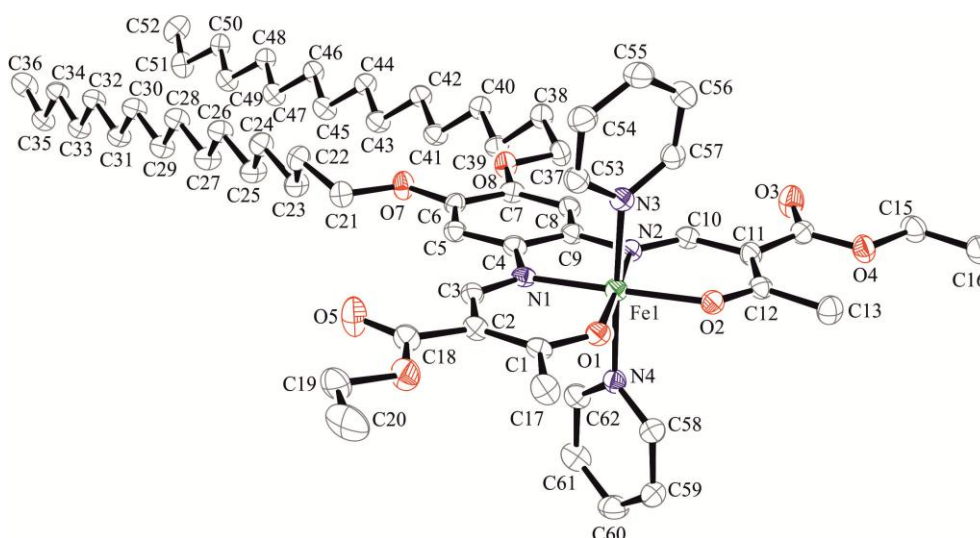
Figure 1. ORTEP drawing of the asymmetric unit of **1** in the HS (top) and LS (bottom) states. Hydrogen atoms and the water molecule have been omitted for clarity. Displacement ellipsoids are shown at the 50 % probability level.

The average bond lengths within the first coordination sphere of the iron(II) centres in the HS structure are 2.07 Å (Fe–N_{eq}), 2.00 Å (Fe–O_{eq}) and 2.28 Å (Fe–L_{ax}). Those and the observed O–Fe–O angle (106°) are in the region expected for HS complexes of this ligand type.[10,11] Upon the HS to LS transition a shortening of the bond lengths of about 10% is observed, as observed for other iron(II) SCO complexes.[2,11] The average bond lengths in the LS-structure are 1.90 Å (Fe–N_{eq}), 1.94 Å (Fe–O_{eq}) and 2.02 Å (Fe–L_{ax}) with a O–Fe–O angle of 89°.

Table 1. Selected bond lengths [Å] and angles [°] within the inner coordination sphere of **1** in the HS and LS state.

	Fe–N_{eq}	Fe–O_{eq}	Fe–N(L_{ax})	O–Fe–O	L_{ax}–Fe–L_{ax}	∠ L_{ax}[b]
HS	2.059(3)	2.001(2)	2.284(3)	106.10(9)	173.73(12)[a]	
	2.086(2)	1.999(2)	2.280(4)[a]		176.95(23)[a]	21.5[a]
			2.288(7)[a]			47.5[a]
LS	1.897(2)	1.935(2)	2.021(2)	88.80(7)	175.06(8)	83.6
	1.907(2)	1.947(2)	2.014(2)			

a: disorder; b: angle between the pyridine planes

In the HS state, a disorder is observed of one pyridine and at the end of one of the C16 alkyl chains. The pyridine ring including N4 is contorted in two directions in a relative ratio of 60:40, the same ratio is observed for the ethyl endgroup (C35 and C36) in the alkyl chain bound by O7. The planes spanned by the two axial pyridine rings are staggered in the HS state. Upon cooling the disordered pyridine ring changes its orientation resulting in a nearly perpendicular arrangement in the LS state. An additional water molecule is observed in the crystal packing with an approximate occupation number of 0.25. Several hydrogen bonds and short contacts are observed between the complex molecules and the water (Table S2).

In the crystal the molecules are packed in a lipid layer like arrangement as illustrated in Fig. 2 with the layers running along the *a-b*-plane. Within one layer, the alkyl chains of the Schiff base like ligand are packed in the middle and the SCO centres are on the outer sides.
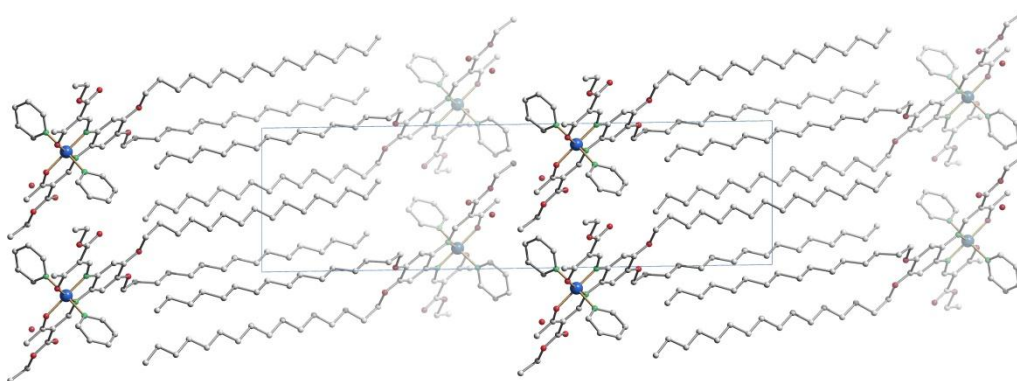
Figure 2. Packing of the molecules of **1**×0.25H$_2$O in the crystal projected along [1 0 0] in the HS state.

In the LS state a network of hydrogen bonds is formed between the SCO centres between the layers and within the layer, the additional water molecule being also involved, as illustrated in Fig. S2. In the HS state the rearrangement of the pyridine ring and the alkyl chain results in changes for the short contacts. Now, short contacts are only observed between the molecules of one lipid like layer but not between the layers as illustrated in Fig. S2 and S3.

Magnetic susceptibility data of **1**×0.25H$_2$O were recorded on cooling and warming over the temperature range 300–5 K (Fig. 3). At room temperature the $\chi_M T$ product is 3.0 cm^{3}Kmol^{-1} which is in the range expected for an iron(II) complex in the HS state. In the first cycle (squares) upon cooling the magnetic moment remains constant until 229 K where an abrupt

spin transition (ST) takes place with about 60% of the molecules and $T_c^{(60)\downarrow} = 222$ K. In the temperature range between 214 K and 185 K the magnetic moment decreases gradually from $\chi_M T$ (214 K) = 1.1 cm^{3}Kmol^{-1} to $\chi_M T$ (185 K) = 0.6 cm^{3}Kmol^{-1}. Below 185 K a second abrupt step is observed involving the remaining 20% of the molecules $T_c^{(20)\downarrow} = 182$ K. At 100 K the remaining $\chi_M T$ product is 0.1 cm^{3}Kmol^{-1} which is in the range expected for an iron(II) complex in the LS state.
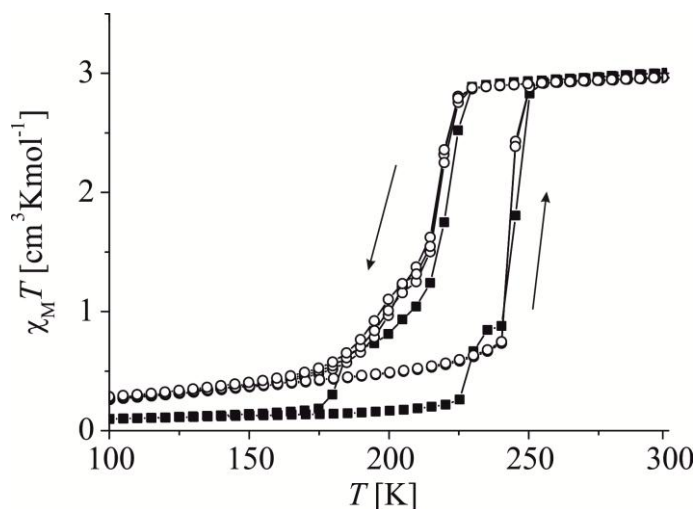
Figure 3. $\chi_M T$ vs. T plot of **1** of the first cycle (squares) and all the following cycles (open cycles). Displayed in the temperature range 300–10 K.

Upon heating the ST occurs in two steps with about 30% of the molecules involved in the first $(T_c^{(30)\uparrow} = 229$ K) and about 70% of the molecules involved in the second step $(T_c^{(70)\uparrow} = 245$ K). The width of the thermal hysteresis loop is 23 K for the first and 47 K for the second step. The second and third thermal cycles reveal the absence of the second gradual step and the remaining $\chi_M T$ product is 0.3 cm^{3}Kmol^{-1} at 100 K indicating an iron(II) complex almost completely in the LS state.

The sample has been studied by differential scanning calorimetry (DSC) over the temperature range 300–98 K on cooling and warming modes, at 10 K min^{-1}, in order to extract thermodynamical parameters associated to the spin transition, and probe the order of the phase transitions. On warming from 98 K, two major endothermic peaks corresponding to a first order phase transition proceeding in two steps were detected (Fig. 4). The first one is ob-

served at $T_{max}^{(1)\uparrow} = 235(1)$ K and a broader peak is found at $T_{max}^{(2)\uparrow} = 250(1)$ K. These data matches the transition temperatures derived from SQUID measurements (see Fig. 3). A very less intense peak, whose shape indicates a continuous or weakly first-order phase transition, is observed at $T^{(3)} = 240$ K corresponding to the plateau region between the two phase transitions. On cooling from room temperature, broader exothermic peaks arise at different temperatures, confirming the hysteretic character of the ST process.
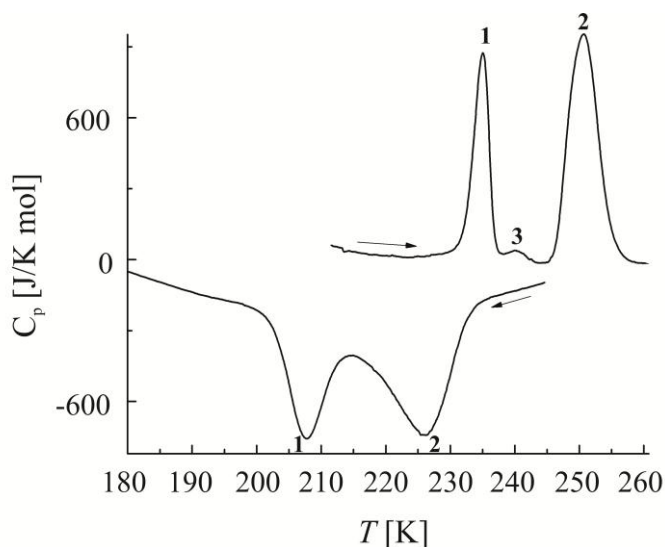
Figure 4. Heat capacity *vs. T* of **1** over the temperature range 261–180 K at a scanning rate of 10 K min^{-1} in the cooling ($\leftarrow$) and warming ($\rightarrow$) modes.

A peak is found at $T_{max}^{(2)\downarrow} = 226(1)$ K, in agreement with the first ST branch, which is followed by a second peak at $T_{max}^{(1)\downarrow} = 207(1)$ K, which only corresponds to the onset of the plateau region of the magnetic curve. The tiny second step in the cooling mode of the first cycle of the SQUID measurements around 182 K is not seen by DSC. Such a DSC profile was confirmed by two successive cooling and heating cycles. Interestingly, two peaks are still observed in the warming and cooling process after the first cycling. One is clearly related to the spin transition (2) whereas the other peak (1) relates to a thermal anomaly that plays a role on the spin state during the first cycle but not later, still existing but not affecting it. Enthalpy and entropy associated to these peaks are given in Table S3.

This unprecedented ST behaviour can be explained thanks to the results from X-ray structure analysis. Step-wise spin transitions are often related to the presence of two or more

inequivalent iron centres.[12] In our case, the disorder of the pyridine ring in the HS state could be responsible for inequivalent iron centres and thus the steps in the transition curve. Such a situation was recently discussed by Matouzenko *et al.*[13] with the same symmetries in the HS and LS state and a symmetry breaking on the plateau.[14] As different intermolecular interactions are observed for the disordered parts of the HS state (Fig. S2) the differences in the hysteresis width can be explained with differences in the H-bond network. It should be noted that the space group does not change upon ST and thus the observed hysteresis cannot be related to a structural phase transition but must be related to other cooperative effects. Due to the long alkyl chains in the outer periphery of the complex the observed change in the cell volume ($\Delta V/V = 2.9\%$) is very small, especially when the contribution from the thermal contraction is considered. Thus the hysteresis cannot solely be related to elastic interactions. The changes in the hydrogen bond network are one possible explanation for the cooperative spin transition.[15] A very interesting feature concerns the second peak in the DSC measurements that is related to the gradual part in the ST curve. This thermal anomaly could result from an order–disorder transition of the pyridine ring,[16] which is disordered in the HS state and that orders in the LS, as dectected by X-ray diffraction. Such types of transitions are known to be able to control the course of a ST leading to gradual regions.[17] The disappearance of the small step after the first cooling/heating cycle could be related to small changes in the molecule structure or the intermolecular interactions due to this order–disorder transition.

4.3   Conclusion

The introduction of long alkyl chains in the outher pheriphery of Schiff base like ligands did lead to head–tail molecules that crystallise in a lipid layer like structure and show a cooperative spin transition with a wide thermal hysteresis loop (up to ~50 K). The X-ray structure solved in the HS and LS states allows a deeper insight into the ST mechanism of **1** which results from an interplay involving the H-bond network and order–disorder transition of the pyridine rings.

4.4 Experimental Section

Synthesis of H$_2$L and the iron complex [FeL(py)$_2$] (1)

The free ligand H$_2$L was synthesised according to [18] and [19] with slight modifications. In a first step, catechol and 2 equivalents of 1-bromohexadecane were converted with K$_2$CO$_3$ in DMF to give, after filtration and washing with plenty of water and methanol, 1,2-dihexadecyloxybenzene (**A**) in good yields. This white precipitate was nitrated according to [20] and [21]. It was suspended in acetic acid and a mixture of HNO$_3$ and fuming HNO$_3$ were added dropwise. The dinitro product (**B**) appears bright yellow coloured. Reducing of the functional groups with Palladium on activated charcoal and hydrazine-monohydrate similar to [21] gives the white diamino product (**C**) which is air sensitive. Further reaction with Ethoxymethyleneethylacetoacetate (**D**) [22] in an approximate ratio of 1:2 gives the yellow ligand **H$_2$L** which is not any more air sensitive and reaction with iron(II) acetate [23] in methanol the corresponding brown microcrystalline iron(II) complex [**Fe(L)(MeOH)$_2$**]. To obtain the pyridine complex **1**, [**Fe(L)(MeOH)$_2$**] was converted in pyridine under reflux conditions and a crystallisation approach was made with water diffunding into the black solution. Several reproductions with different concentrations of possible product in the solution turned out that it takes at least 40-50 days of formation until greenish-black thin platelet-like crystals can be isolated.
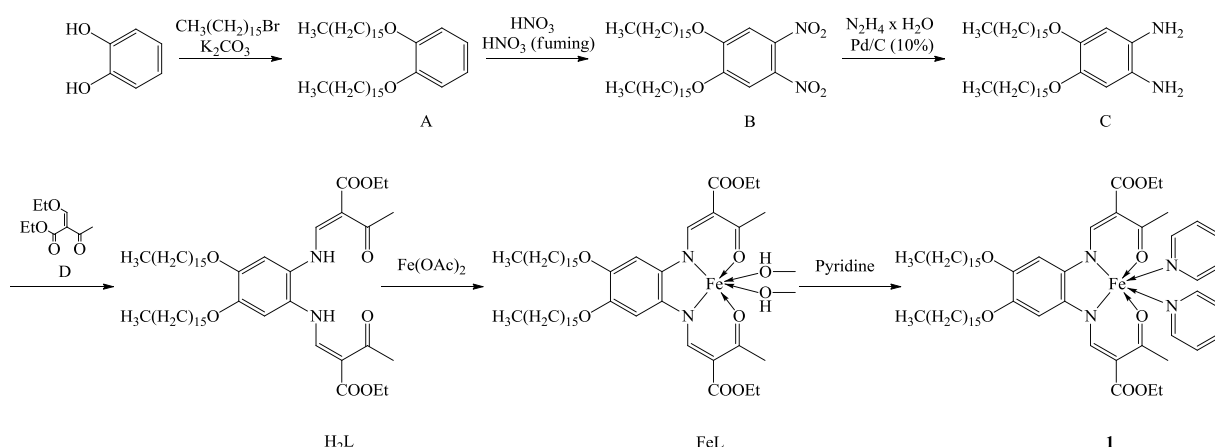
1,2-dihexadecyloxybenzene (A). In a two neck round-bottom flask (1 L) fitted with a condenser and a dropping funnel 8 g (72.65 mmol, 1 eq.) catechol and 20.08 g (145.3 mmol, 2 eq.) K_2CO_3 were stirred at room temperature in 500 mL DMF for 45 min under nitrogen atmosphere. 44.4 g (145.4 mmol, 2 eq.) 1-Bromododecane were added dropwise to the turquoise suspension and the mixture was heated to 90 °C for 8 h. After cooling overnight the white solid was filtered off, washed with water and methanol and dried under reduced pressure. Yield: 22.15 g (87%). $C_{38}H_{70}O_2$ (558.96); MS (DEI+) [*m/z* (%)] 559 (100) [M]$^+$, 334 (7), 110 (33); Anal. calcd. C 81.65, H 12.62; found C 81.50, H 11.47. δ ^{1}H (CDCl$_3$, 399.81 MHz, 296 K): 0.87 (6H, t, 7.0 Hz, CH$_3$), 1.07-1.39 (48H, m, CH$_2$), 1.39-1.51 (4H, m, CH$_2$), 1.74-1.85 (4H, m, CH$_2$), 3.97 (4H, t, 6.7 Hz, CH$_2$–O), 6.87 ppm (4H, s, H$_{Arom.}$). δ ^{13}C (CDCl$_3$, 399.81 MHz, 296 K): 14.1 (CH$_3$), 22.7 (CH$_2$), 26.1 (CH$_2$), 29.3 (CH$_2$), 29.4 (2 CH$_2$), 29.6 (CH$_2$), 29.7 (7 CH$_2$), 31.9 (CH$_2$), 69.2 (CH$_2$, CH$_2$–O), 114.1 (CH, C$_{Arom.}$), 121.0 (CH, C$_{Arom.}$), 149.2 ppm (C$_q$, C$_{Arom.}$–O).

4,5-dihexadecyloxy-1,2-dinitrobenzene (B). 22 g (39.36 mmol) **A** were suspended in 150 mL acetic acid for 1 h. Under stirring, a mixture of 20 mL nitric acid and 150 mL fuming nitric acid were added dropwise over 1.5 h. The yellow suspension was stirred at room temperature for 20 h and poured into 1.5 L ice-water. The yellow precipitate was filtered off and washed with water until neutrality. It was recrystallised from 500 mL Ethanol, washed with methanol and dried overnight. Yield: 23.90 g (94 %). $C_{38}H_{68}N_2O_6$ (648.96); MS (DEI+) [*m/z* (%)] 649 (100) [M]$^+$, 584 (97), 377 (24), 359 (26); Anal. calcd. C 70.33, H 10.56, N 4.32; found C 70.40, H 10.33, N 4.26. δ ^{1}H (CDCl$_3$, 399.81 MHz, 296 K): 0.86 (6H, t, 7.0 Hz, CH$_3$), 1.15-1.38 (48H, m, CH$_2$), 1.40-1.50 (4H, m, CH$_2$), 1.79-1.90 (4H, m, CH$_2$), 4.08

(4H, t, 6.5 Hz, CH$_2$–O), 7.27 ppm (2H, s, H$_{Arom.}$). δ ^{13}C (CDCl$_3$, 399.81 MHz, 296 K): 14.1 (CH$_3$), 22.7 (CH$_2$), 25.8 (CH$_2$), 28.7 (CH$_2$), 29.2 (CH$_2$), 29.4 (CH$_2$), 29.5 (CH$_2$), 29.6 (CH$_2$), 29.7 (6 CH$_2$), 31.9 (CH$_2$), 70.2 (CH$_2$, CH$_2$–O), 107.8 (CH, C$_{Arom.}$), 136.4 (C$_q$, C$_{Arom.}$–NO$_2$), 151.8 ppm (C$_q$, C$_{Arom.}$–O).

1,2-diamino-4,5-dihexadecyloxybenzene (C). Under nitrogen atmosphere, 23.65 g (36.44 mmol) **B** and 2.46 g palladium on activated charcoal (10 % Pd) were suspended in 800 mL ethanol and 67.50 g (1.35 mol, 37 eq.) hydrazine-monohydrate were added dropwise under stirring. The mixture was heated to reflux for 6 h till the yellow suspension turned into white. It was filtered off hot through Celite$^®$545 coarse. After cooling, the white precipitate was filtered off, washed twice with 20 mL ethanol and dried under reduced pressure. Yield: 10.70 g (50 %). C$_{38}$H$_{72}$N$_2$O$_2$ (588.99); MS (DEI+) [*m/z* (%)] 588 (100) [M−H]$^{+}$, 139 (37); Anal. calcd. C 77.49, H 12.32, N 4.76; found C 77.30, H 11.32, N 4.78.

Ethoxymethyleneethylacetoacetate (D) was synthesised according to literature [22].

(E,E)-[{diethyl-2,2'-[4,5-dihexadecyloxy-1,2-phenylenebis(iminomethylidyne)]bis-3-oxo-butanato}] (H$_2$L). Under nitrogen atmosphere, 2 g (3.40 mmol) **C** was dissolved in 200 mL ethanol. A slight excess of **D** (1.40 g, 7.47 mmol, 2.2 eq.) was added and the yellow solution was heated to reflux for 70 min. After cooling to room temperature, the yellow precipitate was filtered off, washed with ethanol and methanol and dried in presence of air. Yield: 2.5 g (85 %). C$_{52}$H$_{88}$N$_2$O$_8$ (869.26); MS (EI) 869 (23) [M]$^{+}$, 823 (100), 777 (33), 614 (45); Anal. calcd. C 71.85, H 10.20, N 3.22; found C 71.44, H 10.06, N 3.28. δ ^{1}H (CDCl$_3$, 399.81 MHz, 296 K): 0.85 (6H, t, 7.1 Hz, CH$_3$), 1.14-1.38 (48H, m, CH$_2$), 1.30 (6H, t, 6.5 Hz, CH$_3$(Et)), 1.39-1.50 (4H, m, CH$_2$), 1.75-1.85 (4H, m, CH$_2$), 2.52 (6H, s, CH$_3$), 3.98 (4H, t, 6.5 Hz, CH$_2$–O), 4.22 (4H, q, 7.1 Hz, CH$_2$(Et)), 6.72 (2H, s, H$_{Arom.}$), 8.24 (2H, d, 12.5 Hz, CH=), 12.84 ppm (2H, d, 12.5 Hz, NH). δ ^{13}C (CDCl$_3$, 399.81 MHz, 296 K): 14.1 (CH$_3$), 14.5 (CH$_3$), 22.7 (CH$_2$), 26.0 (CH$_2$), 29.2 (CH$_2$), 29.3 (CH$_2$), 29.4 (CH$_2$), 29.6 (3 CH$_2$), 29.7 (7 CH$_2$), 31.2 (CH$_3$), 31.9 (CH$_2$), 60.0 (CH$_2$, CH$_2$(Et)), 70.0 (CH$_2$, CH$_2$–O), 103.7 (C$_q$), 106.5 (CH, C$_{Arom.}$), 124.9 (C$_q$, C$_{Arom.}$–N), 148.5 (C$_q$, C$_{Arom.}$–O), 154.1 (CH), 166.9 (C$_q$, O–C=O), 201.0 ppm (C$_q$, C=O).

(E,E)-[{diethyl-2,2'-[4,5-dihexadecyloxy-1,2-phenylenebis(iminomethylidyne)]bis-3-oxo-butanato}](2−)iron(II) × 2 MeOH (**[Fe(L)(MeOH)₂]**). Under nitrogen atmosphere, 2 g (2.30 mmol) **H₂L** and 0.85 g (4.89 mmol, 2.13 eq.) Fe(OAc)₂ (synthesis see lit. [23]) were dissolved in 95 mL methanol and heated to reflux for 2 h 15 min. Already while boiling, a brown solid precipitated from the black solution that was filtered off after cooling to room temperature. It was washed twice with 15 mL methanol and dried under reduced pressure so one obtained a brown, microcrystalline powder. Yield: 2.05 g (90 %). $C_{54}H_{94}FeN_2O_{10}$ (987.18); Anal. calcd. C 65.70, H 9.60, N 2.84; found C 65.96, H 9.44, N 2.90.

[Fe(L)(Py)₂] (1). 0.20 g (0.20 mmol) **[Fe(L)(MeOH)₂]** was dissolved in 20 mL pyridine and the black solution was heated to reflux for 5 h. The solution was allowed to cool slowly to room temperature, and a crystallisation approach was made with water diffunding into the solution. After 50 days, the product was formed as greenish-black thin crystals. The overlaying solution was decanted and the remaining H_2O/pyridine was removed in vacuo. Yield: 0.18 g (83 %). $C_{62}H_{96}FeN_4O_8$ (1081.29); Anal. calcd. C 68.87, H 8.95, N 5.18; found C 68.49, H 8.67, N 4.78.

Magnetic susceptibility data of **1**·0.25 H_2O were collected using a Quantum Design MPMSR2 SQUID magnetometer under an applied field of 0.5 T over the temperature range 50–400 K in the settle mode. All samples were placed in gelatine capsules held within plastic straws. The data were corrected for the diamagnetic magnetization of the ligands, which were estimated using tabulated Pascal's constants and of the sample holder.

Differential scanning calorimetry data were recorded on a Perkin–Elmer DSC Pyris 1 instrument equipped with a cryostat operating down to 98 K following a described procedure.[24]

X-ray diffraction: The intensity data of **1**×0.25H_2O were collected on a Nonius Kappa CCD diffractometer using graphite-monochromated MoK_α radiation. The data were corrected for Lorentz and polarisation effects. The structure was solved by Direct Methods (Sir 97)[25] and refined by full-matrix least-square techniques against F_0^2 (Shelxl-97)[26]. The hydrogen atoms were included at calculated positions with fixed displacement parameters. All non-hydrogen atoms were refined anisotropically. Ortep-III[27] was used for the structure representation,

Schakal-99[28] and Mercury for the representation of the molecule packing. Cell parameters and refinement results are summarised in Table S1. CCDC 821515 (**1**×0.25H$_2$O, HS) and CCDC 821516 (**1**×0.25H$_2$O, LS) contain the supplementary crystallographic data for this paper. These data can be obtained free of charge from The Cambridge Crystallographic Data Centre via www.ccdc.cam.ac.uk/data_request/cif.

4.5   References

[1]   (a) L. Cambi, L. Szegö, *Ber. Dtsch. Chem. Ges. A* **1931**, *64*, 167; (b) L. Cambi, L. Malatesta, *Ber. Dtsch. Chem. Ges. B* **1937**, *70*, 2067.

[2]   (a) H. A. Goodwin, *Coord. Chem. Rev.* **1976**, *18*, 293; (b) E. König, *Struct. Bonding* **1991**, *76*, 51; (c) P. Gütlich, A. Hauser, H. Spiering, *Angew. Chem., Int. Ed. Engl.* **1994**, *33*, 2024 and references therein; (d) ''Spin Crossover in Transition Metal Compounds I—III'', ed. P. Gütlich and H. A. Goodwin, *Topics in Current Chemistry*, Springer-Verlag Berlin Heidelberg, New York, **2004**; (e) J. A. Real, A. B. Gaspar, M. C. Munoz, *Dalton Trans.* **2005**, 2062; (f) K. Nakano, N. Suemura, K. Yoneda, S. Kawata, S. Kaizaki, *Dalton Trans.* **2005**, 740; (g) O. Sato, J. Tao, Y.-Z. Zhang, *Angew. Chem.* **2007**, *119*, 2200 (*Angew. Chem., Int. Ed.* **2007**, *46*, 2152); (h) J. A. Kitchen, S. Brooker, *Coord. Chem. Rev.* **2008**, *252*, 2072; (i) K. S. Murray, Eur. J. Inorg. Chem. **2008**, 3101; (j) M. A. Halcrow, *Coord. Chem. Rev.* **2009**, *253*, 2493–2514; (k) S. Brooker, J. A. Kitchen, *Dalton Trans.* **2009**, 7331; (l) C. J. Kepert, *Aust. J. Chem.* **2009**, *62*, 1079; (m) K. S. Murray, *Aust. J. Chem.* **2009**, *62*, 1081; (n) A. B. Koudriavtsev, W. Linert, *J. Struct. Chem.* **2010**, *51*, 335.

[3]   (a) O.Kahn, C. J.Martinez, *Science* **1998**, *279*, 44; (b) O. Kahn, C. Jay, J. Kröber, R. Claude, F. Grolière, Patent, EP06665611995; (c) J.-F. Létard, O. Nguyen, N. Daro, Patent, FR05124762005; (d) J.-F. Létard, P. Guionneau, L. Goux-Capes, in Topics in Current Chemistry, ed. P. Gütlich and H. A. Goodwin, Springer Wien New York, **2004**, vol. 235, p. 221; (e) A. Galet, A. B. Gaspar, M. C. Munoz, G. V. Bukin, G. Levchenko, J. A. Real, *Adv. Mater.* **2005**, *17*, 2949.

[4]   Y. Garcia, V. Ksenofontov, P. Gütlich, *Hyperfine Interact.* **2002**, *139–140*, 543.

[5]   Y. Garcia, V. Ksenofontov, S. Mentior, M. M. Dîrtu, C. Gieck, A. Bhatthacharjee, P. Gütlich, *Chem.–Eur. J.* **2008**, *14*, 3745.

[6]   (a) I. Boldog, A. B. Gaspar, V. Martinez, P. Pardo-Ibanez, V. Ksenofontov, A. Bhattacharjee, P. Gütlich, J. A. Real, *Angew. Chem., Int. Ed.* **2008**, *47*, 6433–6437; (b) S. Cobo, G. Molnar, J. A. Real, A. Bousseksou, *Angew. Chem., Int. Ed.* **2006**, *45*, 5786–5789; (c) G. Molnár, S. Cobo, J. A. Real, F. Carcenac, E. Daran, C. Vieu, A. Bousseksou, *Adv. Mater.* **2007**, *19*, 2163; (d) M. Cavallini, I. Bergenti, S. Milita, G. Ruani, I. Salitros, Z.-R. Qu, R. Chandrasekar, M. Ruben, *Angew. Chem., Int. Ed.* **2008**, *47*, 8596; (e) A. D. Naik, L. Stappers, J. Snauwaert, J. Fransaer, Y. Garcia, *Small* **2010**, *6*, 2842.

[7]   (a) M. Seredyuk, A. B. Gaspar, V. Ksenofontov, Y. Galyametdinov, M. Verdaguer, F. Villain, P. Gütlich, *Inorg. Chem.* **2008**, *47*, 10232–10245; (b) M. Seredyuk, A. B. Gaspar, V. Ksenofontov, Y. Galyametdinov, J. Kusz, P. Gütlich, *Adv. Funct. Mater.* **2008**, *18*, 2089; (c) M. Seredyuk, A. B. Gaspar, V. Ksenofontov, Y. Galyametdinov, J. Kusz, P. Gütlich, *J. Am. Chem. Soc.* **2008**, *130*, 1431.

[8]   (a) J. A. Real, A.B.Gaspar, V. Niel, M.C.Muñoz, *Coord. Chem. Rev.* **2003**, *236*, 121; (b) A. Bousseksou, G. Molnár, J. A. Real, K. Tanaka, *Coord. Chem. Rev.* **2007**, *251*, 1822–1833.

[9]   (a) A. B. Gaspar, V. Ksenofontov, M. Seredyuk, P. Gütlich, *Coord. Chem. Rev.* **2005**, *249*, 2661–2676; (b) A. B. Gaspar, M. Seredyuk, P. Gütlich, *J. Mol. Struct.* **2009**, *924–926*, 9–19.

[10]   (a) B. Weber, *Coord. Chem. Rev.* **2009**, *253*, 2432; (b) B. Weber, E.-G. Jäger, *Eur. J. Inorg. Chem.* **2009**, 465.

[11]   (a) B. Weber, E. Kaps, J. Weigand, C. Carbonera, J.-F. Létard, K. Achterhold, F. Parak, *Inorg. Chem.* **2008**, *47*, 487; (b) B. Weber, J. Obel, D. Henner-Vásquez, W. Bauer, *Eur. J. Inorg. Chem.* **2009**, 5527.

[12]   (a) Y. Garcia, O. Kahn, L. Rabardel, B. Chansou, L. Salmon, J.-P. Tuchagues, *Inorg. Chem.* **1999**, *38*, 4663; (b) G. S. Matouzenko, J.-F. Letard, S. Lecocq, A. Bousseksou, L. Capes, L. Salmon, M. Perrin, O. Kahn, A. Collet, *Eur. J. Inorg. Chem.* **2001**, 2935; (c) W. Hibbs, P. J. van Koningsbruggen, A. M. Arif, W. W. Shum, J. S. Miller, *Inorg. Chem.* **2003**, *42*, 5645; (d) P. Poganiuch, S. Decurtins, P. Gütlich, *J. Am. Chem. Soc.* **1990**, *112*, 3270; (e) L. Wiehl, *Acta Crystallogr., Sect. B: Struct. Sci.* **1993**, *49*, 289; (f) R. Hinek, H. Spiering, D. Schollmeyer, P. Gütlich, A. Hauser, *Chem.–Eur. J.* **1996**, *2*, 1427; (g) B. Weber, C. Carbonera, C. Desplanches, J.-F. Létard, *Eur. J. Inorg. Chem.* **2008**, 1589; (h) B. Li, R.-J. Wei, R.-B. Huang, L.-S. Zheng, Z. Zheng, *J. Am.*

Chem. Soc. **2010**, *132*, 1558–1566; (i) R.-J. Wei, J. Tao, R.-B. Huang, L.-S. Zheng, Z. Zheng, *Inorg. Chem.* **2011**, *50*, 1170–1172.

[13]   G. S. Matouzenko, D. Luneau, G. Molnár, N. Ould-Moussa, S. Zein, S. A. Borshch, A. Bousseksou, F. Averseng, *Eur. J. Inorg. Chem.* **2006**, 2671–2682.

[14]   M. B.-L. Cointe, N. O. Moussa, E. Trzop, A. Moréac, G. Molnar, L. Toupet, A. Bousseksou, J. F. Létard, G. S. Matouzenko, *Phys. Rev. B* **2010**, *82*, 214106.

[15]   (a) B. Weber, W. Bauer, J. Obel, *Angew. Chem.* **2008**, *120*, 10252 (*Angew. Chem., Int. Ed.* **2008**, *47*, 10098–10101); (b) B. Weber, W. Bauer, T. Pfaffeneder, M. M. Dîrtu, A. D. Naik, A. Rotaru, Y. Garcia, *Eur. J. Inorg. Chem.* **2011**, in press.

[16]   (a) I. Szafraniak, P. Czarnecki, *J. Phys.: Condens. Matter* **2002**, *14*, 3321; (b) D. Vujosevic, K. Muller, E. Roduner, *J. Phys. Chem. B* **2006**, *110*, 8598.

[17]   (a) V. A. Money, J. Elhaik, I. R. Evans, M. A. Halcrow, J. A. K. Howard, *Dalton Trans.* **2004**, 65–69; (b) B. Weber, E. S. Kaps, J. Obel, K. Achterhold, F. G. Parak, *Inorg. Chem.* **2008**, *47*, 10779.

[18]   M. Schlögl, B. Rieger, *Z. Naturforsch. B*, **2004**, 233–240.

[19]   K. Tahara, S. Furukawa, H. Uji-I, T. Uchino, T. Ichikawa, J. Zhang, W. Mamdouh, M. Sonoda, F. C. de Shryver, S. de Feyter, Y. Tobe, *J. Am. Chem. Soc.*, **2006**, *128*, 16613–16625.

[20]   N. L. Drake, H. D. Anspon, J. D. Draper, S. T. Haywood, J. van Hook, S. Melamed, R. M. Peck, J. Sterling Jr., E. W. Walton, A. Whiton, *J. Am. Chem. Soc.* **1946**, *68*, 1541.

[21]   M. J. Howard, F. R. Heirtzler, S. I. G. Diaz, *J. Org. Chem.* **2008**, *73*(7), 2548–2553.

[22]   L. Wolf, E.-G. Jäger, *Z. anorg. allg. Chem.* **1966**, *346*, 76–91.

[23]   B. Weber, R. Betz, W. Bauer, S. Schlamp, *Z. anorg. allg. Chem.* **2011**, *637*, 103–107.

[24]   A. Rotaru, M. M. Dîrtu, C. Enachescu, R. Tanasa, J. Linares, A. Stancu, Y. Garcia, Polyhedron **2009**, *28*, 2531.

[25]   A. Altomare, M.C. Burla, G.M. Camalli, G. Cascarano, C. Giacovazzo, A. Guagliardi, A.G.G. Moliterni, G. Polidori, R. Spagna, *J. Appl. Crystallogr.* **1999**, *32*, 115.

[26]   G.M. Sheldrick, shelxl-97; University of Göttingen: Göttingen, Germany, **1993**.

[27]   a) C.K. Johnson, M.N. Burnett, Ortep-III; Oak-Ridge National Laboratory: Oak-Ridge, TN, **1996**; b) L.J. Farrugia, *J. Appl. Cryst.* **1997**, *30*, 565.

[28]   E. Keller, Schakal-99; University of Freiburg: Freiburg, Germany, **1999**.

4.6   Supporting Information

Table S1. Parameters for crystal structure determination.

	1×0.25H$_2$O, HS	**1**×0.25H$_2$O, LS
sum formula	C$_{62}$H$_{94}$FeN$_4$O$_8$	C$_{62}$H$_{96}$FeN$_4$O$_8$
formula weight	1081.28	1081.28
crystal system	triclinic	triclinic
space group	$P\bar{1}$	$P\bar{1}$
a /Å	9.9758(2)	9.0910(3)
b /Å	10.0579(2)	9.9180(3)
c /Å	31.5743(7)	34.3520(11)
α /°	90.3395(11)	90.0897(19)
β /°	97.4097(11)	93.550(2)
γ /°	97.2664(12)	101.8404(15)
V /Å^3	3115.54(11)	3025.29(17)
Z	2	2
$\rho_{calcd.}$ /g cm^{-3}	1.153	1.187
μ /mm^{-1}	0.295	0.304
F(000)	1172	1172
crystal size /mm	0.23×0.09×0.03	0.23×0.09×0.03
temperature /K	250	125
radiation /Å	Mo-K_α, 0.71073	Mo-K_α, 0.71073
θ-min, θ-max /°	3.2, 27.5	3.2, 27.4
hkl	−12: 12; −13: 12; −40: 40	−11: 11; −12: 12; −44: 44
measured reflections	24716	4071
independent reflections	14173	13662

R_{int}	0.089	0.064
reflections with $I \geq 2\sigma(I)$	5818	8937
reflections	14173	13662
parameters	727	682
R	0.0703	0.0594
wR_2	0.2016	0.1485
S	0.99	1.03
shift/*error*$_{max}$	0.00	0.00
$\Delta\rho_{max}$	0.84	0.96
$\Delta\rho_{min}$	−0.36	−0.38

Table S2. Geometric parameters and symmetry codes of short contacts and non-classic hydrogen bonds in **1**×0.25H$_2$O in the LS and HS state (Å, °).

	D—H⋯A	D—H	H⋯A	D⋯A	D—H⋯A	
LS	C62—H62⋯O99	0.95	2.31	3.19	153.6	−1+x, 1+y, z
	C16—H16C⋯O99	0.98	2.33	3.12	137.4	1−x, −y, 1−z
	C13—H13A⋯O99	0.98	2.36	2.24	148.8	
	O2⋯O99			2.80		
	O3⋯O99			2.87		
	C61—H61⋯O3	0.95	2.44	3.15	130.9	1+x, y, z
	C62A—H62A⋯O99	0.94	2.52	2.28	99.3	−1+x, 1+y, z
	C15—H15A⋯O99	0.98	2.19	3.13	158.8	x, 1+y, z
HS	O2⋯O99			2.97		
	O3⋯O99			3.31		

C61A—H61A···O3	0.94	2.57	3.12	118.2	1+x, y, z
C62A—H62A···O3	0.94	2.42	3.05	124.5	1+x, y, z
H61B···H36F		1.67			

Table S3. Thermodynamic parameters of **1**×0.25H_2O derived from DSC.

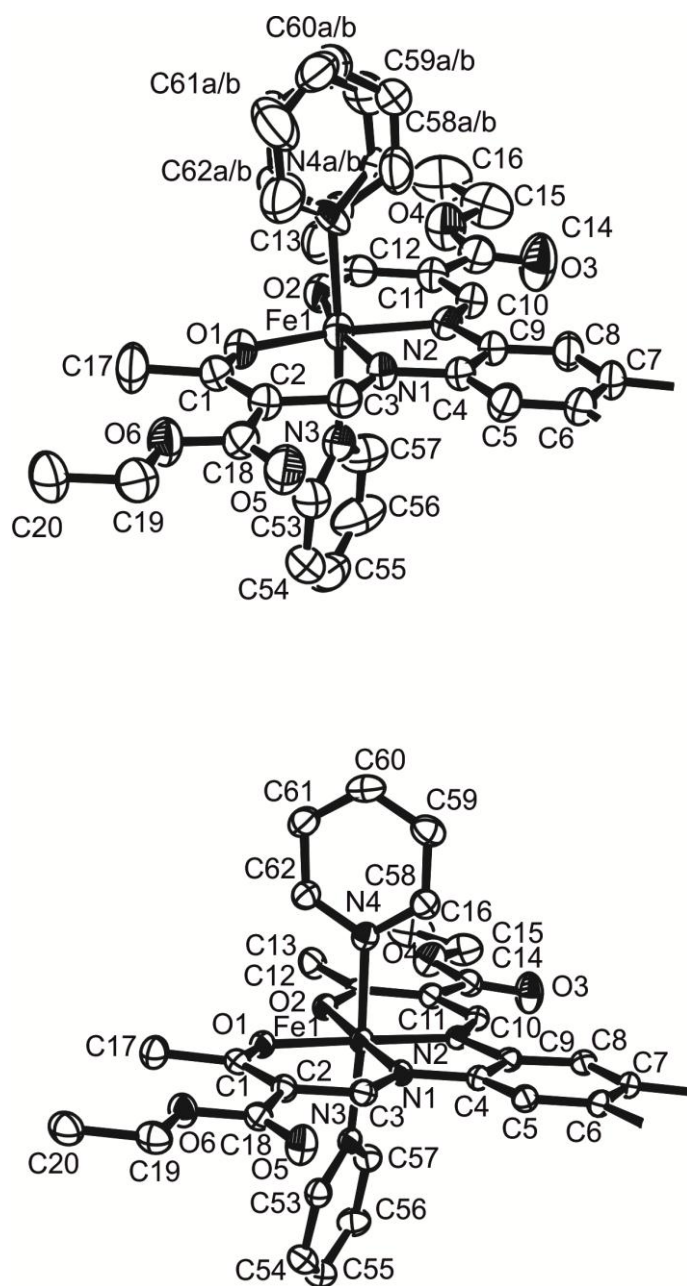| Mode	Peak	T_{max} (K)	ΔH (kJ/mol)	ΔS (J/mol/K)
Cooling	2	226(1)	6(1)	27.6(1)
300K to 98 K	1	207(1)	4(1)	23.3(1)
Warming	1	235(1)	4(1)	17.1(1)
98 K to 300 K	2	250(1)	9(1)	36.6(1)

Figure S1. Excerpt of the coordination environment of the ORTEP drawing of the asymmetric unit of **1** in the HS (top) and LS (bottom) states. Hydrogen atoms and the water molecule have been omitted for clarity. Displacement ellipsoids are shown at the 50 % probability level.
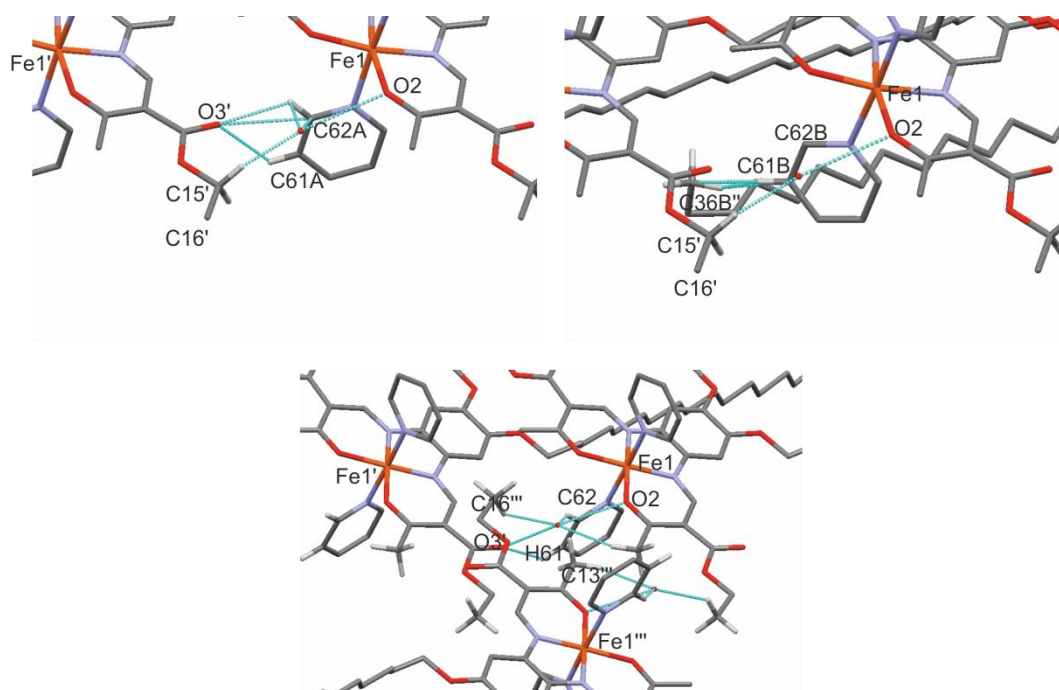
Figure S2. Excerpt of the packing of the molecules of **1**×0.25H$_2$O in the crystal projected along c-axis for a better illustration of the changes in the H-bond network upon spin transition. Top: HS state with the disorder resolved in two separate pictures, bottom: LS state. Short intermolecular contacts are illustrated as dashed lines. Hydrogen atoms and molecules not involved in the H-bond network were omitted for clarity.

Figure S3. Packing of the molecules of **1**×0.25H$_2$O in the crystal projected along [0 1 0]. Top: HS state, bottom: LS state, short intermolecular contacts are illustrated as dashed lines.

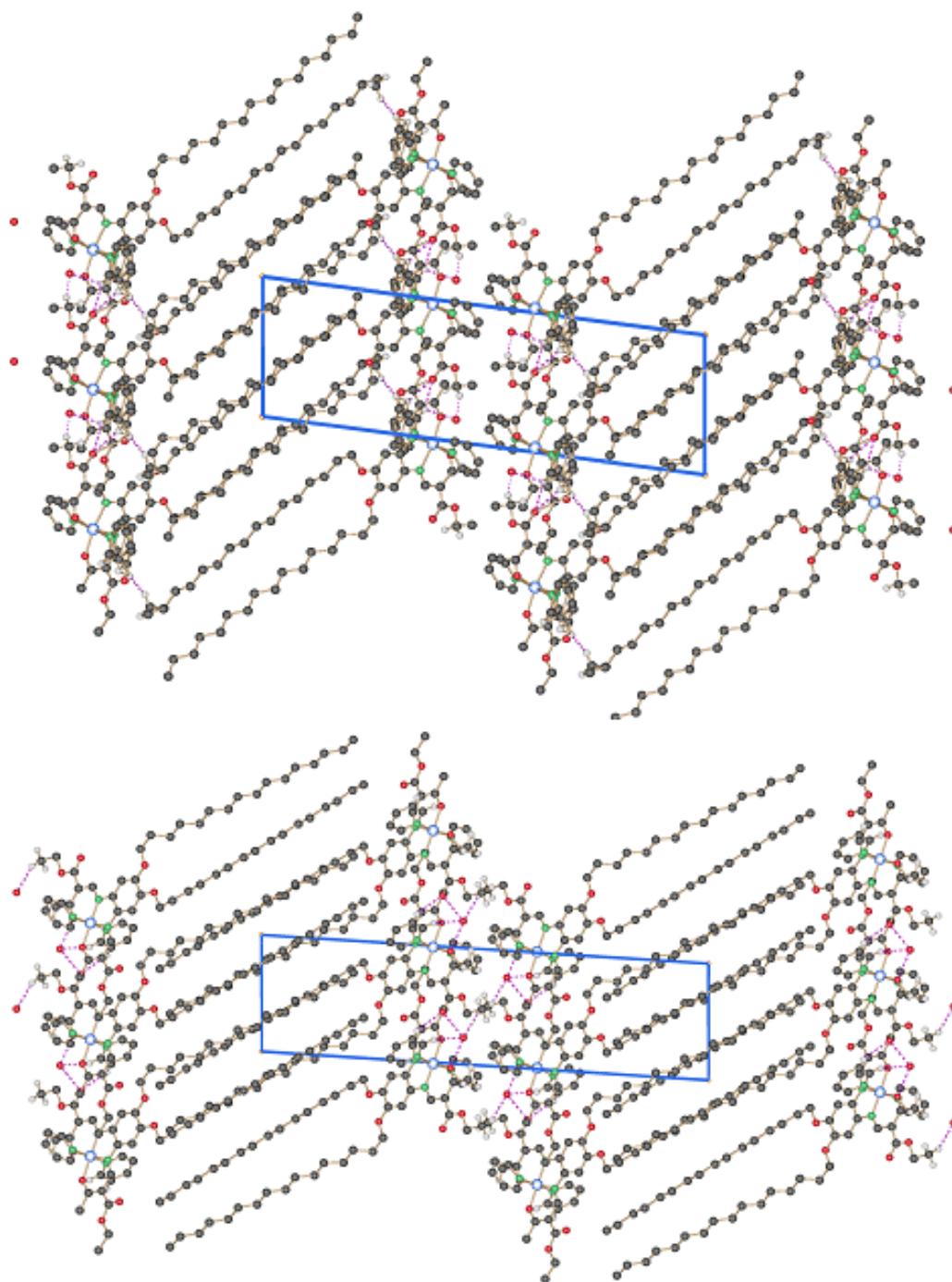# 5 New Octahedral, Head–Tail Iron(II) Complexes with Spin Crossover Properties

Stephan Schlamp,[a] Peter Thoma,[a] Birgit Weber*[a]

[a] Lehrstuhl für Anorganische Chemie II, Universität Bayreuth, Universitätsstraße 30, NW 1, 95440 Bayreuth, Germany; Fax: +49-92155-2157; E-mail: weber@uni-bayreuth.de

Abstract: The synthesis and characterisation of four new Schiff base-like ligands with long alkyl chains in the outer periphery and their iron(II) complexes with methanol and pyridine as axial ligands is reported. Two of the methanol complexes crystallise in a lipid layer-like arrangement with the alkyl chain (tail) packed in the middle and the iron centres (head) in the outer sites. The pyridine complexes show varying types of spin transition (stepwise, incomplete, with hysteresis), which depends on the alkyl chain length and substituents in the outer periphery of the ligand. Investigations in solution using ^{1}H NMR spectroscopy demonstrate that the differences in the spin transition behaviour are due to packing effects as the same transition curve is obtained independently of the alkyl chain length.

5.1 Introduction

Iron(II) spin crossover (SCO) complexes are a fascinating class of molecules that can be switched on the molecular level between the paramagnetic high-spin (HS, $S = 2$) and the diamagnetic low-spin (LS, $S = 0$) state by external perturbations such as temperature, pressure or light.[1–3] This switching progress is associated with a colour change that results in an interest in this substance class as pressure and/or temperature sensors with a simple optical readout or as cold channel control units in the food and medical sectors.[4] In order to realise application it is important to explore different possibilities for the nanostructuration of SCO

materials[5] and to investigate if additional properties can be combined (e.g. liquid crystal behaviour,[6] magnetic exchange interactions)[7] to result in multifunctional SCO materials.[3] To this end, we have modified Schiff base-like ligands used for the synthesis of SCO complexes[2,8] by adding long alkyl chains to the outer periphery. Such an approach can induce new possibilities for the self-assembly of the complexes in solution or the solid state.[9] Using this approach, we have succeeded with the synthesis of an iron(II) complex that crystallises in a lipid layer-like structure and shows a cooperative spin transition (ST) with an up to 50 K wide hysteresis loop.[10] In order to investigate this interesting new class of iron complexes in more detail we have prepared a series of ligands with varying chain lengths (n = 7, 11, 15) and varying substituents R^1 for n = 11 (Scheme 1). The structural and magnetic properties of the corresponding iron(II) complexes with methanol and pyridine as axial ligands are reported here together with the results of temperature T-dependent NMR spectroscopy in solution for selected examples. The influence of the different alkyl chain lengths and substituents on the crystal packing and ST behaviour is discussed.
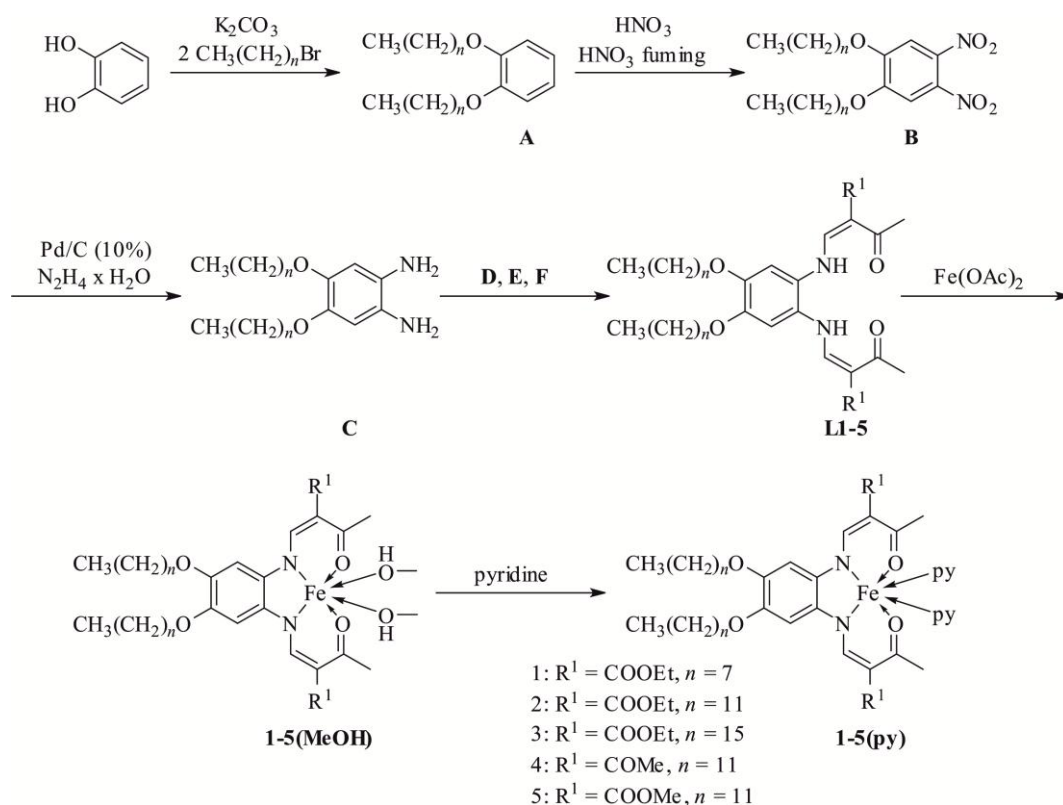
Scheme 1. General procedure for the synthesis of the new ligands and their iron complexes with the abbreviations.

5.2   Results and Discussion

5.2.1   Synthesis and General Characterisation

The general procedure for the synthesis of the new ligands and their iron complexes and the abbreviations used are given in Scheme 1. The preparation of the desired octahedral complexes with pyridine as the axial ligands followed an eight-step synthesis, which started with the conversion of pyrocatechol with an alkyl bromide according to a modification of a literature procedure.[11] Nitration,[12,13] subsequent reduction to the diaminoproduct[13] and reaction with different ketoenol ethers[14,15] led to the free ligands **L1–5**, which were reacted with iron(II) acetate[16] to give the iron(II) complexes with methanol as the axial ligands. In the last step, methanol was replaced by pyridine. The intermediate products were characterised by elemental analysis, NMR spectroscopy and mass spectrometry. In addition, the iron complexes were characterised by *T*-dependent magnetic susceptibility measurements. For the methanol complexes **2(MeOH)** and **5(MeOH)** the structural details were explored by X-ray structure analysis. For complexes **1–3(py)**, *T*-dependent paramagnetic ^{1}H NMR measurements were performed in a pyridine/toluene solution.

5.2.2   Description of the X-ray Structures

Crystallisation of **2(MeOH)** and **5(MeOH)** succeeded, and their molecular structures were elucidated. The asymmetric units of the two complexes are displayed in Figure 1. The crystallographic data are summarised in Table 4, and in Table 1 selected bond lengths and angles within the first coordination sphere are given. Both complexes crystallise in the triclinic space group $P\bar{1}$, and the unit cells each contain two formula units. The cell dimensions of the two complexes are very similar, in **5(MeOH)** the *a*, *c* and *α*, *β*, *δ* values are slightly smaller as is the cell volume.

Table 1. Selected bond lengths [Å] and angles [°] of **2(MeOH)** and **5(MeOH)** within the first coordination spheres.

Complex	Fe–N$_{eq}$	Fe–O$_{eq}$	Fe–O$_{ax}$	O1–Fe–O2	L$_{ax}$–Fe–L$_{ax}$
2(MeOH)	2.093(2),	2.009(1),	2.203(1),	108.93(5)	169.72(5)
	2.095(2)	2.030(1)	2.230(2)		
5(MeOH)	2.088(2),	2.007(2),	2.201(2),	109.37(8)	166.73(7)
	2.094(2)	2.021(2)	2.233(2)		

The iron(II) centres are in the plane of the Schiff base-like equatorial ligand with bond lengths of about 2.0 Å to the two equatorial O atoms and 2.1 Å to the two N atoms. This and the O$_{eq}$–Fe–O$_{eq}$ angle of 109° clearly indicates the high spin state of the complexes,[8,15,17] which is confirmed by magnetic measurements. The Fe–O distances to the axially coordinating methanol molecules are about 2.2 Å, and the O$_{ax}$–Fe–O$_{ax}$ angles deviate slightly from the ideal 180° (O$_{ax}$– Fe–O$_{ax}$ 170° for **2(MeOH)** and 167° for **5(MeOH)**). The equatorial ligand, with exception of the alkyl chains, is nearly planar for both complexes. In **2(MeOH)**, one CH$_3$ group (C16) of the ester group is bent out of this plane by nearly 90°. The plane spanned by the alkyl chains is folded with respect to the plane of the remaining ligand by 23° in **2(MeOH)** and 19° in **5(MeOH)**. A further difference between the two complexes is the relative orientation of the alkyl chains. In the case of **2(MeOH)** with the slightly larger R^1 substituents, they point outwards with nearly planar C5–C6–O7–C21 and C8–C7–O8–C33 torsion angles, respectively, and a C21⋯C33 distance of 5.3 Å. In **5(MeOH)**, the alkyl chain starting with C21 is oriented similarly with a nearly planar C5–C6–O9–C21 torsion angle. However, the second alkyl chain is bent towards the first chain, which results in a significantly shorter C21⋯C33 distance of 4.2 Å and a C8–C7–O10–C33 torsion angle of 121°. At the end of the alkyl chains the C32⋯C44 distance of 4.0 Å is nearly identical for both complexes.
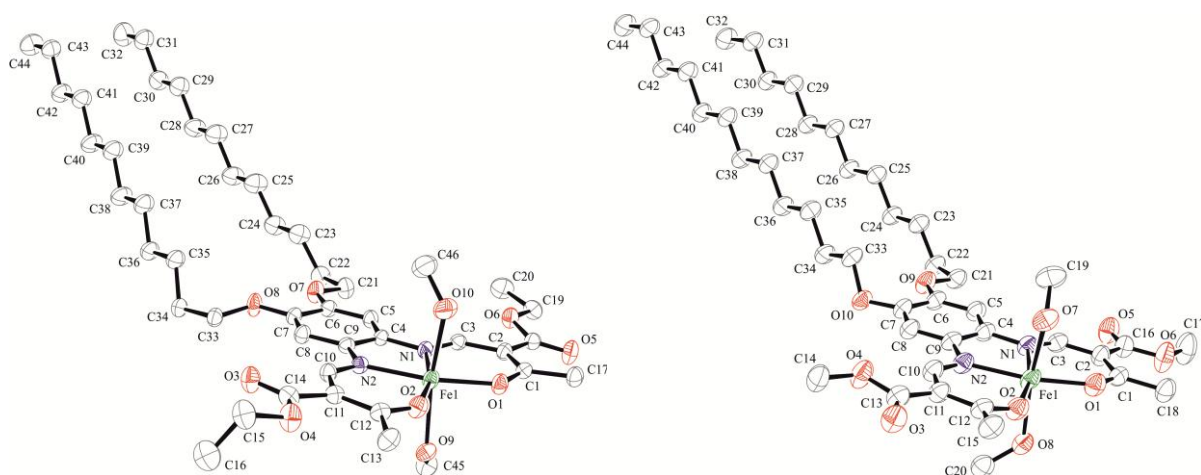
Figure 1. ORTEP drawing of the asymmetric unit of **2(MeOH)** (left) and **5(MeOH)** (right) with atom labels (anisotropic displacement ellipsoids drawn at 50% probability level). H atoms omitted for clarity.

The molecular packing of the complexes reveals a lipid layer-like arrangement as illustrated in Figure 2 for **2(MeOH)** and **5(MeOH)**, respectively. Such an arrangement was recently observed for a very similar pyridine complex of the same ligand type.[10] The layers run along the *ab* plane and, within one layer, the alkyl chains of the Schiff base-like ligand (tail) are packed in the middle and the iron centres (heads) are on the outer sides. Two opposed heads of two neighbouring layers are connected by a hydrogen bond between the hydrogen atom of the methanol OH group of the axial ligand [H9 and H45 for **2(MeOH)** and **5(MeOH)**, respectively] and the oxygen atom of the carbonyl group coordinated to the iron centre [O1 and O2 for **2(MeOH)** and **5(MeOH)**, respectively]. A further hydrogen bond is observed bet-
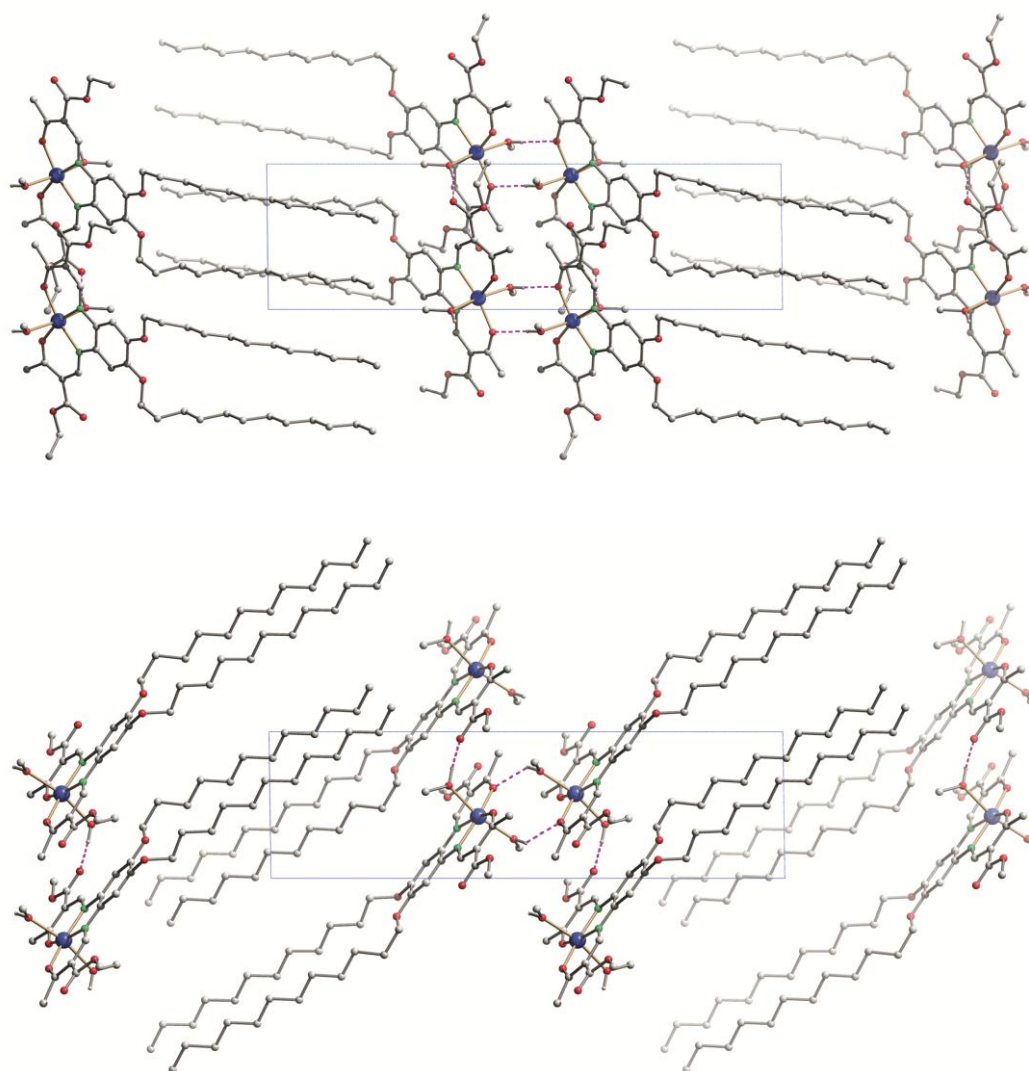
Figure 2. Packing of the molecules of **2(MeOH)** (top) and **5(MeOH)** (bottom) in the crystal projected along [0 1 0]. Hydrogen atoms not involved in the H-bond network are omitted for clarity.

ween the heads within a layer that involves the hydrogen atom of the second coordinated methanol molecule and one of the carbonyl oxygen atoms of the ester group of the ligand [H47···O3 for **2(MeOH)** and H7···O5 for **5(MeOH)**], which connects the iron centres into infinite chains that run along [1 0 0] in both complexes. Details of the hydrogen bonds are given in Tables 2 and 3.

Table 2. Distances [Å] and angles [°] of the hydrogen bonds in **2(MeOH)**.

2(MeOH)	D—H	H···A	A···D	D—H···A
O9—H9···O1[a]	0.79	2.04	2.82	174
O10—H47···O3[b]	0.79	1.95	2.72	166

[a] −x, −y, 1−z. [b] −1+x, y, z.

Table 3. Distances [Å] and angles [°] of the hydrogen bonds in **5(MeOH)**.

5(MeOH)	D—H	H···A	A···D	D—H···A
O7—H7···O5[a]	0.95	2.08	2.7098	123
O8—H45···O2[b]	0.95	2.11	2.7402	123

[a] 1+x, y, z. [b] 3−x, −y, 1−z.

5.2.3 Magnetic Properties

Magnetic susceptibility measurements were performed from 300–10 K for all iron(II) complexes with a Quantum Design MPMSR-2 SQUID magnetometer. The methanol complexes were HS in the entire temperature range with an average room temperature magnetic moment of 3.2 cm^3Kmol^{-1}. Replacement of methanol by pyridine shifts the overall ligand field strength into a region where the observation of *T*-induced ST is possible. Accordingly, all pyridine complexes of L1–5 show SCO behaviour, with different kinds of ST. The ST properties of **3(py)** (hysteresis) have been published previously.[10] The thermal dependence of the $\chi_M T$ product (χ_M = molar susceptibility) for **1(py), 4(py)** and **5(py)** is given in Figure 5.
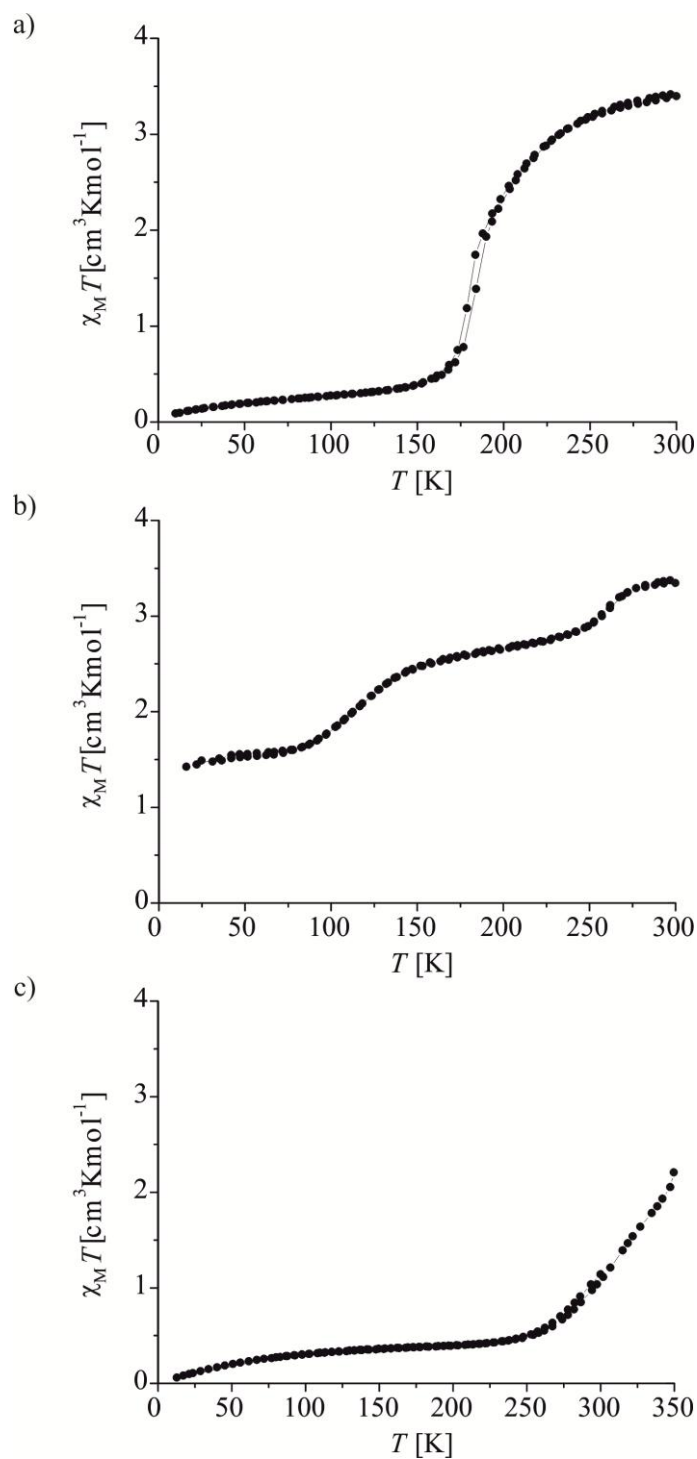
Figure 5. Plots of $\chi_M T$ product vs. T for compounds **1(py)** at 0.05 T (a), **4(py)** at 0.05 T (b) and **5(py)** at 0.2 T (c).

Complexes **1–3(py)** with the same R1 but different chain lengths are all in the HS state at room temperature. Complex **1(py)** with $n = 7$ shows a complete and abrupt ST with $\chi_M T$

(300 K) = 3.41 cm^{3}Kmol^{-1} and $\chi_M T$ (50 K) = 0.20 cm^{3}Kmol^{-1}. The transition temperature ($T_{1/2}$) is 182 K in the cooling mode and 186 K in the heating mode and reveals a 4 K wide hysteresis loop. In contrast to this, **2(py)** with n = 11 shows a gradual, stepwise and incomplete SCO. At room temperature the $\chi_M T$ product is with 2.67 cm^{3}Kmol^{-1} almost completely in the HS state. The $T_{1/2}$ values are 168 K and 98 K for the first and second step, respectively. The $\chi_M T$ product at 50 K with 0.98 cm^{3}Kmol^{-1} indicates that about a third of the iron centres are still in the HS state. The ST properties of **3(py)** with n = 15 have already been reported. A wide hysteresis loop is observed with $T_{1/2\downarrow}$ = 222 K and $T_{1/2\uparrow}$ = 245 K.[10] The differences in the curve progression can be explained by the different number of carbon atoms in the chains as the different space required by the alkyl chains influences the molecular packing. The influence of the alkyl chains (and the resulting packing effects) on $T_{1/2}$ appears to be less pronounced. As for the already published example of **3(py)**, different amounts of water molecules are observed in the crystal packing. However, as no X-ray structures are available, no conclusions can be drawn with regard to the possible existence of a hydrogen-bond network. The complexes with different substituents but the same chain length of n = 11 also display considerable differences in ST behaviour, here also with temperature. For **4(py)** the ST is still stepwise and incomplete but with a higher $T_{1/2}$ for both steps. At room temperature, $\chi_M T$ = 3.34 cm^{3}Kmol^{-1} and the complex is completely in the HS state. At 50 K, $\chi_M T$ = 1.52 cm^{3}Kmol^{-1} and the spin transition stops at a plateau with a HS mol fraction (γ_{HS}) of ca. 0.5, which is frequently observed for 1D chain compounds with this ligand type.[18,19] The $T_{1/2}$ values of 262 K and 113 K are significantly higher than those of **2(py)**. At 250 K, **5(py)** is in the LS state with a $\chi_M T$ value of about 0.50 cm^{3}Kmol^{-1}. Upon heating, the $\chi_M T$ value continuously increases to 2.21 cm^{3}Kmol^{-1} at 350 K, which indicates a gradual spin transition that takes place at around room temperature ($T_{1/2} \approx 325$). Unfortunately, further heating led to decomposition, so the pure HS state could not be reached. The different R^1 substituents influence both $T_{1/2}$ and the curve progression. Investigations in solution on similar pyridine complexes without the alkyl chains indicate that variations in R^1 have a marginal influence on $T_{1/2}$ in solution.[20] Thus the differences in the ST behaviour are mainly related to packing effects.

5.2.4   Paramagnetic ^{1}H NMR Spectroscopy

In order to more clearly evaluate the influence of packing effects on the SCO properties, **1(py)**, **2(py)** and **3(py)** (n = 7, 11 and 15, respectively) were investigated by paramagnetic ^{1}H NMR measurements in solution. Evans method[21] is a powerful technique to determine the spin state of a complex in solution, however, it has some disadvantages, e.g. relatively high error,[22] which depends on the concentration of the sample. We have shown[18,20,23–25] that the SCO of iron(II) complexes can be investigated in solution using the isotropic shift, which is an extraordinary improvement as the same results can be obtained with minor laboratory complexity. Complexes **1–3(py)** were dissolved in a pyridine/toluene mixture (1:1) to ensure the formation of octahedral complexes due to the excess of pyridine. Toluene was used as a noncoordinating solvent to realise a wide temperature range for the solution NMR experiments.[20] Both parts of the complexes (head and tail) are soluble in this solvent mixture, and no indication of self-assembly in solution was observed. Sealed samples were measured in from 360–185 K every 5 K beginning at high temperature. The assignment of the resonances was accomplished by comparison to known results for complexes without alkyl chains[20] or with hydroxyl groups.[25] The assignment of the three iron(II) complexes at room temperature is displayed in Figure 6. The shifts of the CH_2 group b and the CH_3 groups a and c are clearly visible and distinguishable from all the other alkyl and solvent signals. Integration of the signals gave the expected values of 2:3:3 for the ethyl group at the ester unit and the methyl group on the carbonyl unit directly attached to the iron(II) centre. It can be assumed that no pentacoordinate species are present due to the high excess of pyridine in the solution. All other signals of the complex were not assigned because of overlap in the alkyl region and/or bad resolution in a region away from the main spectra (olefinic HC–N protons).[20]
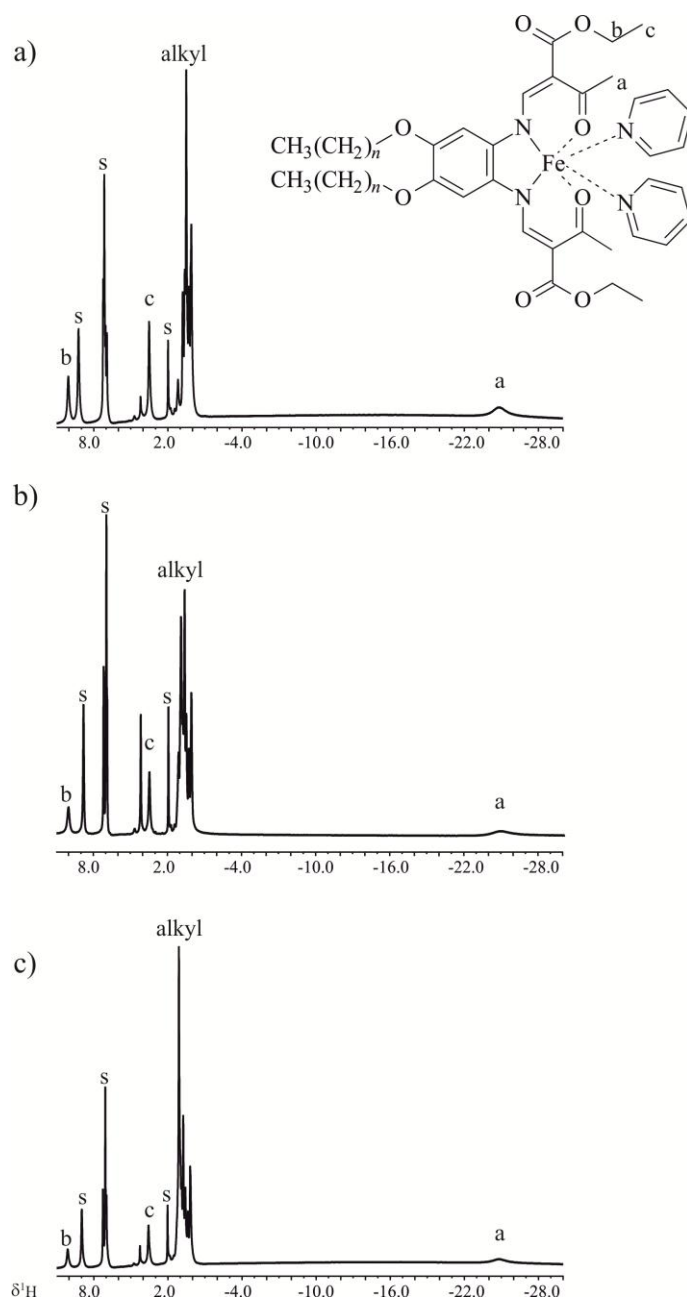
Figure 6. Assignment of the NMR resonances for a) **1(py)**, b) **2(py)** and c) **3(py)** at room temp. S denotes the solvent pyridine/toluene.
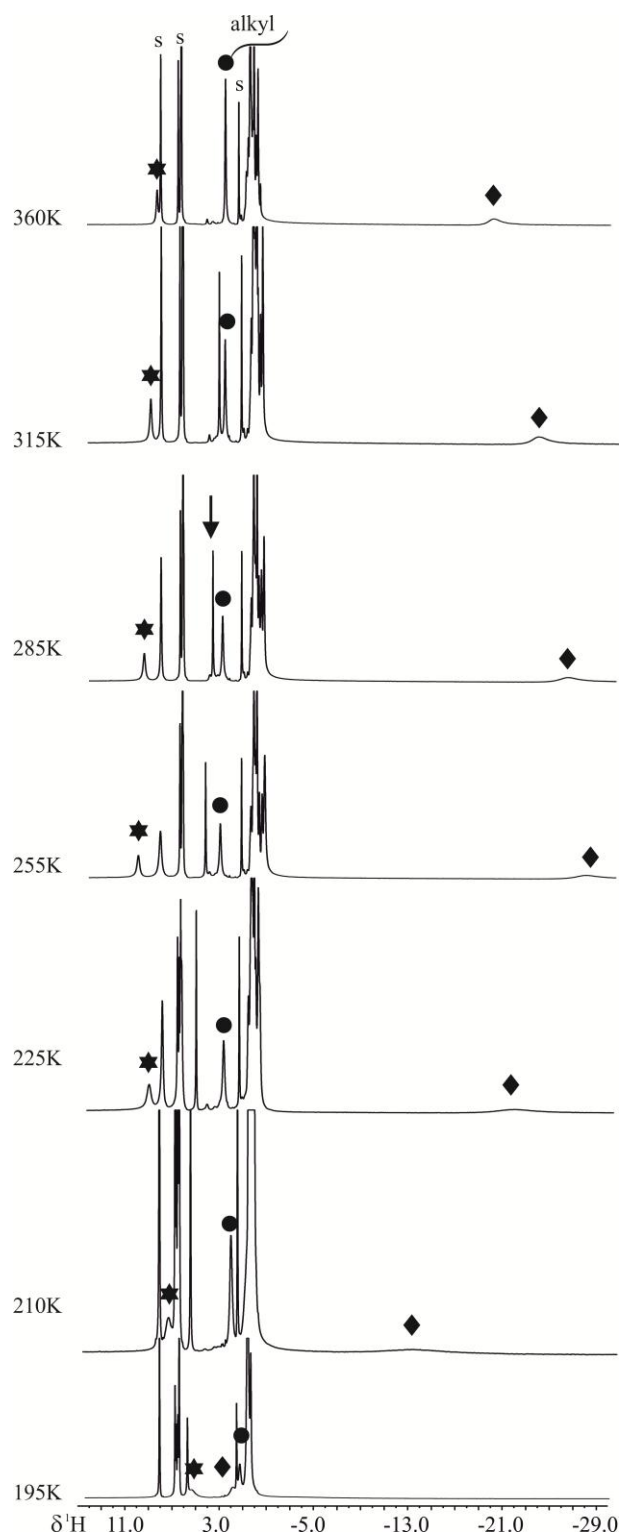
Figure 7. Temperature dependence of the chemical shifts of the signals of **2(py)**. Signals are marked with a diamond (a), star (b) and filled circle (c) to illustrate the temperature-dependent shift of the signals. One paramagnetic impurity is marked with an arrow. S denotes the solvent pyridine/toluene.

The *T*-dependent ^{1}H spectra of **2(py)** are displayed in Figure 7. The roaming of the monitored signals is clearly visible. Correction of these shifts by the diamagnetic shifts of the free ligand signals gives the paramagnetic (or isotropic) shift that can be plotted *vs.* inverse *T* as shown in Figure 8 (a) for **1(py)** for the three ligand signals. As shown before,[18,20,23–25] the isotropic shift moves starting at high temperatures towards the more paramagnetic region and shows the Curie behaviour expected for an iron(II) HS complex. This behaviour changes below *T* = 255 K (1/*T* = $3.9 \times 10^3 K^{-1}$). Upon further cooling, the paramagnetic shifts move to zero, which is the value expected for a pure LS complex.

Multiplying the isotropic shift with *T* and normalizing the values to one gave γ_{HS} as shown in part b of Figure 8 plotted *vs. T*. The observed ST behaviour of the three monitored signals is nearly identical, and for further comparison the average of the three signals was used. Comparison of **1(py)**, **2(py)** and **3(py)** in Figure 8 (c) shows the same trend for all of the complexes. For **3(py)**, the complete data are not shown due to its low solubility at low temperatures. For the other two complexes, the complete ST can be followed using this method. The curve progression is nearly identical, which demonstrates that the length of the alkyl chain does not influence the ST properties in solution ($T_{1/2} \approx 225$ K in all cases). Thus all the differences observed in the solid state are due to packing effects.
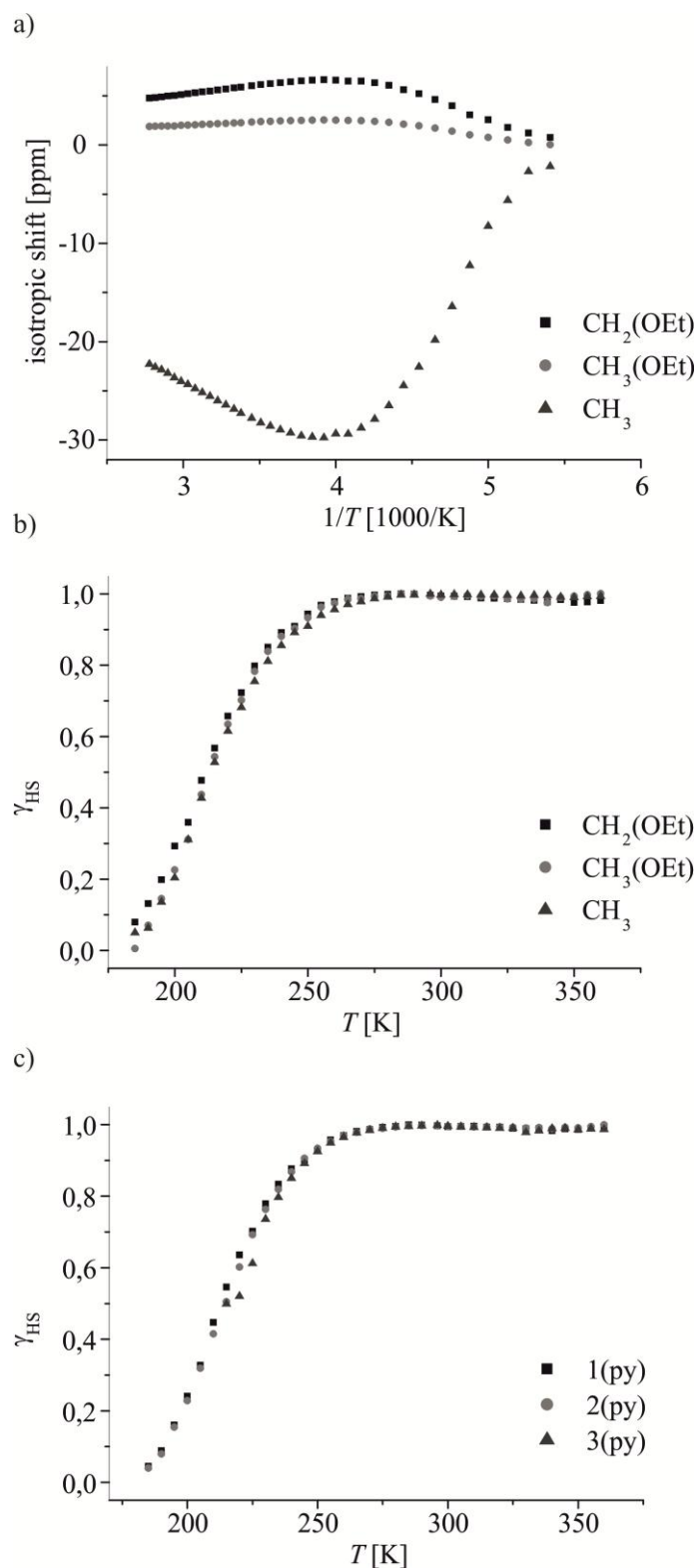
a)

b)

c)

Figure 8. a) Isotropic shift of **1(py)** plotted versus $1/T$ for the three monitored ligand signals; b) HS mole fraction (γ_{HS}) for the three monitored ligand signals of **1(py)** plotted versus T and c) HS mole fraction (γ_{HS}) of the complexes **1-3(py)** plotted versus T.

5.3   Conclusion

We have reported the synthesis and characterisation of five new Schiff base-like ligands and their iron(II) complexes with pyridine or methanol as axial ligands. A special feature of the ligands is the introduction of long alkyl chains in the outer sphere that results in the head–tail character of the complexes. For three complexes of these ligands, we have been able to obtain single crystals of a high enough quality to perform X-ray structure analysis.[10] The structure bearing motif is in all cases a lipid layer-like arrangement of the molecules where the alkyl chains (tails) are packed in the middle and the iron centres (heads) are on the outer sides. In all cases, a network of hydrogen bonds is observed between the layers. Further investigations are needed to verify if this motif is always obtained or if certain structural preconditions are necessary (certain ratio of length of alkyl chain/size of head). At the moment, the later possibility is more likely as with larger pyridine as the axial ligands the complex with $n = 15$ crystallised, whereas with smaller methanol two complexes with $n = 11$ crystallised. Of the complexes with pyridine, the SCO properties are strongly influenced by the different alkyl chain lengths in the solid state, whereas in solution the same transition curve is obtained independent of n. Because of the lack of structural information for all those complexes, no structure–function relationships have been identified. However, the increase in the alkyl chain length does not necessarily lead to a decrease of cooperative interactions during the spin transition. A network of hydrogen bonds between the lipid layers appears to be enough for the transmission of cooperative effects.[10]

5.4 Experimental Section

General: The synthesis of the iron complexes was carried out under an argon atmosphere using Schlenk techniques. The solvents were purified as described in the literature[26] and distilled under an atmosphere of argon. When argon is used for the synthesis of the intermediate products, it is described in the text. Alkylbromides were commercial products (Sigma-Aldrich) and used as received. The synthesis of **3(py)** and its precursors,[10] ethoxymethyleneethylacetoacetate (D),[27] ethoxymethyleneacetylacetone (E),[27] methoxymethylenemethylacetoacetate (F)[15] and iron(II) acetate[16] are described in the literature.

1,2-Dioctyloxybenzene (A1): In a three neck round-bottomed flask (1 L) fitted with a condenser and a dropping funnel, catechol (25 g, 227.0 mmol, 1 equiv.) and K_2CO_3 (78.45 g, 567.7 mmol, 2.5 equiv.) were stirred at room temperature in N,N-dimethylformamide (DMF, 350 mL) for 1 h under a nitrogen atmosphere. 1-Bromooctane (109.62 g, 567.7 mmol, 2.5 equiv.) was added dropwise to the turquoise suspension, and the mixture was heated to 80 °C for 12 h. The suspension was poured into a separatory funnel and H_2O (250 mL) and ethyl ether (400 mL) were added. The solid was removed, the DMF/H_2O phase was separated from the ether phase and washed twice with ether (ca. 150 mL). The combined ether phases were washed twice with H_2O (150 mL) and the solvent was removed in vacuo. Distillation gave **A1** at about 2.0×10^{-4} bar and 160 °C as a colourless liquid; yield 71.3 g (94 %). $C_{22}H_{38}O_2$ (334.54): calcd. C 78.99, H 11.45; found C 79.29, H 12.39. ^{1}H NMR (399.81 MHz, CDCl$_3$, 296 K): δ = 0.87 (t, J = 7.0 Hz, 6 H, CH$_3$), 1.22–1.39 (m, 16 H, CH$_2$), 1.41–1.51 (m, 4 H, CH$_2$), 1.75–1.85 (m, 4 H, CH$_2$), 3.98 (t, J = 6.7 Hz, 4 H, CH$_2$O), 6.87 (s, 4 H, H$_{ar}$) ppm. ^{13}C NMR (100.53 MHz, CDCl$_3$, 296 K): δ = 14.1 (CH$_3$), 22.7 (CH$_2$), 26.0 (CH$_2$), 29.3 (2 CH$_2$), 29.4 (CH$_2$), 31.8 (CH$_2$), 69.2 (CH$_2$, CH$_2$O), 114.1 (CH, C$_{ar}$), 121.0 (CH, C$_{ar}$), 149.2 (C$_q$, C$_{ar}$–O) ppm.

1,2-Didodecyloxybenzene (A2): In a three neck round-bottomed flask (1 L) fitted with a condenser and a dropping funnel, catechol (25 g, 227.0 mmol, 1 equiv.) and K_2CO_3 (62.75 g, 454.0 mmol, 2 equiv.) were stirred at room temperature in DMF (600 mL) for 50 min under a nitrogen atmosphere. 1-Bromododecane (113.14 g, 454.0 mmol, 2 equiv.) was added dropwise to the turquoise suspension. After stirring for 20 min at room temperature, the mix-

ture was heated to 80 °C for 7 h and stored at –25 °C. The white precipitate was collected by filtration and washed with plenty of water. **A2** was recrystallised from ethanol (500 mL), collected by filtration, washed with methanol and dried in vacuo; yield 79.0 g (78 %). $C_{30}H_{54}O_2$ (446.75): calcd. C 80.65, H 12.18; found C 80.53, H 11.55. MS (DEI+): m/z (%) = 447 (100) $[M]^+$, 278 (10), 110 (55). ^{1}H NMR (399.81 MHz, $CDCl_3$, 296 K): δ = 0.87 (t, J = 6.9 Hz, 6 H, CH_3), 1.18–1.38 (m, 32 H, CH_2), 1.39–1.50 (m, 4 H, CH_2), 1.74–1.84 (m, 4 H, CH2), 3.97 (t, J = 6.7 Hz, 4 H, CH_2O), 6.87 (s, 4 H, H_{ar}) ppm. ^{13}C NMR (100.53 MHz, $CDCl_3$, 296 K): δ = 14.1 (CH_3), 22.7 (CH_2), 26.1 (CH_2), 29.3 (CH_2), 29.4 (CH_2), 29.5 (CH_2), 29.6/29.6 (2 CH_2), 29.7/29.7 (2 CH_2), 31.9 (CH_2), 69.3 (CH_2, CH_2–O), 114.1 (CH, C_{ar}), 121.0 (CH, C_{ar}), 149.2 (C_q, C_{ar}–O) ppm.

1,2-Dinitro-4,5-dioctyloxybenzene (B1): **A1** (34.15 g, 102.0 mmol) was dissolved in acetic acid (130 mL) and nitric acid (50 mL, 65%) was added dropwise over 45 min. The solution became yellow and solidified, and the temperature was increased to 45 °C. Fuming nitric acid (115 mL) was added dropwise over 45 min, whereby the reaction mixture became liquid again, and the temperature was increased to 65 °C. After 2 h stirring, the solution was poured into iced water (750 mL), and the resulting yellow solid was collected by filtration and washed with water until neutral. **B1** was recrystallized from ethanol (450 mL), filtered, washed with methanol and dried in vacuo; yield 29.0 g (67 %). $C_{22}H_{36}N_2O_6$ (424.53): calcd. C 62.24, H 8.55, N 6.60; found C 62.22, H 9.33, N 6.69. ^{1}H NMR (399.81 MHz, $CDCl_3$, 296 K): δ = 0.87 (t, J = 7.0 Hz, 6 H, CH_3), 1.07–1.39 (m, 16 H, CH_2), 1.39–1.51 (m, 4 H, CH_2), 1.78–1.90 (m, 4 H, CH_2), 4.08 (t, J = 6.5 Hz, 4 H, CH_2O), 7.27 (s, 2 H, H_{ar}) ppm. ^{13}C NMR (100.53 MHz, $CDCl_3$, 296 K): δ = 14.1 (CH_3), 22.6 (CH_2), 25.8 (CH_2), 28.7 (CH_2), 29.2 (2 CH_2), 31.7 (CH_2), 70.2 (CH_2, CH_2O), 107.9 (CH, C_{ar}), 136.5 (C_q, C_{ar}–NO_2), 151.8 (C_q, C_{ar}–O) ppm.

4,5-Didodecyloxy-1,2-dinitrobenzene (B2): **A2** (45.6 g, 102 mmol) was dissolved in acetic acid (480 mL) over several hours. Nitric acid (25 mL, 65%) and then fuming nitric acid (300 mL) were added dropwise. Slight warming at times was necessary to ensure that continuous stirring was possible. The reaction mixture was stirred for 20 h at room temperature and poured slowly with vigorous stirring into iced water (2 L). The yellow solid was collected by filtration, washed with water until neutral and dried overnight. Recrystallisation from ethanol (700 mL) gave **B2** as a bright yellow powder; yield 41.6 g (76 %). $C_{30}H_{52}N_2O_6$ (536.74): calcd. C 67.13, H 9.76, N 5.22; found C 66.92, H 9.87, N 5.34.

MS (DEI+): m/z (%) = 537 (100) [M]$^+$. ^{1}H NMR (399.81 MHz, CDCl$_3$, 296 K): δ = 0.86 (t, J = 7.0 Hz, 6 H, CH$_3$), 1.14–1.39 (m, 32 H, CH$_2$), 1.39– 1.50 (m, 4 H, CH$_2$), 1.78–1.90 (m, 4 H, CH$_2$), 4.07 (t, J = 6.6 Hz, 4 H, CH$_2$–O), 7.27 (s, 2 H, H$_{ar}$) ppm. ^{13}C (100.53 MHz, CDCl$_3$, 296 K): 14.1 (CH$_3$), 22.7 (CH$_2$), 25.8 (CH$_2$), 28.7 (CH$_2$), 29.2 (CH$_2$), 29.4 (CH$_2$), 29.5 (CH$_2$), 29.6 (2 CH$_2$), 29.7 (CH$_2$), 31.9 (CH$_2$), 70.2 (CH$_2$, CH$_2$O), 107.8 (CH, C$_{ar}$), 136.4 (C$_q$, C$_{ar}$–NO$_2$), 151.8 (C$_q$, C$_{ar}$–O). ^{1}H NMR (399.81 MHz, C$_6$D$_6$, 296 K): δ = 1.32 (t, J = 6.8 Hz, 6 H, CH$_3$), 1.58–1.78 (m, 36 H, CH$_2$), 1.83–1.92 (m, 4 H, CH$_2$), 3.62 (t, J = 5.8 Hz, 4 H, CH$_2$O), 7.54 (s, 2 H, H$_{ar}$) ppm. ^{13}C NMR (100.53 MHz, C$_6$D$_6$, 296 K): δ = 14.3 (CH$_3$), 23.1 (CH$_2$), 26.2 (CH$_2$), 28.9 (CH$_2$), 29.6 (CH$_2$), 29.8 (CH$_2$), 30.0 (CH$_2$), 30.1 (2 CH$_2$), 30.2 (CH$_2$), 32.3 (CH$_2$), 69.5 (CH$_2$, CH$_2$–O), 107.6 (CH, C$_{ar}$), 136.8 (C$_q$, C$_{ar}$–NO$_2$), 151.7 (C$_q$, C$_{ar}$–O) ppm.

1,2-Diamino-4,5-dioctyloxybenzene (C1): Under an argon atmosphere, **B1** (17.7 g, 41.7 mmol) and Pd on activated charcoal (2.6 g, 10 %) were suspended in ethanol (250 mL) for 10 min. Hydrazine monohydrate (62.6 g, 1250.0 mmol, 30 equiv.) was added dropwise over 30 min. The mixture was heated to reflux for 2 h, and the colour turned from purple to yellow. Slightly warm, the mixture was filtered through Celite® 545 coarse and stored at 5 °C overnight. After the resulting yellow solid was collected by filtration, it was hydrated again by the same procedure with hydrazine monohydrate (31 g) and Pd on activated charcoal (1.3 g) in ethanol (200 mL) to obtain **C1** as a white powder; yield 8.2 g (59 %). C$_{22}$H$_{40}$N$_2$O$_2$ (364.57): calcd. C 72.48, H 11.06, N 7.68; found C 72.72, H 10.67, N 7.54. ^{1}H NMR (399.81 MHz, CDCl$_3$, 296 K): δ = 0.86 (t, J = 7.1 Hz, 6 H, CH$_3$), 1.16–1.36 (m, 16 H, CH$_2$), 1.36–1.46 (m, 4 H, CH$_2$), 1.64–1.77 (m, 4 H, CH$_2$), 3.15 (br, 4 H, NH$_2$), 3.86 (t, J = 6.7 Hz, 4 H, CH$_2$–O), 6.35 (s, 2 H, H$_{ar}$) ppm. ^{13}C NMR (100.53 MHz, CDCl$_3$, 296 K): δ = 14.1 (CH$_3$), 22.7 (CH$_2$), 26.1 (CH$_2$), 29.3 (CH$_2$), 29.4 (CH$_2$), 29.6 (CH$_2$), 31.8 (CH$_2$), 70.7 (CH$_2$, CH$_2$O), 106.7 (CH, C$_{ar}$), 128.4 (C$_q$, C$_{ar}$–NH$_2$), 143.4 (C$_q$, C$_{ar}$–O) ppm.

1,2-Diamino-4,5-didodecyloxybenzene (C2): Under an argon atmosphere, **B2** (41.6 g, 77.5 mmol) was stirred at room temperature with Pd on activated charcoal (7.5 g) in ethanol (1.1 L) for 10 min. Hydrazine monohydrate (147.7 g, 7392.8 mmol, 37 equiv.) was added dropwise over 1 h, and the mixture was heated to reflux for 2 h until the colour turned to white. The mixture was filtered hot through Celite® 545 coarse and stored at 5 °C overnight. **C2**, a white solid, was collected by filtration and dried in vacuo; yield 33.1 g (90 %). C$_{30}$H$_{56}$N$_2$O$_2$ (476.78): calcd. C 75.57, H 11.84, N 5.88; found C 75.41, H 11.75, N 5.95. MS

(DEI+): m/z (%) = 477 (100) [M]$^+$, 139 (50). ^{1}H NMR (399.81 MHz, CDCl$_3$, 296 K): δ = 0.86 (t, J = 7.0 Hz, 6 H, CH$_3$), 1.14–1.35 (m, 32 H, CH$_2$), 1.36– 1.46 (m, 4 H, CH$_2$), 1.66–1.77 (m, 4 H, CH$_2$), 3.15 (br, 4 H, NH$_2$), 3.86 (t, J = 6.6 Hz, 4 H, CH$_2$–O), 6.35 (s, 2 H, H$_{ar}$) ppm. ^{13}C NMR (100.53 MHz, CDCl$_3$, 296 K): δ = 14.1 (CH$_3$), 22.7 (CH$_2$), 26.1 (CH$_2$), 29.4 (CH$_2$), 29.5 (CH$_2$), 29.4 (CH$_2$), 29.6 (CH$_2$), 29.7 (3 CH$_2$), 31.9 (CH$_2$), 70.7 (CH$_2$, CH$_2$O), 106.8 (CH, C$_{ar}$), 138.3 (C$_q$, C$_{ar}$–NH$_2$), 143.4 (C$_q$, C$_{ar}$–O) ppm.

Diethyl (2E,2$'E$)-2,2$'$-{[4,5-Bis(octyloxy)-1,2-phenylene]bis[imino-(E)-methylylidene]}bis (3-oxobutanoate) (L1): Under an argon atmosphere, **C1** (2.76 g, 7.6 mmol) was diluted in ethanol (40 mL) and **D** (3.1 g, 16.7 mmol, 2.2 equiv.) was added. The yellow mixture was heated to reflux for 1.5 h and stored at −30 °C. The yellow solid was collected by filtration and recrystallised twice from ethanol (25 mL); yield 2.53 g (52 %). C$_{36}$H$_{56}$N$_2$O$_8$ (644.84): calcd. C 67.05, H 8.75, N 4.34; found C 67.00, H 9.07, N 4.52. ^{1}H NMR (399.81 MHz, CDCl$_3$, 296 K): δ = 0.86 (t, J = 6.5 Hz, 6 H, CH$_3$), 1.20–1.34 (m, 16 H, CH$_2$), 1.29 [t, J = 7.5Hz, 6 H, CH$_3$(Et)], 1.38– 1.52 (m, 4 H, CH$_2$), 1.73–1.86 (m, 4 H, CH$_2$), 2.51 (s, 6 H, CH$_3$), 3.98 (t, J = 6.3Hz, 4 H, CH$_2$O), 4.22 [q, J = 7.5 Hz, 4 H, CH$_2$(Et)], 6.72 (s, 2 H, H$_{ar}$), 8.23 (d, J = 12.5 Hz, 2 H, CH=), 12.83 (d, NH, J = 12.5 Hz, 2 H) ppm. ^{13}C NMR (100.53 MHz, CDCl$_3$, 296 K): δ = 14.0 (CH$_3$), 14.4 (CH$_3$), 22.7 (CH$_2$), 26.0 (CH$_2$), 29.2 (2 CH$_2$), 29.3 (CH$_2$), 31.1 (CH$_3$), 31.8 (CH$_2$), 60.0 [CH$_2$, CH$_2$(Et)], 70.0 (CH$_2$, CH$_2$–O), 103.7 (C$_q$), 106.5 (CH, C$_{ar}$), 124.8 (C$_q$, C$_{ar}$–N), 148.4 (C$_q$, C$_{ar}$–O), 154.1 (CH), 166.8 (O–C=O), 200.1 (C=O) ppm.

Diethyl (2E,2$'E$)-2,2$'$-{[4,5-Bis(dodecyloxy)-1,2-phenylene]bis[imino-(E)-methylylidene]} bis(3-oxobutanoate) (L2): Under an argon atmosphere, **C2** (5.0 g, 10.5 mmol) was diluted in ethanol (90 mL) and **D** (4.3 g, 23.1 mmol, 2.2 equiv.) was added. The yellow mixture was heated to reflux for 1.5 h and stored at −30 °C. The yellow solid was collected by filtration, washed with ethanol and recrystallized from ethanol (60 mL); yield 6.9 g (87 %). C$_{44}$H$_{72}$N$_2$O$_8$ (757.05): calcd. C 69.81, H 9.59, N 3.70; found C 69.67, H 9.43, N 3.60. MS (DEI+): m/z (%) = 757 (100) [M]$^+$, 711 (22), 627 (20), 285 (17). ^{1}H NMR (299.83 MHz, CDCl$_3$, 296 K): δ = 0.85 (t, J = 6.8 Hz, 6 H, CH$_3$), 1.17–1.36 (m, 32 H, CH$_2$), 1.29 [t, J = 7.1 Hz, 6 H, CH$_3$(Et)], 1.38–1.51 (m, 4 H, CH$_2$), 1.73–1.86 (m, 4 H, CH$_2$), 2.51 (s, 6 H, CH$_3$), 3.98 (t, J = 6.6 Hz, 4 H, CH$_2$O), 4.22 [q, J = 7.1 Hz, 4 H, CH$_2$(Et)], 6.72 (s, 2 H, H$_{ar}$), 8.24 (d, J = 12.5 Hz, 2 H, CH=), 12.83 (d, NH, J = 12.5 Hz, 2 H) ppm. ^{13}C NMR (75.39 MHz, CDCl$_3$, 296 K): δ = 14.1

(CH$_3$), 14.4 (CH$_3$), 22.6 (CH$_2$), 26.0 (CH$_2$), 29.2 (CH$_2$), 29.3 (2 CH$_2$), 29.6 (3 CH$_2$), 29.7 (CH$_2$), 31.1 (CH$_3$), 31.9 (CH$_2$), 60.0 [CH$_2$, CH$_2$(Et)], 70.0 (CH$_2$, CH$_2$O), 103.7 (C$_q$), 106.5 (CH, C$_{ar}$), 124.8 (C$_q$, C$_{ar}$–N), 148.4 (C$_q$, C$_{ar}$–O), 154.1 (CH), 166.8 (O–C=O), 200.1 (C=O) ppm.

3,3′-{[4,5-Bis(octyloxy)-1,2-phenylene]bis(iminomethylylidene)}dipentane-2,4-dione

(L4): Under an argon atmosphere, **C2** (1.45 g, 3.0 mmol) was diluted in ethanol (180 mL) and **E** (1.0 g, 6.6 mmol, 2.2 equiv.) was added. The mixture was heated to reflux for 1 h and stored at −30 °C. The yellow solid was collected by filtration, washed with ethanol and recrystallised from ethanol (100 mL); yield 0.86 g (41 %). C$_{42}$H$_{68}$N$_2$O$_6$ (697.00): calcd. C 72.37, H 9.83, N 4.02; found C 72.27, H 9.90, N 4.06. MS (DEI+): *m/z* (%) = 687 (100) [M]$^+$. ^{1}H NMR (299.83 MHz, CDCl$_3$, 296 K): δ = 0.85 (t, *J* = 6.6 Hz, 6 H, CH$_3$), 1.16–1.39 (m, 32 H, CH$_2$), 1.39–1.52 (m, 4 H, CH$_2$), 1.74–1.87 (m, 4 H, CH$_2$), 2.31 (s, 6 H, CH$_3$), 2.51 (s, 6 H, CH$_3$), 3.99 (t, *J* = 6.6 Hz, 4 H, CH$_2$–O), 6.71 (s, 2 H, H$_{ar}$), 7.98 (d, *J* = 12.2 Hz, 2 H, CH=), 12.82 (d, NH, *J* = 12.2 Hz, 2 H) ppm. ^{13}C NMR (79.39 MHz, CDCl$_3$, 296 K): δ = 14.1 (CH$_3$), 22.7 (CH$_2$), 26.0 (CH$_2$), 27.5 (CH$_3$), 29.2 (CH$_2$), 29.3 (CH$_2$), 29.4 (CH$_2$), 29.6 (3 CH$_2$), 29.7 (CH$_2$), 31.9 (CH$_3$), 70.1 (CH$_2$, CH$_2$–O), 106.9 (CH, C$_{ar}$), 114.2 (C$_q$), 125.0 (C$_q$, C$_{ar}$–N), 148.7 (C$_q$, C$_{ar}$–O), 154.1 (CH), 194.6 (C=O), 201.2 (C=O) ppm.

Dimethyl(2*E*,2′*E*)-2,2′-{[4,5-Bis(dodecyloxy)-1,2-phenylene]bis-[imino-(*E*)methylylidene]}bis(3-oxobutanoate) (L5): Under an argon atmosphere, **C2** (5.0 g, 10.5 mmol) was diluted in ethanol (90 mL) and **F** (4.0 g, 23.2 mmol, 2.2 equiv.) was added. The yellow mixture was heated to reflux for 1.5 h and stored at −30 °C. The yellow solid was collected by filtration, washed with ethanol and recrystallised from ethanol (60 mL); yield 7.0 g (91 %). C$_{42}$H$_{68}$N$_2$O$_8$ (729.00): calcd. C 69.20, H 9.40, N 3.84; found C 69.03, H 9.35, N 3.87. ^{1}H NMR (299.83 MHz, CDCl$_3$, 296 K): δ = 0.85 (t, *J* =6.7 Hz, 6 H, CH$_3$), 1.15–1.39 (m, 32 H, CH$_2$), 1.39–1.52 (m, 4 H, CH$_2$), 1.73–1.87 (m, 4 H, CH$_2$), 2.52 (s, 6 H, CH$_3$), 3.75 (s, 6 H, CH$_3$), 3.98 (t, *J* = 6.3Hz, 4 H, CH$_2$O), 6.72 (s, 2 H, H$_{ar}$), 8.23 (d, *J* = 12.3 Hz, 2 H, CH=), 12.87 (d, NH, *J* = 12.3 Hz, 2 H) ppm. ^{13}C NMR (75.39 MHz, CDCl$_3$, 296 K): δ = 14.1 (CH$_3$), 22.7 (CH$_2$), 26.0 (CH$_2$), 29.2 (CH$_2$), 29.3 (CH$_2$), 29.4 (CH$_2$), 29.6 (3 CH$_2$), 29.7 (CH$_2$), 31.0 (CH$_3$), 31.9 (CH$_2$), 51.2 (CH$_3$), 70.0 (CH$_2$, CH$_2$O), 103.4 (C$_q$), 106.4 (CH, C$_{ar}$), 124.8 (C$_q$, C$_{ar}$–N), 148.5 (C$_q$, C$_{ar}$–O), 154.1 (CH), 167.2 (O–C=O), 200.1 (C=O) ppm.

L1-Iron(II)·2MeOH [1(MeOH)]: **L1** (3.48 g, 5.4 mmol) was reacted with Fe(OAc)$_2$ (2.0 g, 11.5 mmol, 2.1 equiv.) in methanol (100 mL) under reflux conditions for 1 h. After cooling to room temperature, black needles were isolated, washed twice with methanol (10 mL) and dried under vacuum; yield 3.14 g (76 %). C$_{38}$H$_{62}$FeN$_2$O$_{10}$ (762.75): calcd. C 59.84, H 8.19, N 3.67; found C 60.05, H 7.70, N 3.97.

L2-Iron(II)·2MeOH [2(MeOH)]: **L2** (0.72 g, 1.0 mmol) was reacted with Fe(OAc)$_2$ (0.40 g, 2.3 mmol, 2.4 equiv.) in methanol (80 mL) under reflux conditions for 1 h. After cooling to room temperature, black crystals were isolated, which were collected by filtration, washed twice with methanol (10 mL) and dried under vacuum; yield 0.68 g (78 %). C$_{46}$H$_{78}$FeN$_2$O$_{10}$ (874.96): calcd. C 63.14, H 8.99, N 3.20; found C 62.72, H 8.72, N 3.20. MS (DEI+): *m/z* (%) = 811 (100) [M − 2 MeOH]$^+$. Crystals suitable for X-ray structure analysis were obtained.

L4-Iron(II) (4): **L4** (0.49 g, 0.7 mmol) was reacted with Fe(OAc)$_2$ (0.21 g, 1.2 mmol, 1.7 equiv.) in methanol (60 mL) under reflux conditions for 70 min. After cooling, a brown solid precipitated, which was collected by filtration, washed twice with methanol (15 mL) and dried in vacuo; yield 0.36 g (69 %). C$_{42}$H$_{66}$FeN$_2$O$_6$ (750.83): calcd. C 67.19, H 8.86, N 3.73; found C 67.13, H 9.13, N 3.85. MS (DEI+): *m/z* (%) = 750 (100) [M]$^+$.

L5-Iron(II)·2MeOH [5(MeOH)]: **L5** (3 g, 4.1 mmol) was reacted with Fe(OAc)$_2$ (1.35 g, 7.0 mmol, 1.7 equiv.) in methanol (80 mL) under reflux conditions for 90 min. After cooling to room temperature, black needles precipitated, which were collected by filtration, washed twice with methanol (10 mL) and dried under reduced pressure; yield 3.1 g (89 %). C$_{44}$H$_{74}$FeN$_2$O$_{10}$ (846.91): calcd. C 62.40, H 8.81, N 3.31; found C 62.15, H 9.03, N 3.37. Crystals suitable for X-ray structure analysis were obtained.

L1-Iron(II)·2py [1(py)]: Compound **1(MeOH)** (0.3 g, 0.4 mmol) was dissolved in pyridine (7 mL) and heated to reflux for 1 h. After cooling to room temperature, water (1 mL) was added. The obtained precipitate was collected by filtration and drying in vacuo gave the product as a black solid; yield 0.29 g (83 %). C$_{46}$H$_{64}$FeN$_4$O$_8$×H$_2$O (874.88): calcd. C 63.15, H 7.60, N 6.40; found C 62.92, H 7.11, N 6.42.

L2-Iron(II)·2py [2(py)]: Compound **2(MeOH)** (0.48 g, 0.6 mmol) was treated with pyridine (9 mL) for 45 min under reflux conditions. After cooling, water (2.3 mL) was added, and the mixture heated again to reflux for 2 min. Within 2 d of storage at 4 °C, black crystals were formed. The product was collected by filtration and dried in vacuo; yield 0.28 g (53 %). $C_{54}H_{80}FeN_4O_8 \times 0.5H_2O$ (978.09): calcd. C 66.31, H 8.35, N 5.73; found C 66.27, H 8.87, N 5.53.

L4-Iron(II)·2py [4(py)]: Compound **4** (0.3 g, 0.4 mmol) was treated with pyridine (7 mL) for 45 min under reflux conditions. After cooling to room temperature, water (1 mL) was added. The obtained precipitate was collected by filtration and drying in vacuo gave the product as a black solid; yield 0.26 g (72 %). $C_{52}H_{76}FeN_4O_6$ (909.03): calcd. C 68.71, H 8.43, N 6.16; found C 68.53, H 8.31, N 6.48.

L5-Iron(II)·2py [5(py)]: Compound **5(MeOH)** (0.44 g, 0.5 mmol) was treated with pyridine (10 mL) for 1 h under reflux conditions. After cooling, water (2.4 mL) was added, and the mixture heated again to reflux for 2 min. A red-brown fine crystalline powder was formed at 4 °C, which was collected by filtration and dried in vacuo; yield 0.28 g (67 %). $C_{52}H_{76}FeN_4O_8 \times 0.5H_2O$ (950.04): calcd. C 65.74, H 8.17, N 5.90; found C 65.67, H 8.22, N 5.87.

NMR Spectroscopy: [D_8]toluene (D, 99.50 %), [D_5]pyridine (D, 99.50 %), [D_6]benzene (D, 99.50%) and $CDCl_3$ (D, 99.80%) were purchased from Euriso-top. Solvents for organic compounds (C_6D_6 and $CDCl_3$) were degassed and stored over molecular sieves. Samples were prepared using 5 mm tubes and Schlenk techniques (concentration ca. 5–10 %). The solvent for the paramagnetic ^1H NMR investigations was a [D_8]toluene/[D_5]pyridine mixture (50:50, *V/V*), which was degassed using at least seven pump–freeze cycles and stored under argon. The NMR samples of the iron(II) complexes (ca. 15 mg in 0.6 mL of solvent) were prepared in 5 mm tubes under argon using Schlenk techniques and degassed using pump–freeze cycles prior to sealing with a butane gas burner. The NMR spectra were recorded with Varian Inova 300 and 400 spectrometers at 23 °C (organic compounds) or variable temperatures [–93 °C to +87 °C, iron(II) complexes]. Chemical shifts are given relative to Me_4Si, δ $^1H(CHCl_3) = 7.24$, δ $^1H(C_6D_5H) = 7.15$, δ $^1H(C_6D_5CD_2H) = 2.03$; Me_4Si, δ $^1H(CDCl_3) = 77.0$, δ $^1H(C_6D_6) = 128.0$ ppm.

Magnetic Susceptibilities: Data for **1–5(py)** were collected with a Quantum Design MPMSR2 SQUID magnetometer under an applied field of 0.05, 0.1 and 0.2 T over 10–400 K in the sweep mode. All samples were placed in gelatine capsules held within plastic straws. The data were corrected for the diamagnetic magnetization of the ligands, which were estimated using Pascal's constants, and the sample holder.

X-ray Diffraction: The intensity data of **2(MeOH)** were collected with a Nonius Kappa CCD diffractometer using graphite-monochromated Mo-K_α radiation (Table 4). The intensity data of **5(MeOH)** were collected with a Stoe IPDS II diffractometer using graphite-monochromated Mo-K_α radiation. The data were corrected for Lorentz and polarisation effects. The structure was solved by direct methods (Sir 97)[28] and refined by full-matrix least-square techniques against $F_0{}^2$ (SHELXL-97).[29] The hydrogen atoms were included at calculated positions with fixed displacement parameters. All non-hydrogen atoms were refined anisotropically. ORTEP-III[30] was used for the structure representation, Schakal-99[31] and Mercury[32] for the representation of the molecule packing. CCDC-847611 [for **2(MeOH)**] and -847612 [for **5(MeOH)**] contain the supplementary crystallographic data for this paper. These data can be obtained free of charge from The Cambridge Crystallographic Data Centre via www.ccdc.cam.ac.uk/data_request/cif.

Elemental Analysis: Elemental analysis was performed with a VarioEL III CHN instrument using tin boats purchased from Elementar and Acetanilid (Merck) as a standard.

Mass Spectrometry: Mass spectra were recorded with a Varian MAT CH7 instrument (direct inlet system, electron impact ionization 70 eV) or a Jeol MS-700 instrument.

Table 4. Crystallographic data of **2(MeOH)** and **5(MeOH)**.

	2(MeOH)	**5(MeOH)**
Empirical formula	$C_{46}H_{78}FeN_2O_{10}$	$C_{44}H_{74}FeN_2O_{10}$
Formula weight	874.95	846.90
Temperature [K]	200	133
Crystal size [mm]	0.23×0.12×0.03	0.28×0.25×0.17

Crystal system	triclinic	triclinic
Space group	$P\bar{1}$	$P\bar{1}$
λ	Mo-K_α, 0.71073	Mo-K_α, 0.71069
a	8.1996(1)	8.0145(4)
b	10.7339(1)	11.3292(6)
c	28.4255(4)	26.7290(15)
α	82.4756(9)	78.299(4)
β	88.8122(8)	86.789(4)
δ	75.9810(8)	70.243(4)
$V\,[\text{Å}^3]$	2406.26(5)	2236.4(2)
Z	2	2
$\rho_{calcd.}\,[\text{g/cm}^3]$	1.208	1.258
$\mu\,[\text{1/mm}]$	0.368	0.394
$F(000)$	948	916
Θ range [°]	3.3–25.4	1.6–25.7
Index ranges	−9/ 9	−9/ 9
	−12/12	−13/13
	−34/34	−32/32
Reflections collected	16749	30421
Reflections unique	8776	8436
Data/restraints/parameters	8776/0/546	8436/0/522
R_1 (all)	0.0402	0.0517
wR_2	0.1016	0.1235
GooF	1.04	0.87

5.5 References

[1]   a) P. Gütlich, A. Hauser, H. Spiering, *Angew. Chem. Int. Ed.* **1994**, *33*(20), 2024–2054; b) P. Gütlich, H. Goodwin, Eds, *Spin Crossover in Transition Metal Compounds I-III,* Springer Berlin / Heidelberg, **2004**; c) J.-F. Letard, *J. Mater. Chem.* **2006**, *16*(26), 2550–2559; d) O. Sato, J. Tao, Y.-Z. Zhang, *Angew. Chem. Int. Ed.* **2007**, *46*(13), 2152–2187; e) J. A. Kitchen, S. Brooker, *Coord. Chem. Rev.* **2008**, *252*(18-20), 2072–2092; f) M. A. Halcrow, *Coord. Chem. Rev.* **2009**, *253*(21-22), 2493–2514; g) K. S. Murray, *Aust. J. Chem.* **2009**, *62*(9), 1081; h) S. Brooker, J. A. Kitchen, *Dalton Trans.* **2009**, *36*, 7331–7340; i) A. B. Koudriavtsev, W. Linert, *J. Struct. Chem.* **2010**, *51*(2), 335–365; j) M. A. Halcrow, *Chem. Soc. Rev.* **2011**.

[2]   B. Weber, *Coord. Chem. Rev.* **2009**, *253*(19-20), 2432–2449.

[3]   A. Gaspar, M. Seredyuk, P. Gütlich, *J. Mol. Struc.* **2009**, *924-926*, 9–19.

[4]   a) J.-F. Létard, P. Guionneau, L. Goux-Capes in *Spin Crossover in Transition Metal Compounds I-III*, *Topics in Current Chemistry*, *233-235* (Eds: P. Gütlich, H. Goodwin), Springer Berlin / Heidelberg, **2004**, pp. 221–249; b) Y. Garcia, V. Ksenofontov, S. Mentior, M. M. Dîrtu, C. Gieck, A. Bhatthacharjee, P. Gütlich, *Chem. Eur. J.* **2008**, *14*(12), 3745–3758.

[5]   a) I. Boldog, A. B. Gaspar, V. Martínez, P. Pardo-Ibañez, V. Ksenofontov, A. Bhattacharjee, P. Gütlich, J. A. Real, *Angew. Chem. Int. Ed.* **2008**, *47*(34), 6433–6437; b) S. Cobo, G. Molnár, J. A. Real, A. Bousseksou, *Angew. Chem. Int. Ed.* **2006**, *45*(35), 5786–5789; c) G. Molnár, S. Cobo, J. A. Real, F. Carcenac, E. Daran, C. Vieu, A. Bousseksou, *Adv. Mater.* **2007**, *19*(16), 2163–2167; d) M. Cavallini, I. Bergenti, S. Milita, G. Ruani, I. Salitros, Z.-R. Qu, R. Chandrasekar, M. Ruben, *Angew. Chem. Int. Ed.* **2008**, *47*(45), 8596–8600; e) A. D. Naik, L. Stappers, J. Snauwaert, J. Fransaer, Y. Garcia, *Small* **2010**, *6*(24), 2842–2846.

[6]   a) M. Seredyuk, A. B. Gaspar, V. Ksenofontov, Y. Galyametdinov, J. Kusz, P. Gütlich, *Adv. Funct. Mater.* **2008**, *18*(14), 2089–2101; b) M. Seredyuk, A. B. Gaspar, V. Ksenofontov, Y. Galyametdinov, J. Kusz, P. Gütlich, *J. Am. Chem. Soc.* **2008**, *130*(4), 1431–1439; c) S. Hayami, Y. Kojima, D. Urakami, K. Ohta, K. Inoue, *Polyhedron* **2009**, *28*(9-10), 2053–2057.

[7]   a) A. Bousseksou, G. Molnar, J. A. Real, K. Tanaka, *Coord. Chem. Rev.* **2007**, *251*(13-14), 1822–1833; b) J. A. Real, A. B. Gaspar, V. Niel, M. C. Muñoz, *Coord. Chem. Rev.* **2003**, *236*(1-2), 121–141.

[8]   B. Weber, E.-G. Jäger, *Eur. J. Inorg. Chem.* **2009**, *4*, 465–477.

[9]   a) C. Gandolfi, T. Cotting, P. N. Martinho, O. Sereda, A. Neels, G. G. Morgan, M. Albrecht, *Dalton Trans.* **2011**, *40*(9), 1855–1865; b) C. Gandolfi, C. Moitzi, P. Schurtenberger, G. G. Morgan, M. Albrecht, *J. Am. Chem. Soc.* **2008**, *130*(44), 14434–14435; c) P. N. Martinho, C. J. Harding, H. Müller-Bunz, M. Albrecht, G. G. Morgan, *Eur. J. Inorg. Chem.* **2010**, *5*, 675–679.

[10]   S. Schlamp, B. Weber, A. D. Naik, Y. Garcia, *Chem. Commun.* **2011**, *47*(25), 7152–7154.

[11]   a) M. Schlögl, B. Rieger, *Z. Naturforsch. B* **2004**, *59b*, 233–240; b) K. Tahara, S. Furukawa, H. Uji-i, T. Uchino, T. Ichikawa, J. Zhang, W. Mamdouh, M. Sonoda, F. C. de Schryver, S. de Feyter, Y. Tobe, *J. Am. Chem. Soc.* **2006**, *128*(51), 16613–16625.

[12]   W. M. Lauer, C. Rondestvedt, R. T. Arnold, N. L. Drake, J. van Hook, J. Tinker, *J. Am. Chem. Soc.* **1946**, *68*(8), 1546–1548.

[13]   M. J. Howard, F. R. Heirtzler, S. I. G. Dias, *J. Org. Chem.* **2008**, *73*(7), 2548–2553.

[14]   L. Wolf, E.-G. Jäger, *Z. anorg. allg. Chem.* **1966**, *346*(1-2), 76–91.

[15]   W. Bauer, T. Ossiander, B. Weber, *Z. Naturforsch. B* **2010**, *65b*, 323–328.

[16]   B. Weber, R. Betz, W. Bauer, S. Schlamp, *Z. Anorg. Allg. Chem.* **2011**, *637*(1), 102–107.

[17]   a) B. Weber, E.-G. Jäger, *Z. Anorg. Allg. Chem.* **2009**, *635*(1), 130–133; b) S. Thallmair, W. Bauer, B. Weber, *Polyhedron* **2009**, *28*(9-10), 1796–1801.

[18]   W. Bauer, W. Scherer, S. Altmannshofer, B. Weber, *Eur. J. Inorg. Chem.* **2011**, 2803–2818.

[19]   a) W. Bauer, T. Pfaffeneder, K. Achterhold, B. Weber, *Eur. J. Inorg. Chem.* **2011**, *21*, 3183–3192; b) T. M. Pfaffeneder, S. Thallmair, W. Bauer, B. Weber, *New J. Chem.* **2011**, *35*(3), 691–700.

[20]   B. Weber, F. A. Walker, *Inorg. Chem.* **2007**, *46*(16), 6794–6803.

[21]   a) D. F. Evans, *J. Chem. Soc.* **1959**, 2003–2005; b) D. Ostfeld, I. A. Cohen, *J. Chem. Educ.* **1972**, *49*(12), 829; c) E. M. Schubert, *J. Chem. Educ.* **1992**, *69*, 62.

[22]   L. A. Yatsunyk, F. A. Walker, *Inorg. Chem.* **2004**, *43*(2), 757–777.

[23]   B. Weber, E. S. Kaps, J. Obel, K. Achterhold, F. G. Parak, *Inorg. Chem.* **2008**, *47*(22), 10779–10787.

[24]   B. Weber, C. Carbonera, C. Desplances, J.-F. Létard, *Eur. J. Inorg. Chem.* **2008**, *10*, 1589–1598.

[25]   B. Weber, J. Obel, D. Henner-Vasquez, W. Bauer, *Eur. J. Inorg. Chem.* **2009**, *36*, 5527–5534.

[26]   H. G. O. Becker, *Organikum*, Organisch-chemisches Grundpraktikum, Johann Ambrosius Barth, Berlin, **1993**.

[27]   L. Claisen, *Justus Liebigs Ann. Chem.* **1897**, *297*(1-2), 1–98.

[28]   A. Altomare, M. C. Burla, M. Camalli, G. L. Cascarano, C. Giacovazzo, A. Guagliardi, A. G. G. Moliterni, G. Polidori, R. Spagna, *J. Appl. Cryst.* **1999**, *32*(1), 115–119.

[29]   G. Sheldrick, *Acta Cryst. A* **2008**, *64*(1), 112–122.

[30]   a) C. K. Johnson, M. N. Burnett, *ORTEP-III;* Oak-Ridge National Laboratory, Oak-Ridge, TN, **1996**; b) L. Farrugia, *J. Appl. Cryst.* **1997**, *30*(5), 565.

[31]   E. Keller, *Schakal-99,* University of Freiburg, Freiburg, Germany, **1999**.

[32]   C. F. Macrae, P. R. Edgington, P. McCabe, E. Pidcock, G. P. Shilds, R. Taylor, M. Towler, J. van de Streek, *J. Appl. Cryst.* **2006**, *39*, 453–457.

6   Amphiphilic iron(II) complexes with short alkyl chains – crystal packing and spin transition properties

Stephan Schlamp,[a] Katja Dankhoff,[a] Birgit Weber*[a]

[a] Lehrstuhl für Anorganische Chemie II, Universität Bayreuth, Universitätsstraße 30, NW 1, 95440 Bayreuth, Germany; Fax: +49-92155-2157; E-mail: weber@uni-bayreuth.de

Abstract: An amphiphilic iron(II) spin crossover complex with relatively short octyl chains was synthesised and the crystal structures of the high spin and the low spin state could be determined. In further reactions, a second modification of the hexa-coordinated complex and two different penta-coordinated complexes could be obtained and characterised by X-ray structure analysis. The examples demonstrate an influence of the alkyl chains on the stoichiometry of the final product. Different arrangements of the alkyl chains were observed in the crystal packing. Despite those differences, the spin transition of the hexa-coordinated complexes is always gradual and comparable to that observed in solution.

6.1   Introduction

Since the discovery of the spin crossover (SCO) phenomenon in 1931,[1] a vast amount of compounds showing spin transition with a huge variety of ligands and metal centres were synthesised.[2,3] In recent times, the interest increases to add multifunctionality to these compounds so that they exhibit not only spin crossover but additionally functionalities like liquid crystallinity,[4] gel formation[5] or magnetic exchange interactions,[6] just to mention three examples. Also the nanostructuring of spin crossover compounds, either by the synthesis

75

of nanoparticles[7] or through pattering methods[8] is a recent field of research that is an important step towards possible future applications.

For cooperative SCO materials intermolecular interactions like hydrogen bonds, π-π interactions or also van der Waals (vdW) interactions are of uttermost importance. Studies on compounds exhibiting huge hysteresis showed that particularly hydrogen bonds are related to strong cooperative effects leading to the hysteresis phenomenon.[9] This work is focused on the influence of vdW interactions on the spin crossover behaviour. The addition of long alkyl chains in the periphery of the ligand adds a new functionality to the spin crossover system by the generation of amphiphilic molecules.[10] In previous work we did show that such complexes with Schiff base-like ligands can self-assemble to lipid layer like arrangements.[11,12] Additionally, an influence of the alkyl chains on the spin transition behaviour is possible. A rearrangement of the alkyl chains could trigger the spin transition or vice versa.[13] Thus the modification of the ligand could help to increase the cooperativity of spin crossover complexes based on the Schiff base-like ligand system used in our group. In a crystal engineering approach we want to study the influence of these alkyloxy substituents as a structure determining element on the packing of the complexes in the crystal and therefore on the SCO behaviour. So far, lipid layer like structures are the only motif observed for such complexes with dodecyl or hexadecyl alkyl chains.[11,12] Thus the question arises, if other structural motifs are possible and to what extend the alkyl chains influence the crystal packing and by this the magnetic properties. Here we present X-ray structures and magnetic properties of complexes with comparatively short octyl chains.

6.2   Results and Discussion

6.2.1   Synthesis and General Characterisation

The synthesis of the new amphiphilic ligand, visualised in Scheme 1, is realised in a four step reaction. In the Supporting Information, Figure S1, the NMR spectrum of the free ligand **H₂L** is displayed with the signal assignment. Conversion with iron(II)-acetate[14] results in the hexa-coordinated complex **[Fe(L)(MeOH)₂]** with two methanol as axial ligands. Replacement of the methanol molecules through 4-dimethylaminopyridine (dmap) leads, depending on the exact reaction conditions, to the desired compound [Fe(L)(dmap)₂] (**1**) (with varying amounts

of included methanol molecules) or the penta-coordinated complex [Fe(L)(dmap)] (**2**). In a first approach a 30 fold excess of dmap was used with the aim to obtain an octahedral complex.[18] Indeed, the desired complex [Fe(L)(dmap)$_2$] · MeOH (**1a**) could be isolated. However, slight variations in the reaction conditions (reaction time, temperature of precipitation), keeping the stoichiometry constant, resulted in the isolation of the penta-coordinated complex [Fe(L)(dmap)] (**2**). Here two different samples (**2a** and **2b**), both with the same composition but differences in the relative orientation of the alkyl chains, were obtained. This was unexpected as the characteristic colour change of the solution upon cooling with liquid nitrogen suggested the presence of a hexa-coordinated species in solution. Due to the contrary results further syntheses with a different excess of axial ligand were carried out to obtain a clear synthetic protocol for the compounds **1** and **2**. The excess of the axial dmap ligand was systematically varied and stoichiometries of 1: 20, 30, 50, 70, 90 and 110 were used. It turned out that the penta-coordinated product (**2**) is obtained selectively with a 20 fold excess. By taking 30 equivalents of axial ligand, it is difficult to predict if the penta- or hexa-coordinated complex will be obtained. In our synthetic approaches a 50:50 ratio between the two possibilities was reached. But the system can be forced to precipitate hexa-coordinated when a 50 fold excess or higher is used. In this frame, another modification of the hexa-coordinated complex, **1b** ([Fe(L)(dmap)$_2$] · 1.5 MeOH), was obtained, that could be characterised by single crystal X-ray structure analysis. For the approaches with a higher excess of dmap, fine crystalline samples with additionally included dmap/MeOH molecules were obtained.

The compounds were characterised by elemental analysis, IR and mass spectrometry, magnetic measurements and, if possible, X-ray structure analysis.
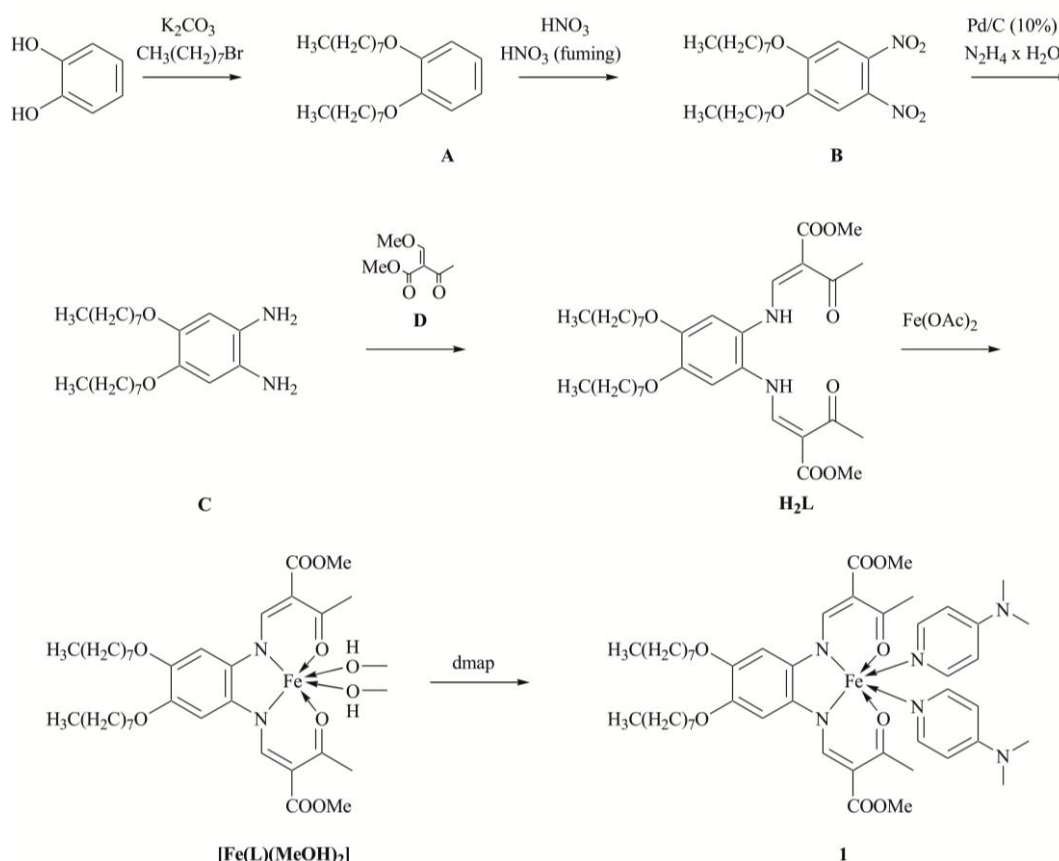
Scheme 1. General procedure for the synthesis of the new amphiphilic Schiff base-like ligand and its iron(II) complexes.

6.2.2 Description of the X-ray structures

Single crystals suitable for X-ray structure analysis were obtained for two hexa-coordinated (**1a** and **1b**) and two penta-coordinated (**2a** and **2b**) samples. The quality of the data of **1b** was low (high R_{int}) thus only the conformation of the complex and the relative orientation of the molecules in the crystal packing can be presented. In the case of **2a** the disorder of the alkyl chains could not be solved satisfactorily (due to the low quality of the data set and twinning of the crystal) thus only the conformation of the molecule is presented. Attempts to reproduce the crystals to obtain diffraction data of higher quality led to the sample **2b**. In the Supporting Information, Table S1, the crystallographic data are given.

1a precipitated in the form of platelet-like crystals out of a black solution with a 30 fold excess of dmap. The crystal structure was determined at 273 K and 133 K, what corresponds

to the high spin (HS) and the low spin (LS) state of the system (see magnetic measurements). In Figure 1 the asymmetric unit of **1a** in the HS and the LS state is displayed. Selected bond lengths and angles are summarised in Table 1.

1a crystallises in the triclinic space group $P\bar{1}$ that does not change upon spin transition. The bond lengths and angles within the first coordination sphere, Fe–N_{eq} / Fe–O_{eq}, are with an average of 2.07/2.01 Å (HS) and 1.91/1.95 Å (LS) in the region expected for this ligand system with a bond length change of about 5 % upon spin transition.[15, 18] The average Fe–N distances to the axially attached ligands (2.22 Å (HS) and 2.02 Å (LS)) change about 10 % (see Table 1) due to the higher flexibility of the axial ligands. The O–Fe–O angle is with 91.7° (LS) and 107.2° (HS) in the expected region for complexes of this type of Schiff base-like ligands.[15, 18] The change of the unit cell volume is with $\Delta V/V = 4.0$ % at the lower limit of what is expected for an iron(II) spin crossover complex,[3] but the value is higher than the one previously reported for an SCO complex with C16-alkyl chains.[12]
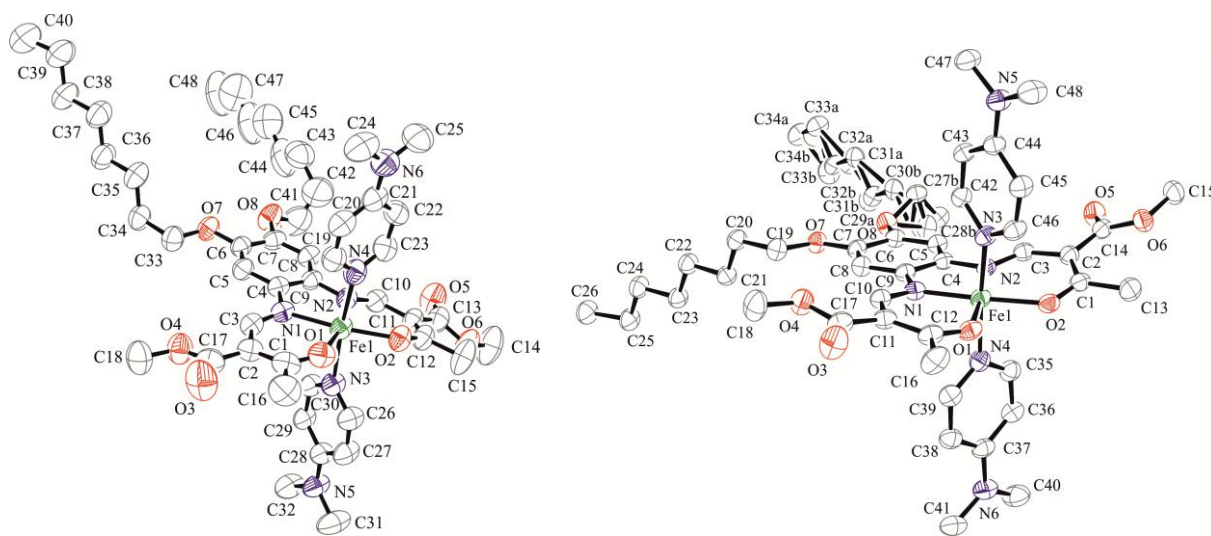

Figure 1. ORTEP drawing of **1a** at 273 K (HS) (left) and 133 K (LS) (right). Ellipsoids are drawn at the 50% probability level. Hydrogen atoms and methanol molecules are omitted for clarity.

Table 1. Selected bond lengths /Å and angles /° within the inner coordination sphere of **1a**(LS) and **1a**(HS), **1b**, **2a** and **2b**.

	Fe–N_{eq} /Å	Fe–O_{eq} /Å	Fe–N_{ax} /Å	O–Fe–O /°
1a(LS)	1.909(2)/1.915(2)	1.948(1)/1.957(1)	2.013(2)/2.018(2)	91.68(6)
1a(HS)	2.065(3)/2.080(3)	2.002(3)/2.012(3)	2.216(3)/2.217(3)	107.16(11)
1b	1.9	2.0	2.0	92
2a	2.1	2.0	2.1	100
2b	2.073(4)/ 2.085(4)	2.002(3)/ 1.980(3)	2.127(4)	101.62 (14)

One of the alkyl chains and the methanol molecule are disordered in the LS state. Due to increase of thermal motion of the atoms at higher temperatures, this disorder cannot be solved in the HS state. The relative orientation of the aromatic planes of the dmap to each other changes marginally from 89.3° to 88.1°, the N_{ax}–Fe–N_{ax} angle from 175.7° to 174.9° upon switching from the LS to the HS state, thus the axially ligands are nearly perpendicular in both spin states.

1b precipitated as spicular crystals, space group $P2_1/c$, from the synthetic approach with 50 fold excess of dmap and the X-ray structure was determined at 133 K. Due to insufficient quality of the data one can only talk about a motif. Average values of selected bond lengths and angles are summarised in Table 1.
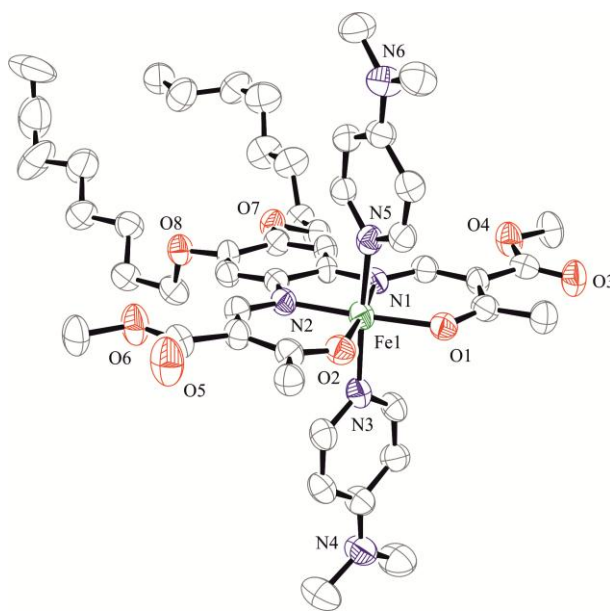
Figure 2. ORTEP drawing of **1b**. Ellipsoids are shown at the 50% probability level. Hydrogen atoms and methanol molecules are omitted for clarity.

Figure 2 shows the asymmetric unit of **1b**. At the temperature used for the determination of the X-ray structure the complex should be in the LS state according to the magnetic measurements. Indeed, the bond lengths and angles within the first coordination sphere are very similar to those of **1a** in the LS state. The average values are 1.9 Å/2.0 Å for Fe–N_{eq} / Fe–O_{eq} and 2.0 Å for Fe–N_{ax}. The O–Fe–O angle is about 92°, the N_{ax}–Fe–N_{ax} angle is 174° and the dmap rings are twisted towards each other in an angle of around 94° and are therefore also nearly perpendicular. The main difference between the two samples lies in the additional half of a solvent molecule, the conformation (orientation of the alkyloxy chains) and the packing of the molecules in the crystal.

In the molecular packing of **1a**, displayed in Figure 3 for the LS state, the disordered methanol molecule forms a hydrogen bond to the O5 atom in the outer periphery of the equatorial ligand. This hydrogen bond is weakened in the HS state. A few further short contacts (more than 0.2 Å shorter than the sum of the vdW radii) are observed, that are given in Table 2. The major distinction between the molecule packing of **1a** compared to the previously discussed structures is the absence of a lipid layer like structure. Instead, the axial dmap ligand of one complex is "embraced" from the C8 chains of the neighbouring complex.

For the previously published structures the distance between the alkyl chains are between 0.3 and 0.4 Å longer than the sum of the vdW radii, indicative for stabilising interactions between the chains.[11,12] For **1a** in the LS state several short contacts are observed between the alkyl chains, and the alkyl chains and the embraced dmap, respectively. However, the contacts are too short to be considered for a stabilising effect. In the HS state they are a bit longer. The strength of such stabilising interactions (London dispersion forces) depends on the length of the alkyl chains. Obviously, for the complex discussed here, the C8 alkyl chains are not long enough to form lipid layer like structures.
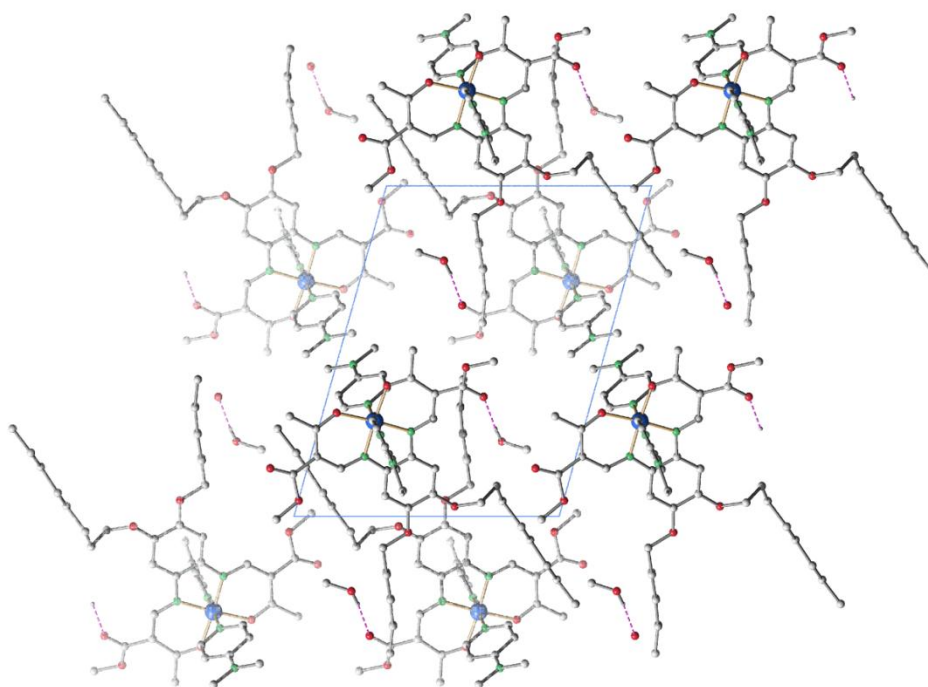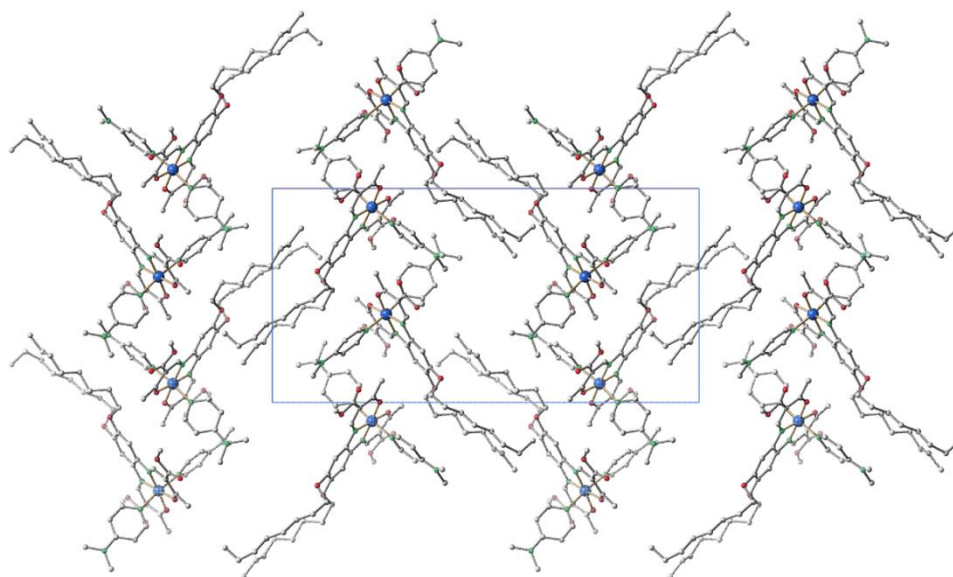

Figure 3. Molecular packing of **1a**(LS) along [1 0 0]. Hydrogen bonds are drawn as dashed lines. Disorder omitted for clarity.

Table 2. Short contacts and hydrogen bonds /Å and corresponding angle /° of the obtained crystal structures.

	D—H···A	D—H	H···A	D···A	D—H···A
1a(LS)	C47—H47B···O7[a]	0.98	2.60	3.436(3)	143
	C29A—H29B···C42[b]	0.97	2.637	3.519(8)	151
	C41—H41C···O2[c]	0.98	2.57	3.393(3)	142
	O31B—H31F···O5[d]	0.84	1.92	2.760(3)	174
1a(HS)	C32—H32B···C6[e]	0.96	2.606	3.550(6)	165
	O9A—H9A···O5[f]	0.82	2.04	2.785(14)	151
2b	C23—H23C···O4[g]	0.98	2.400	3.347(7)	162

[a] 1+x, y, z; [b] 1−x, 1−y, −z; [c] 1−x, 2−y, 1−z; [d] x, y, z; [e] 1+x, y, z; [f] 1−x, 1−y, 1−z; [g] −1+x, y, z.

The packing of the molecules in the crystal of **1b** is very different to that of **1a** (Figure 4). Two molecules form pairs where the alkyl chains are arranged such that stabilising vdW interactions can be considered. The next pair is rotated by 90° with the two axial dmap ligands pointing together. As only a structural motif is obtained, no intermolecular contacts can be discussed. It can, however, be pointed out that, as for **1a**, no lipid layer like arrangement of the complex molecules is obtained.

Figure 4. Molecular packing of **1b** along [1 0 0]. Methanol molecules omitted for clarity.

The two penta-coordinated complexes crystallise in the space group $P2_1/c$ (**2a**) and $P\bar{1}$ (**2b**), respectively. In Figure 5 ORTEP drawings of the asymmetric units of **2a** and **2b** are displayed. In Table 1 selected bond lengths and angles within the first coordination sphere are given. For these two samples, no additional methanol molecules are included in the crystal packing.

Due to insufficient quality of the data of the spicular crystals of **2a**, only the conformation of the molecule is discussed in comparison to that of **2b**.
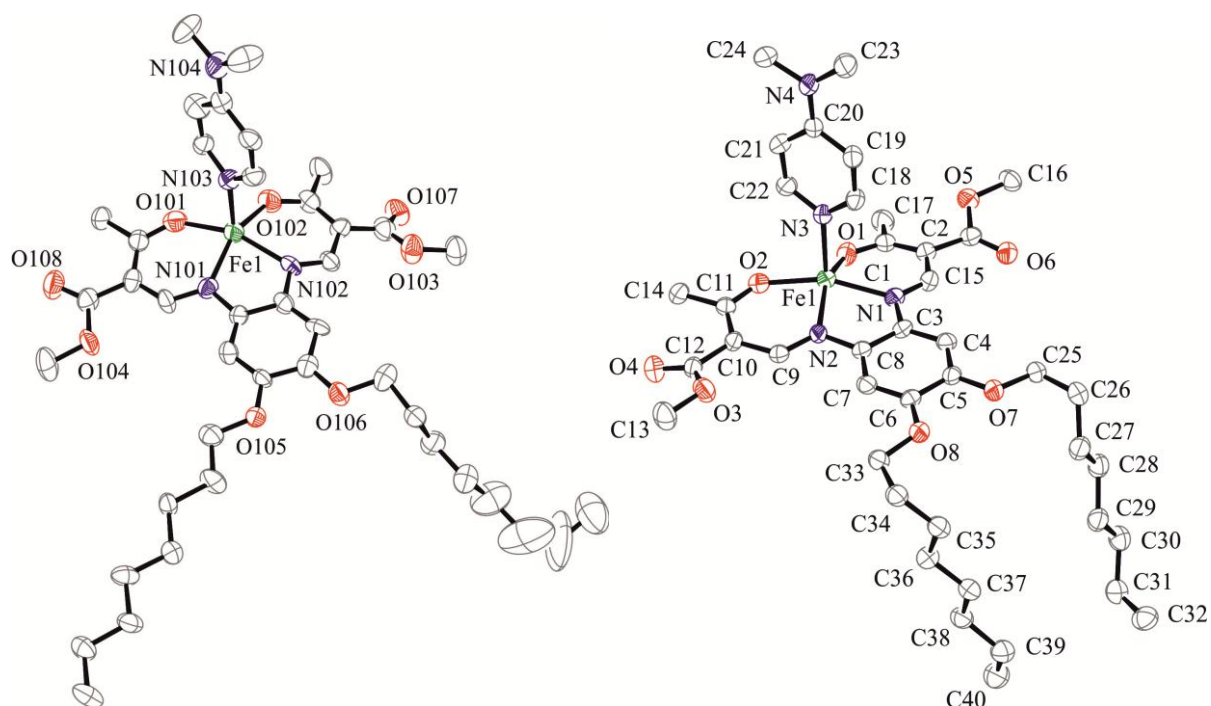

Figure 5. ORTEP drawing of **2a** (left) and **2b** (right). Ellipsoids are shown at the 50% probability level. Hydrogen atoms are omitted for clarity.

The average bond lengths of the inner coordination spheres of the two penta-coordinated species are with about 2.1 Å (Fe–N_{eq}) and 2.0 Å (Fe–O_{eq}) very similar to the lengths of the HS structure of **1a** and in the same order of magnitude as observed for other penta-coordinated complexes of this ligand system.[16,17] The Fe–N_{ax} bond lengths are about 0.1 Å shorter than in **1a**(HS), due to the penta-coordination. The O–Fe–O angles are with 100° in

the region expected for complexes with this kind of Schiff base-like ligands and are between the values of HS and LS state, respectively.[16,17]

In the case of **2a** the C8 alkyl chains are spread widely out with an angle of almost 90° between the two chains. In contrast to this, for **2b** they are arranged parallel to each other, similar to **1b**. However, differently to **1b**, in **2b** the alkyl chains are not in plane with the axial ligand but bent by almost 90° in the direction of the axial dmap ligand.
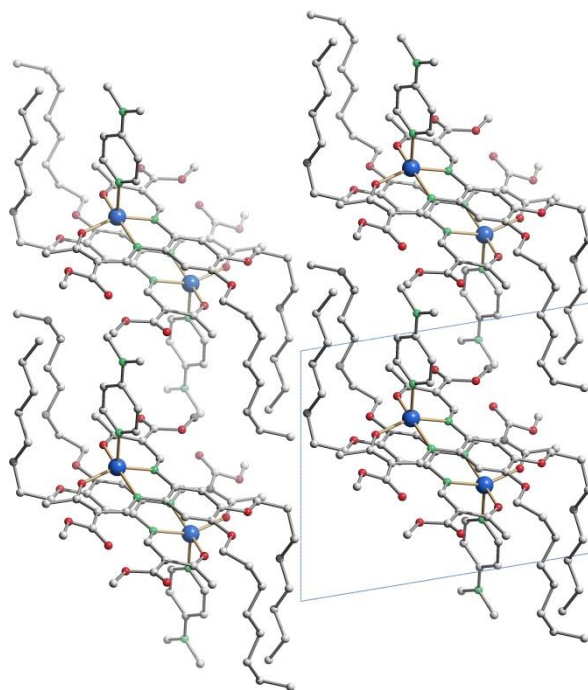

Figure 6. Molecular packing of **2b** along [1 0 0].

In Figure 6 the molecular packing in the unit cell of **2b** is displayed. In this case, pairs are build where the almost planar planes of the equatorial ligand including the iron(II) (the iron-N1N2O1O2 plane distance is 0.36 Å) are stacked above each other and the C8 alkyl chains are bended in the direction of the axial dmap of the neighbouring molecule. A short contact with a distance of 0.2 Å smaller than the sum of the vdW radii connects one molecule at the atom H23C of the dmap ligand with the oxygen atom O4 of the outer periphery of the ligand of the neighbouring molecule. The dmap ligands are arranged parallel to each other and also almost parallel to the alkyl chains. The same is observed for the alkyl chains that are themselves arranged parallel to each other. That means that the alkyl chains of one molecule

are again interacting with the chains of another molecule whose axial ligand points to the opposite direction so that they form a lipid layer like arrangement. The distances between the alkyl chains support the idea of stabilising vdW interactions. Additionally, the distances between the stacked planes of the equatorial ligand (about 3.5 Å) suggest stabilising π-π-interactions.

6.2.3   Magnetic measurements

Temperature dependent magnetic measurements in the 325–10 K range were performed for all complexes discussed in this work. Additionally, the temperature dependent magnetic susceptibility was determined in a methanol solution of the iron complex **1** with a 50 fold excess of dmap. The concentration of the complex in the solution is *ca.* 14.5 mg/mL. The presence of the octahedral complex [Fe(L)(dmap)$_2$] in solution was confirmed by the colour change upon cooling due to the spin transition. This is illustrated in the Supporting Information, Figure S4. In Figure 7 the results for **1a**, **1b** and for the methanol solution of the complex are given. At 325 K **1a** is in the high spin state, with a $\chi_M T$ value of 3.15 cm^{3}Kmol^{-1}. Upon cooling a gradual decrease of the $\chi_M T$ product down to 2.10 cm^{3}Kmol^{-1} at 255 K is observed, where a small plateau is visible. Further cooling causes a slow drop of the $\chi_M T$ product until the compound is in the low spin state at about 100 K (0.17 cm^{3}Kmol^{-1}). The plateau is due to a mixture of powder and crystalline parts in the sample used for the magnetic measurements. According to X-ray structure analysis the crystals contain disordered methanol molecules. Results from CHN analysis indicate the absence of additional methanol molecules in the fine crystalline bulk material. The step and the small hysteresis disappear completely if the compound is measured again after complete removal of the methanol. This is confirmed by a measurement on freshly prepared crystals (**1c**) where in the first cycle an apparent hysteresis is observed (see Supporting Information, Figure S3) that is lost in a second cycle. The transition curve of sample **1a** can be reproduced by displaying a combined curve of the weighted contributions (50:50) of **1b** and **1c**.

The magnetic properties of **1b** are very similar to that of **1a**. The spin transition is very gradual and complete and takes place in the same temperature region. The $\chi_M T$ value at 325 K is with 3.10 cm^{3}Kmol^{-1} comparable to that of **1a**. Decreasing of the temperature leads to a gradual decrease of the $\chi_M T$ product until 120 K (0.31 cm^{3}Kmol^{-1}) where a small plateau can

be observed. At 100 K the compound is completely in the LS state ($\chi_M T = 0.06$ cm^{3}Kmol^{-1}). Although methanol molecules are included in the crystal packing of **1b**, they are strongly disordered and are, apparently, not involved in cooperative interactions as a very gradual spin transition is observed.
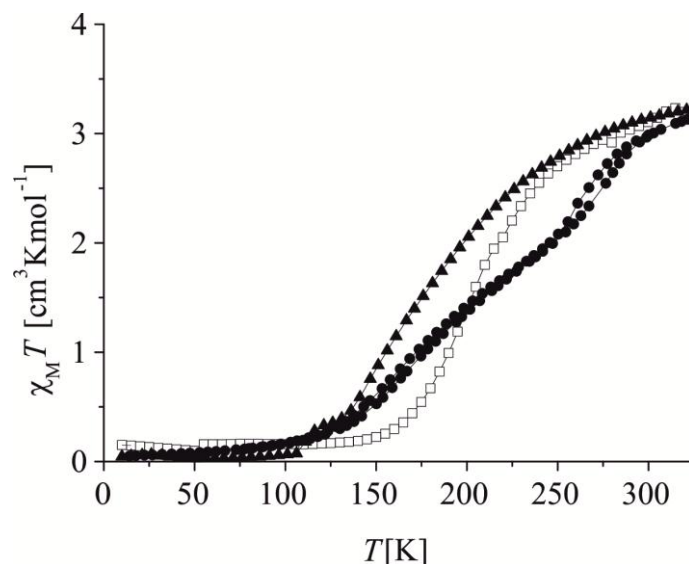

Figure 7. Magnetic measurement of **1a** (circles), **1b** (triangles) and a methanol solution of **1** with a 50 fold excess of dmap (open squares) in the temperature range of 325–10 K.

In Figure S2, Supporting Information, the spin transition curves of the products of the different synthetic approaches are compared. The penta-coordinated samples (**2a**, **2b** and **2** from the approach with 20 fold excess of dmap) remain as expected in the HS state. The $\chi_M T$ vs. *T* plot of **2** is shown as typical example. All samples, where 50 equivalents of dmap and more was used, show the same kind of spin transition as **1b**, independent of additional solvent or dmap molecules in the crystal packing. This is unexpected as for spin transition compounds often significant changes in the spin transition behaviour are observed, if the crystal packing is slightly modified or additional solvent molecules are included. The behaviour observed for the different samples of **1** indicates the total absence of cooperative interactions, thus the spin transition should be comparable to that of the complex is solution. As can be seen in Figure 7, indeed the transition curves are almost identical. Only the transition temperature is shifted to slightly higher temperatures in solution.

It was already shown that abrupt ST is realisable with compounds that bear lipid layer like arrangements.[12] The increase of vdW interactions influences the packing in the crystal through the formation of lipid layer like arrangements and by this cooperative effects like a network of hydrogen bonds between the polar groups can be enhanced. For the complexes described here, no layered structure can be achieved because of the relatively short C8 alkyl chains. Additionally, the molecule is very bulky and the volume change upon spin transition relative to the overall volume is relatively small and almost in the region of the thermal contraction. Therefore, cooperativity is decreased in the crystal and only a gradual SCO as in solution is observed. This is the reason why the spin transition is independent of the conformation of the molecule and the crystal packing. A similar effect was recently described for the nanostructuring of mononuclear complexes.[19]

6.3   Conclusion

In this article, several molecular setups and arrangements of hexa- and penta-coordinated amphiphilic iron(II) complexes **1a**(HS), **1a**(LS), **1b**, **2a** and **2b** with dimethylaminopyridine as axial ligands were investigated with the help of X-ray structure analysis and magnetic measurements. The complex can precipitate hexa-coordinated as well as penta-coordinated depending on the excess taken of the axial ligand. With 30 equivalents of dmap the system can crystallise in both modifications, below this value it is penta-coordinated and above, it can be forced to crystallise hexa-coordinated. In the case of the octahedral complexes **1a** and **1b**, a gradual spin crossover can be observed starting at about 325 K in the high spin state and ending at about 125 K in the low spin state. It should be pointed out that the spin transition is always the same despite the significant differences in the composition and crystal packing of the different samples. The crystal structures show no lipid layer like arrangement due to the relatively short C8 alkyl chains. In the crystal packing of the penta-coordinated compound vdW interactions between the C8 alkyl chains are observed. This in combination with the π-π-interactions could be the reason for the complex to precipitate penta-coordinated up to a relatively high excess of the used dmap ligand. The gradual spin transition behaviour can be explained with missing lipid layer like arrangement and the absence of other factors that are responsible for cooperative interactions. Thus the same spin transition as in solution is observed.

6.4   Experimental Section

Synthesis

The synthesis of the iron complexes were carried out under an argon atmosphere using Schlenk tube techniques. The solvents therefore were purified as described in the literature[20] and distilled under an atmosphere of argon. The precursors methoxymethylenemethylacetoacetate,[21] iron(II) acetate,[14] 1,2-dioctyloxybenzene, 1,2-dinitro-4,5-dioctyloxybenzene, 1,2-diamino-4,5-dioctyloxybenzene,[22] were synthesised as described.

(*E*,*E*)[{dimethyl-2,2'[4,5-dioctyloxy-1,2phenylenebis(iminomethylidyne)]bis-3-oxobutanato}] (**H₂L**) Under argon, 2.1 g (5.76 mmol) 1,2-diamino-4,5-dioctyloxybenzene and 2.4 g (15.18 mmol, 2.6 eq.) methoxymethylenemethylacetoacetate were dissolved in 60 mL degassed ethanol and the yellow solution was heated to reflux for 90 min. After storing the reaction mixture at 5°C overnight, the precipitate was collected, washed with ethanol and recrystallised from 35 mL ethanol. The bright yellow fine crystalline ligand was dried on air. Yield: 3.1 g (87 %). Elem. anal. calcd. for $C_{34}H_{52}N_2O_8$ (616.79 g/mol): C 66.21, H 8.50, N 4.54; found: C 66.64, H 9.28, N 4.64. MS (DEI+): *m/z* (%) = 616 (100) $[M]^+$, 584 (62), 552 (61) 501 (54). ^{1}H NMR (299.86 MHz, CDCl$_3$, 298 K): δ = 0.90 (t, J = 6.8 Hz, 6H, CH$_3$), 1.30–1.40 (m, 16 H, CH$_2$), 1.45–1.55 (m, 4H, CH$_2$), 1.80–1.89 (m, 4H, CH$_2$), 2.57 (s, 6H, CH$_3$), 3.79 (s, 6H, CH$_3$), 4.03 (t, 4H, J = 6.5 Hz, CH$_2$O), 6.76 (s, 2H, H$_{ar}$), 8.28 (d, 2H, J = 12.5 Hz, CH=), 12.90 (d, 2H, J = 12.5 Hz, NH) ppm. ^{13}C NMR (75.40 MHz, CDCl$_3$, 298 K): δ = 14.3 (CH$_3$), 22.9 (CH$_2$), 26.2 (CH$_2$), 29.4 (CH$_2$), 29.5 (CH$_2$), 29.6 (CH$_2$) 31.3 (CH$_3$), 32.1 (CH$_2$), 45.0 (C$_q$), 51.5 (CH$_3$), 70.3 (CH$_2$, CH$_2$O), 103.7 (C$_q$), 106.7 (CH, C$_{ar}$), 125.0 (C$_q$, C$_{ar}$–N), 148.8 (C$_q$, C$_{ar}$–O), 154.3 (CH), 167.4 (O–C=O), 200.4 (C=O) ppm. IR: $\tilde{\nu}$ = 1699 s, 1612 vs, 1521 m, 1420 m, 1243 vs, 1189 vs, 1081 vs.

[Fe(L)(MeOH)₂] 1.5 g (2.43 mmol) **H₂L** and 0.85 g (4.86 mmol, 2 eq.) iron(II) acetate were dissolved in 100 mL methanol and the brown solution was heated to reflux for 1 h. After cooling to room temperature, the brown precipitate was collected, washed twice with 10 mL methanol and dried in vacuum. Yield: 1.35 g (76 %). Elem. anal. calcd. for $C_{36}H_{58}FeN_2O_{10}$ (734.80 g/mol): C 58.85, H 7.96, N 3.81; found: C 59.29, H 7.86, N 4.16. IR: $\tilde{\nu} =$ 2925 m, 2854 w, 1706 m, 1577 s, 1506 w, 1429 s, 1384 s, 1258 vs, 1214 s, 1069 vs, 998 m, 841 m, 769 m.

[Fe(L)(dmap)₂] (**1/1a**) 0.27 g (0.37 mmol) **[Fe(L)(MeOH)₂]** and 1.35 g (11.05 mmol, 30 eq.) dmap were dissolved in 15 mL methanol and heated to reflux for 70 min. After storing the solution at 5°C for 14 d, greenish-black crystals (**1a**) were filtrated and dried in vacuum. Yield: 0.01 g (3 %, crystals), 0.15 g (44 %, fine crystalline powder, **1/1a**) Elem. anal. calcd. for $C_{48}H_{70}FeN_6O_8$ (fine crystalline powder, no methanol included) (914.95 g/mol): C 63.01, H 7.71, N 9.19; found: C 62.67, H 7.78, N 9.59.

[Fe(L)(dmap)] (**2a**) 0.25 g (0.34 mmol) **[Fe(L)(MeOH)₂]** and 1.25 g (10.21 mmol, 30 eq.) dmap were dissolved in 10 mL methanol and heated to reflux for 60 min. After 1 d at room temperature the reaction mixture was stored at −30°C for 3 d. Black crystals precipitated that were filtrated, washed with 2.5 mL methanol and dried in vacuum. Yield: 0.13 g (48 %). Elem. anal. calcd. for $C_{41}H_{60}FeN_4O_8$ (792.78 g/mol): C 62.12, H 7.63, N 7.07; found: C 61.79, H 7.44, N 7.30.

[Fe(L)(dmap)] (**2b**) 0.18 g (0.25 mmol) **[Fe(L)(MeOH)₂]** and 0.90 g (7.37 mmol, 30 eq.) dmap were dissolved in 15 mL methanol and heated to reflux for 60 min. After 5 weeks at room temperature, black needles precipitated that were filtrated and dried in vacuum. Yield: 0.05 g (22 %). $C_{41}H_{60}FeN_4O_8$ (792.78 g/mol). Elem. anal. not possible due to insufficient amount of product. IR: $\tilde{\nu} =$ 2923 m, 2853 w, 1693 m, 1579 s, 1433 s, 1387 s, 1255 vs, 1212 vs, 1065 vs, 1008 s, 804 m, 768 m.

[Fe(L)(dmap)] (20 eq.) 0.25 g (0.34 mmol) **[Fe(L)(MeOH)₂]** and 0.83 g (6.8 mmol, 20 eq.) dmap were dissolved in 15 mL methanol and heated to reflux for 60 min. After 1 d at room temperature, black crystals and brown powder were filtrated and dried in vacuum. Yield:

0.12 g (44 %). Elem. anal. calcd. for $C_{41}H_{60}FeN_4O_8$ (792.78 g/mol): C 62.12, H 7.63, N 7.07; found: C 61.80, H 7.81, N 7.21.

[Fe(L)(dmap)₂] (30 eq.) 0.25 g (0.34 mmol) **[Fe(L)(MeOH)₂]** and 1.25 g (10.2 mmol, 30 eq.) dmap were dissolved in 15 mL methanol and heated to reflux for 60 min. After 1 d at room temperature and 10 d at 6°C black crystals and brown powder were filtrated and dried in vacuum. Yield: 0.16 g (51 %). Elem. anal. calcd. for $C_{48}H_{70}FeN_6O_8$ (914.95 g/mol): C 63.01, H 7.71, N 9.19; found: C 62.77, H 8.15, N 9.30.

[Fe(L)(dmap)₂] (**1b**) (50 eq.) 0.27 g (0.37 mmol) **[Fe(L)(MeOH)₂]** and 2.25 g (18.4 mmol, 50 eq.) dmap were dissolved in 15 mL methanol and heated to reflux for 70 min. After 1 d at room temperature, 16 d at 6°C and 1 d at −30°C black crystals were filtrated, washed with 3 mL methanol and dried in vacuum. Yield: 0.05 g (15 %). Elem. anal. calcd. for $C_{48}H_{70}FeN_6O_8$ (no methanol included) (914.95 g/mol): C 63.01, H 7.71, N 9.19; found: C 62.87, H 8.03, N 9.66.

[Fe(L)(dmap)₂] (70 eq.) 0.25 g (0.34 mmol) **[Fe(L)(MeOH)₂]** and 2.91 g (23.8 mmol, 70 eq.) dmap were dissolved in 15 mL methanol and heated to reflux for 60 min. After 1 d at room temperature, 14 d at 6°C and 13 d at −30°C black crystals were filtrated and dried in vacuum. Yield: 0.15 g (48 %). Elem. anal. calcd. for $C_{48}H_{70}FeN_6O_8 \times$ dmap (1037.12 g/mol): C 63.69, H 7.77, N 10.80; found: C 63.79, H 8.39, N 10.87.

[Fe(L)(dmap)₂] (90 eq.) 0.25 g (0.34 mmol) **[Fe(L)(MeOH)₂]** and 3.74 g (30.6 mmol, 90 eq.) dmap were dissolved in 15 mL methanol and heated to reflux for 60 min. After 1 d at room temperature, 14 d at 6°C and 5 d at −30°C black crystals were filtrated and dried in vacuum. Yield: 0.16 g (51 %). Elem. anal. calcd. for $C_{48}H_{70}FeN_6O_8 \times 2$ dmap $\times 0.5$ MeOH (1175.31 g/mol): C 63.87, H 7.89, N 11.92; found: C 64.06, H 8.24, N 11.68.

[Fe(L)(dmap)₂] (110 eq.) 0.25 g (0.34 mmol) **[Fe(L)(MeOH)₂]** and 4.57 g (37.4 mmol, 110 eq.) dmap were dissolved in 15 mL methanol and heated to reflux for 60 min. After 1 d at room temperature, 10 d at 6°C and 4 d at −30°C, black fine crystalline powder was filtrated and dried in vacuum. Elem. anal. calcd. for $C_{48}H_{70}FeN_6O_8 \times 2$ dmap $\times 0.5$ MeOH (1175.31 g/mol): C 63.87, H 7.89, N 11.92; found C 64.05, H 8.63, N 11.82.

Magnetic measurements on the bulk materials were carried out with a SQUID MPMS-XL5 from Quantum Design with an applied field of 1000, 2000 and 5000 G, respectively, and in the temperature range from 325 to 10 K in the sweep and settle mode. The sample was prepared in a gelatine capsule held in a plastic straw. The raw data was corrected for the diamagnetic part of the sample holder and the diamagnetism of the organic ligand using tabulated Pascal's constants.

For the measurements in solution the sample was prepared in the plastic straw and measured in the settle mode with an applied field of 20000 G. The raw data were corrected for the diamagnetism of the solution and the diamagnetism of the organic ligand using tabulated Pascal's constants.

X-ray Diffraction: The intensity data of **1a**(LS), **1a**(HS), **1b**, **2a** and **2b** were collected with a Stoe IPDS II diffractometer using graphite-monochromated Mo-K_α radiation. The data were corrected for Lorentz and polarisation effects. **1a**(LS) **1b**, **2a** and **2b** (Sir97)[23], **1a**(HS) (SHELXS-97)[24] were solved by direct methods and refined by full-matrix least-square techniques against F_0^2 (SHELXL-97).[24] The hydrogen atoms were included at calculated positions with fixed displacement parameters, allowed to ride on their parent atoms. If not noted differently, for methyl groups and hydroxyl groups the torsion angles were allowed to be refined according to the electron density. For the hydroxyl groups O99-H9A (**1a**), O98–H98 and O99–H99 (both **1b**) no stable refinement was achieved thus idealised torsion angles were used. All non-hydrogen atoms were refined anisotropically. Due to bad quality of the data of **1b** (bad R$_{int}$) and **2a** only the general molecular setup could be investigated. For **2a**, twin refinement was conducted based on twin law

$$\begin{pmatrix} -1.000 & 0.000 & 0.000 \\ 0.000 & -1.000 & 0.000 \\ 0.396 & 0.000 & 1.000 \end{pmatrix}$$

found by PLATON.[25] ORTEP-III[26] was used for the structure representation, Schakal-99[27] and Mercury[28] for the representation of the molecule packing.

6.5 References

[1] L. Cambi and L. Szegö, *Ber. dtsch. Chem. Ges. A/B* **1933**, *66*, 656–661.

[2] M. A. Halcrow, ed., *Spin-Crossover Materials*, John Wiley & Sons Ltd, Oxford, UK, **2013**.

[3] P. Gütlich and H. Goodwin, eds., *Spin Crossover in Transition Metal Compounds I-III*, Springer Berlin / Heidelberg **2004**, 233–235.

[4] a) S. Hayami, Y. Komatsu, T. Shimizu, H. Kamihata and Y. H. Lee, *Coord. Chem. Rev.* **2011**, *255*, 1981–1990. b) C. Gandolfi, T. Cotting, P. N. Martinho, O. Sereda, A. Neels, G. G. Morgan and M. Albrecht, *Dalton Trans.* **2011**, *40*, 1855–1865. c) P. N. Martinho, C. J. Harding, H. Müller-Bunz, M. Albrecht and G. G. Morgan, *Eur. J. Inorg. Chem.* **2010**, 675–679. d) Y. Komatsu, K. Kato, Y. Yamamoto, H. Kamihata, Y. H. Lee, A. Fuyuhiro, S. Kawata and S. Hayami, *Eur. J. Inorg. Chem.* **2012**, 2769–2775. e) Y. Bodenthin, U. Pietsch, H. Möhwald and D. G. Kurth, *J. Am. Chem. Soc.* **2005**, *127*, 3110–3114. f) A. B. Gaspar, M. Seredyuk and P. Gütlich, *Coord. Chem. Rev.* **2009**, *253*, 2399–2413.

[5] P. Grondin, O. Roubeau, M. Castro, H. Saadaoui, A. Colin and R. Clérac, *Langmuir* **2010**, *26*, 5184–5195.

[6] A. Gaspar, M. Seredyuk and P. Gütlich, *J. Mol. Struc.* **2009**, *924-926*, 9–19.

[7] a) S. M. Neville, C. Etrillard, S. Asthana and J.-F. Létard, *Eur. J. Inorg. Chem.* **2010**, *2*, 282–288. b) V. Martínez, I. Boldog, A. B. Gaspar, V. Ksenofontov, A. Bhattacharjee, P. Gütlich and J. A. Real, *Chem. Mater.* **2010**, *22*, 4271–4281. c) J. R. Galán-Mascarós, E. Coronado, A. Forment-Aliaga, M. Monrabal-Capilla, E. Pinilla-Cienfuegos and M. Ceolin, *Inorg. Chem.* **2010**, *49*, 5706–5714.

[8] a) C. Thibault, G. Molnár, L. Salmon, A. Bousseksou and C. Vieu, *Langmuir* **2010**, *26*, 1557–1560. b) M. Cavallini, I. Bergenti, S. Milita, G. Ruani, I. Salitros, Z.-R. Qu, R. Chandrasekar and M. Ruben, *Angew. Chem.* **2008**, *120*, 8724–8728. c) C. M. Quintero, I. A. Gural'skiy, L. Salmon, G. Molnar, C. Bergaud and A. Bousseksou, *J. Mater. Chem.* **2012**, *22*, 3745–3751. d) A. D. Naik, L. Stappers, J. Snauwaert, J. Fransaer and Y. Garcia, *Small* **2010**, *6*, 2842–2846.

[9] a) B. Weber, W. Bauer, T. Pfaffeneder, M. M. Dîrtu, A. D. Naik, A. Rotaru and Y. Garcia, *Eur. J. Inorg. Chem.* **2011**, 3193–3206. b) B. Weber, W. Bauer and J. Obel, *Angew. Chem. Int. Ed.* **2008**, *47*, 10098–10101.

[10]   a) M. Seredyuk, A. B. Gaspar, V. Ksenofontov, Y. Galyametdinov, J. Kusz and P. Gütlich, *J. Am. Chem. Soc.* **2008**, *130*, 1431–1439. b) M. Seredyuk, A. B. Gaspar, V. Ksenofontov, Y. Galyametdinov, J. Kusz and P. Gütlich, *Adv. Funct. Mater.* **2008**, *18*, 2089–2101.

[11]   S. Schlamp, P. Thoma, B. Weber and Y. Garcia, *Eur. J. Inorg. Chem.* **2012**, *16*, 2759–2768.

[12]   S. Schlamp, B. Weber, A. D. Naik and Y. Garcia, *Chem. Commun.* **2011**, *47*, 7152–7154.

[13]   S. Hayami, Y. Kojima, D. Urakami, K. Ohta and K. Inoue, *Polyhedron* **2009**, *28*, 2053–2057.

[14]   B. Weber, R. Betz, W. Bauer and S. Schlamp, *Z. Anorg. Allg. Chem.* **2011**, *637*, 102–107.

[15]   B. Weber, *Coord. Chem. Rev.* **2009**, *253*, 2432–2449.

[16]   B. Weber and E.-G. Jäger, *Eur. J. Inorg. Chem.* **2009**, 465–477.

[17]   S. Schlamp, J. Schulten, R. Betz, T. Bauch, A. V. Mudring and B. Weber, *Z. Anorg. Allg. Chem.* **2012**, *638*, 1093–1102.

[18]   a) B. Weber, E. Kaps, J. Weigand, C. Carbonera, J.-F. Létard, K. Achterhold and F. G. Parak, *Inorg. Chem.* **2008**, *47*, 487–496. b) B. Weber, J. Obel, D. Henner-Vasquez and W. Bauer, *Eur. J. Inorg. Chem.* **2009**, 5527–5534.

[19]   A. Tissot, L. Rechignat, A. Bousseksou and M.-L. Boillot, *J. Mater. Chem.* **2012**, *22*, 3411.

[20]   H. G. O. Becker, *Organikum.* Organisch-chemisches Grundpraktikum, Johann Ambrosius Barth, Berlin, 19th edn., **1993**.

[21]   W. Bauer, T. Ossiander and B. Weber, *Z. Naturforsch. B* **2010**, 323–328.

[22]   a) M. J. Howard, F. R. Heirtzler and S. I. G. Dias, *J. Org. Chem.* **2008**, *73*, 2548–2553. b) W. M. Lauer, C. Rondestvedt, R. T. Arnold, N. L. Drake, J. van Hook and J. Tinker, *J. Am. Chem. Soc.* **1946**, *68*, 1546–1548. c) M. Schlögl and B. Rieger, *Z. Naturforsch. B* **2004**, 233–240. d) K. Tahara, S. Furukawa, H. Uji-i, T. Uchino, T. Ichikawa, J. Zhang, W. Mamdouh, M. Sonoda, F. C. de Schryver, S. de Feyter and Y. Tobe, *J. Am. Chem. Soc.* **2006**, *128*, 16613–16625.

[23]   A. Altomare, M. C. Burla, M. Camalli, G. L. Cascarano, C. Giacovazzo, A. Guagliardi, A. G. G. Moliterni, G. Polidori, R. Spagna, *J. Appl. Crystallogr.* **1999**, *32*, 115–119.

[24]   G. Sheldrick, *Acta Crystallogr., Sect. A* **2008**, *64*, 112–122.

[25]   A. L. Spek, *PLATON - A Multipurpose Crystallographic Tool*, Utrecht University, Utrecht, The Netherlands, **2008**.

[26]   a) C. K. Johnson, M. N. Burnett, *ORTEP-III*, Oak-Ridge National Laboratory, Oak-Ridge, TN, **1996**; b) L. Farrugia, *J. Appl. Crystallogr.* **1997**, *30*, 565.

[27]   E. Keller, *Schakal-99*, University of Freiburg, Germany, **1999**.

[28]   C. F. Macrae, P. R. Edgington, P. McCabe, E. Pidcock, G. P. Shilds, R. Taylor, M. Towler, J. van de Streek, *J. Appl. Crystallogr.* **2006**, *39*, 453–457.
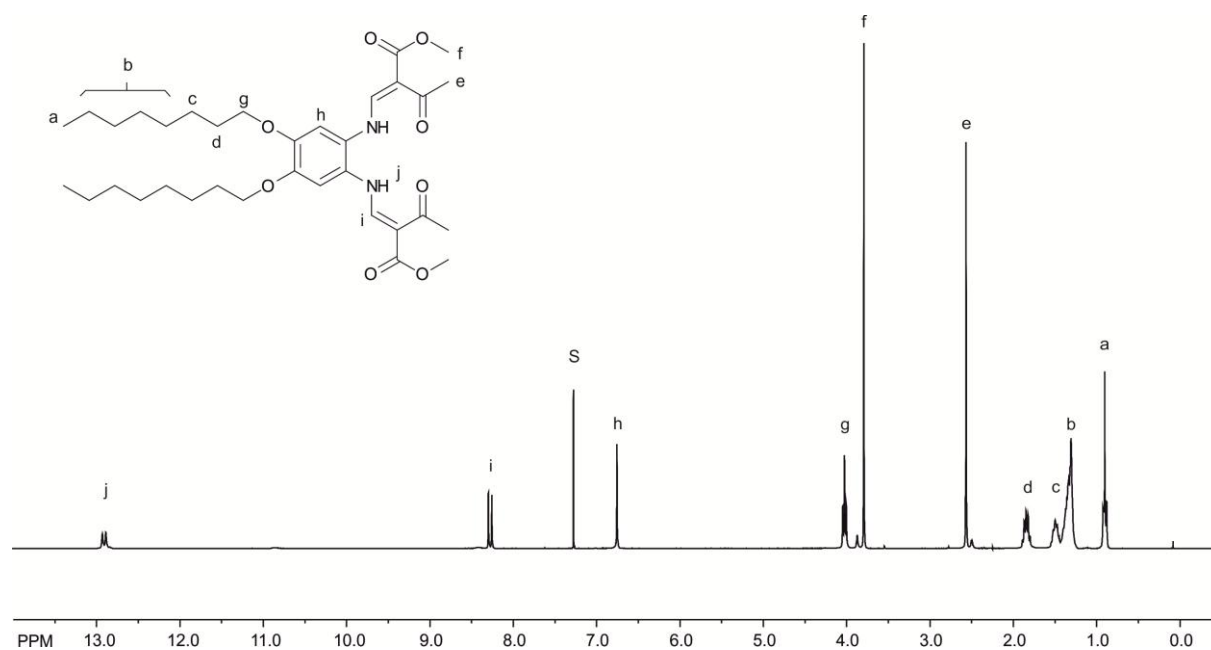
6.6   Supporting Information

Figure S1. ^{1}H NMR of the ligand **H$_2$L** (left). S denotes the residual solvent.

Table S1. Parameters for crystal structure determination of **1a**(HS), **1a**(LS), **1b**, **2a** and **2b**.

Compound reference	**1a**(HS)	**1a**(LS)	**1b**
Chemical formula	$C_{48}H_{70}FeN_6O_8 \cdot MeOH$	$C_{48}H_{70}FeN_6O_8 \cdot MeOH$	$C_{48}H_{70}FeN_6O_8$ $\cdot 1.5MeOH$
M_r/g mol^{-1}	946.99	946.99	963.01
crystal dimensions /mm	0.20×0.27×0.40	0.37×0.40×0.42	0.14×0.19×0.39
radiation /nm	0.71073	0.71073	0.71073
crystal system	triclinic	triclinic	monoclinic
a /Å	12.0361(8)	11.9287(5)	10.599(5)

b /Å	13.4241(10)	13.1406(5)	31.295(5)
c /Å	17.3275(13)	17.0569(7)	15.997(5)
α /°	103.289(6)	103.154(3)	90
β /°	101.608(6)	100.508(3)	101.404(5)
γ /°	99.935(6)	100.246(3)	90
Unit cell volume /Å^3	2597.7(3)	2491.76(18)	5201(3)
Temperature /K	273	133	133
space group	$P\bar{1}$	$P\bar{1}$	$P2_1/c$
Z	2	2	4
μ /mm^{-1}	0.347	0.362	0.349
No. of reflections measured	31745	30301	56290
No. of independent reflections	8697	8344	8715
R_{int}	0.154	0.073	0.185
Final R_1 values ($I > 2\sigma(I)$)	0.0660	0.0384	0.0852
Final R_1 values (all data)	0.1055	0.0531	0.1626
Final $wR(F^2)$ values ($I > 2\sigma(I)$)	0.1737	0.0975	0.2514
Goodness of fit on F^2	0.87	0.93	0.93
CCDC number	CCDC 944437	CCDC 944436	CCDC 944434

Compound reference	**2a**	**2b**
Chemical formula	$C_{41}H_{60}FeN_4O_8$	$C_{41}H_{60}FeN_4O_8$
M_r /g mol^{-1}	792.78	792.78

crystal dimensions /mm	0.20×0.26×0.34	0.11×0.12×0.29
radiation /nm	0.71073	0.71073
crystal system	monoclinic	triclinic
a /Å	19.8161(9)	11.9872(7)
b /Å	8.2415(4)	12.5380(8)
c /Å	25.5905(11)	14.6613(10)
α /°	90	95.394(5)
β /°	98.224(3)	102.327(5)
γ /°	90	106.231(5)
Unit cell volume /Å^3	4136.3(3)	2039.0(2)
Temperature /K	133	133
space group	$P2_1/c$	$P\bar{1}$
Z	4	2
μ /mm^{-1}	0.419	0.425
No. of reflections measured	38465/5508	24231
No. of independent reflections	5508	6827
R_{int}	0.00 (0.142)*	0.142
Final R_1 values ($I > 2\sigma(I)$)	0.1008	0.0632
Final R_1 values (all data)	0.1147	0.1335
Final $wR(F^2)$ values ($I > 2\sigma(I)$)	0.2606	0.1380
Goodness of fit on F^2	1.13	0.88
CCDC number	CCDC 944438	CCDC 944435

* new hkl file generated by PLATON. Original R_{int} in brackets.

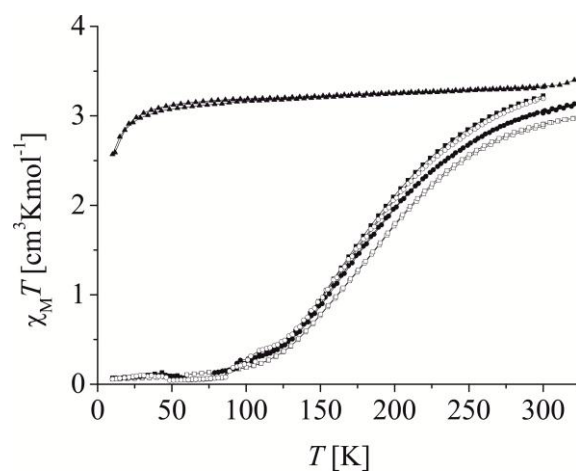**Figure S2**. Spin crossover behaviour of the reaction products of **[Fe(L)(MeOH)₂]** with 20 (triangles), 30 (open squares), 70 (cycles), 90 (squares) and 110 (open cycles) equivalents of dmap.
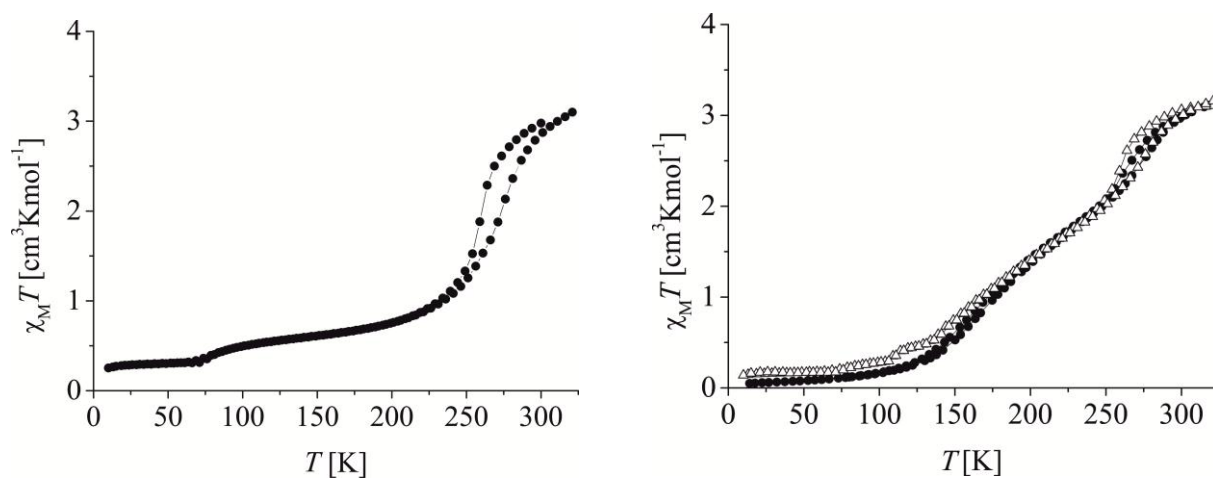

Figure S3. Left: Spin crossover behaviour of fresh crystals of **[Fe(L)(dmap)₂] (1c)**. Right: Spin transition curve of **1a** (cycles) and combined curve of the 50:50 weighted contributions of the spin transition curves of **1b** and **1c** (open triangles).

Figure S4. Left: appearance of the high spin state of the solution of **[Fe(L)(MeOH)₂]** with 50 equivalents of dmap. Right: low spin state of the solution after cooling with liquid nitrogen.

7 Influence of the Alkyl Chain Length on the Self-assembly of Amphiphilic Iron Complexes – An Analysis of X-ray Structures

Stephan Schlamp,[a] Peter Thoma,[a] Birgit Weber*[a]

[a] Lehrstuhl für Anorganische Chemie II, Universität Bayreuth, Universitätsstraße 30, NW 1, 95440 Bayreuth, Germany; Fax: +49-92155-2157; E-mail: weber@uni-bayreuth.de

Dedicated to Prof. Dr. I.-P. Lorenz on the occasion of his 70th birthday

Abstract: Several new amphiphilic iron complexes were synthesized and characterized by single crystal X-ray structure analysis. The Schiff base-like equatorial ligands contain long alkyl chains in their outer periphery with chain lengths of 8, 12, 16 and 22 carbon atoms. As axial ligands methanol, pyridine, 4-aminopyridine, 4-(dimethylamino)pyridine and 1,2-bis(4-pyridyl)ethane were used. X-ray structure analysis of the products reveals different coordination numbers, depending on the combination of equatorial and axial ligand. The driving force for this is the self-assembly to lipid layer-like arrangements. This can be controlled through the chain lengths and the dimension of the axial ligands in a crystal-engineering-like approach. For this an empiric rule is introduced concerning the crystallization behaviour of the complexes. The efficacy of this rule is confirmed with the crystallization of an octahedral complex with two docosyl (C22) chains in the outer periphery. The rule is also applied to other ligand systems.

7.1   Introduction

Designing multifunctional materials is of great importance as they allow exploring many new potential applications. In this frame, adding additional properties to spin crossover (SCO) compounds would lead to materials that can not only be switched from the low spin (LS) to the high spin (HS) state through thermal excitation, or induced by light, pressure or host inclusion[1–5], but exhibit further functionalities. One possibility to introduce additional properties to such materials is the synthesis of amphiphilic spin crossover complexes. This could result in liquid crystalline behaviour of the material, where synergetic effects between phase transition and spin transition (ST) are possible.[6–12] Another interesting aspect is the self-assembly of such complexes in solution that might lead to the formation of micelles or inverse micelles and can influence the ST properties in solution.[13,14] Further the self-assembly of amphiphilic complexes on frontiers can be used for the formation of Langmuir-Blodgett (LB) films.[15] Thus such systems are not only of interest as bulk material but also for the nanostructuring of SCO materials. For a purposeful synthesis of such systems it is important to understand the self-assembly in solution as this will influence the behaviour on frontiers and the crystal packing in the bulk material.

For SCO complexes with iron(II), the most widely used metal ion in spin crossover research,[3] it is commonly necessary to synthesize octahedral complexes. Therefore, we designed N_2O_2-coordinating Schiff base-like equatorial ligands with long alkyl chains in the outer periphery (Scheme 1). In combination with various axial ligands, octahedral iron(II) complexes with thermal spin crossover activity can be realized,[16–18] and the influence of the hydrophobic substituents can be investigated. In a previous work we showed, that the amphiphilic complexes of this family can self-assemble to lipid layer-like arrangements,[16,17] with one of those complexes exhibiting a highly cooperative spin transition with a wide hysteresis loop.[17] The X-ray structure of this complex was solved before and after the spin transition, revealing that the volume change of the unit cell is very small ($\Delta V/V \approx 2.9$ %),[17] and in the region of thermal contraction. Despite of this an up to 47 K wide thermal hysteresis loop is observed that can be explained with a hydrogen bond network between the polar head groups of the amphipilic complexes and significant changes in the structure of the complex upon spin transition.[1,5,17] In contrast to this gradual spin transitions are observed for complexes with relatively short alkyl chain substituents.[16,18] The X-ray structure of one of

those complexes in the HS and the LS state reveals, that the volume change upon spin transition is higher compared to the example with the long alkyl chain. However, with $\Delta V/V \approx$ 4.0 % it is still small for a spin crossover complex.[18] For this example with a very gradual spin transition no lipid layer-like structure was observed.

There appears to be a connection between the appearance of lipid layer-like (lamellar) structures and the cooperativity of the spin transition. Additionally lamellar arrangements are interesting for further nanostructuring (e.g., LB-film formation) or with regard to potential liquid crystalline properties. Thus, the question arises if there are factors which we can control in a crystal-engineering-like approach to obtain the desired lamellar structural motif. A second question to be answered is how to control the formation of octahedral complexes. First investigations on a system with short octyl chains demonstrated that often unwanted penta-coordinated products are obtained.[18]

It is difficult to investigate the self-assembly of the highly air sensitive iron(II) complexes directly in solution. Therefore, we decided to have a look at the structures of the solid products that can be considered as the result of the self-assembly in solution. Thus the X-ray structures of 15 complexes of the amphiphilic Schiff base-like ligands used in our group are compared. The results lead to a rule which allows us to predict, under which conditions the purposeful synthesis of octahedral complexes with lamellar structures is possible. It will become clear, why of the alkyl chain lengths used for the ligand (C8, C12, C16 and C22), the longest chains were necessary for the synthesis of an octahedral complex with two bulky dmap (N,N-dimethylaminopyridine) as axial ligands. Application of this rule to other systems shows that it is not limited to the complexes investigated in our group. In Scheme 1 the general structure of the ligands together with the used abbreviations are given.
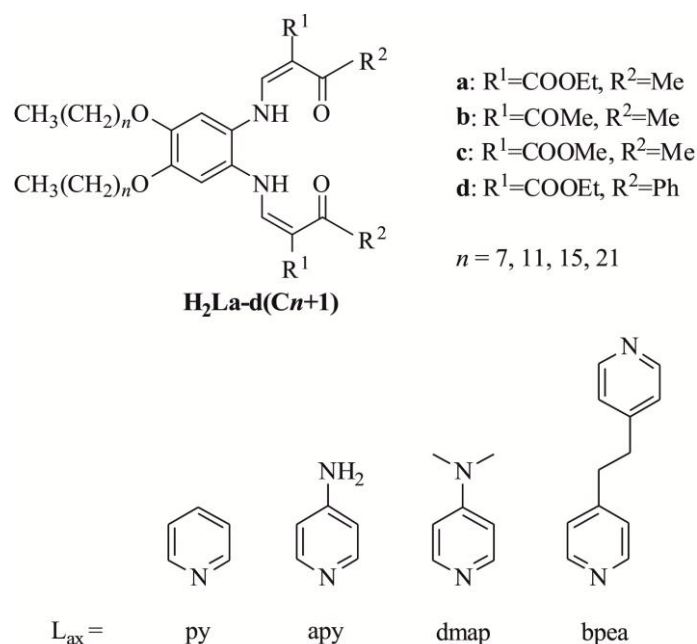
Scheme 1. General structure of the equatorial (top) and axial (bottom) ligands discussed in this work and their abbreviations.

7.2   Results and Discussion

7.2.1   Synthesis of the complexes

In Table 1, an overview of the complexes discussed in this work is given. To obtain octahedral iron(II) complexes, the free Schiff base-like ligands $H_2L(a$-$d)(Cn+1)$ were firstly converted with iron(II) acetate in methanol to give the penta- or hexa-coordinated [Fe(La-d)(Cn+1)(MeOH)$_{1-2}$] complexes with methanol as axial ligand. Further reaction with aromatic N-donor ligands like pyridine or imidazole that replace the methanol in the axial position, leads to a [N$_4$O$_2$] coordination sphere that shifts the iron(II) metal centre into the right energy region for the observation of thermal spin crossover.[4,19]

On the one hand, monomeric spin crossover complexes can be synthesized using axial ligands like pyridine (py), 4-aminopyridine (apy) or (4-dimethylamino)pyridine (dmap). These neutral compounds have been proved to be good candidates for SCO, but are also quite air sensitive

and the thermal stability is not too high.[4,19] On the other hand, coordination polymers can be realized using axial ligands like 4,4'bipyridine (bipy), 1,2-bis(4-pyridyl)ethane (bpea) or 1,2-bis(4-pyridyl)ethene (bpee). They show an increased thermal stability as well as a dramatically increased stability against oxidation in comparison to monomeric SCO complexes and give higher yields due to low solubility.[4,20] Additionally such 1D polymeric SCO complexes are attractive for the formation of nanoparticles.[21]

Table 1. Overview of the complexes discussed in this work.

complex	abbreviation	L_{eq}	L_{ax}	oxidation state	desired product	literature
[FeLa(C8)(dmap)]	**1**	La(C8)	dmap	iron(II)	no	this work
[FeLc(C8)(dmap)]	**2a**	Lc(C8)	dmap	iron(II)	no	[18]
[FeLc(C8)(dmap)]	**2b**	Lc(C8)	dmap	iron(II)	no	[18]
[(FeLc(C8))₂O]	**3**	Lc(C8)	-	iron(III)	no	this work
[FeLc(C8)(dmap)₂]×MeOH LS	**4aLS**	Lc(C8)	dmap	iron(II)	yes	[18]
[FeLc(C8)(dmap)₂]×MeOH HS	**4aHS**	Lc(C8)	dmap	iron(II)	yes	[18]
[FeLc(C8)(dmap)₂]×2MeOH	**4b**	Lc(C8)	dmap	iron(II)	yes	[18]
[FeLc(C8)(apy)]	**5**	Lc(C8)	apy	iron(II)	no	this work
[FeLa(C12)(MeOH)₂]	**6**	La(C12)	MeOH	iron(II)	yes[a]	[16]
[FeLc(C12)(MeOH)₂]	**7**	Lc(C12)	MeOH	iron(II)	yes[a]	[16]
[FeLa(C12)₂(bpea)]	**8**	La(C12)	bpea	iron(II)	no	this work
[{FeLb(C12)(MeOH)}₂(bpea)]	**9**	Lb(C12)	bpea	iron(II)	no	this work
[FeLa(C12)(apy)]	**10**	La(C12)	apy	iron(II)	no	this work
[FeLb(C12)(dmap)(MeOH)]	**11**	Lb(C12)	dmap	iron(II)	no	this work
[FeLa(C16)(py)₂]×0.25H₂O LS	**12LS**	La(C16)	py	iron(II)	yes	[17]
[FeLa(C16)(py)₂]×0.25H₂O HS	**12HS**	La(C16)	py	iron(II)	yes	[17]
[FeLd(C22)(dmap)₂]×0.5EtOH	**13**	Ld(C22)	dmap	iron(II)	yes	this work

[a] starting material.

For the synthesis of the final complexes similar reaction conditions were used as for the well investigated Schiff base-like iron(II) complexes with no alkyl chains in the outer periphery.[4] The combination of four different axial ligands with a total of sixteen different equatorial ligands (the lengths of the two alkyl chains are varied from 8, 12, and 16 up to 22 carbon atoms and four different substituents combinations for R^1 and R^2 are used) should allow the synthesis of a large pool of new octahedral complexes. It soon turned out, that the desired octahedral complexes are not obtained as easily as for the unmodified system.[18] The difference is especially pronounced for the complexes with bridging axial ligands, which are readily formed for the unsubsituted Schiff base-like ligands.[4] In contrast to this, dimeric structures are obtained frequently, as illustrated in Scheme 2. Here, we focus on the synthetic approaches in which single crystals in high enough quality for an X-ray structure analysis of the product were obtained.

7.2.2   X-ray structure analysis

In the following the X-ray structures of eight new amphiphilic complexes are compared with those of seven previously published complexes of this ligand system. The focus is set on the analysis of the crystal packing, especially the arrangement of the alkyl chains and the van der Waals (vdW) interactions between them. For the complexes **1**, **2a**, **3**, **4b**, **5** and **10**, the quality of the diffraction data was low, so only the relative conformation of the complex and the orientation in the crystal is discussed. For the other examples intermolecular interactions are also considered. In the Supporting Information (Table S1) the crystallographic data of the newly presented complexes are summarized. Selected bond lengths and angles within the first coordination sphere are compared in Table 2. The iron centre of the complexes is either penta-coordinated or hexa-coordinated. For the latter case often mixed axial ligands were obtained, of which one is the desired N-heterocyclic ligand whereas the other is methanol (from the solvent). For the parent Schiff base-like complexes only one example for such an octahedral complex is known.[22]

7.2.2.1   Chain length of eight carbon atoms

Crystals suitable for X-ray structure analysis were obtained quite frequently for the complexes with the C8 alkyl chains. However, in most cases the quality of the diffraction data was low. Thus of the seven different structures (compounds **1**, **2a**, **2b**, **3**, **4a**, **4b** and **5**), only two were of good enough quality to be discussed fully (**2b** and **4a**), whereas for the others only the molecular setup and the relative orientation of the alkyl chains is discussed. The different products for the combination of Lc with dmap were presented recently.[18] Two different samples were obtained for both, the octahedral complex **4**, and the penta-coordinated complex **2**.[18] In all cases significant differences were observed for the relative orientation of the alkyl chains. For the penta-coordinated samples indications for vdW interactions were observed between the alkyl chains but not for the octahedral samples.[18] Here, the motif of the crystal structures of the penta-coordinated complexes **1** and **5** and of the iron(III)-μ-oxido complex **3** are presented. The complexes crystallize in the space group $P\bar{1}$ (**1**) and (**3**) and $P2_1/c$ (**5**). The bond lengths around the iron centre are within the expected range for complexes of this type (Fe–O_{eq}/Fe–N_{eq}: 1.9-2.1 Å, Fe–N_{ax}: 2.1 Å).[9] The distances to the bridging oxygen atom in the μ-oxido complex are clearly shorter (*ca.* 1.8 Å). This is also the case for the O–Fe–O angle (91-94°) in comparison to the N-substituted complexes (97-101°; Table 2).

The molecular setup of the complexes **1**, **3** and **5** is displayed in Figure 1. For the complexes with the C8 alkyl chains a wide variety of relative orientations of the alkyl chains is observed. They are either parallel to each other but bent down with regard to the equatorial Schiff base-like ligand (Figure 1, top; **1** and **2b**), parallel to each other and in plane with the equatorial ligand (Figure 1, middle) or spread out and parallel with regard to the equatorial ligand (Figure 1, bottom; **5** and **2a**).
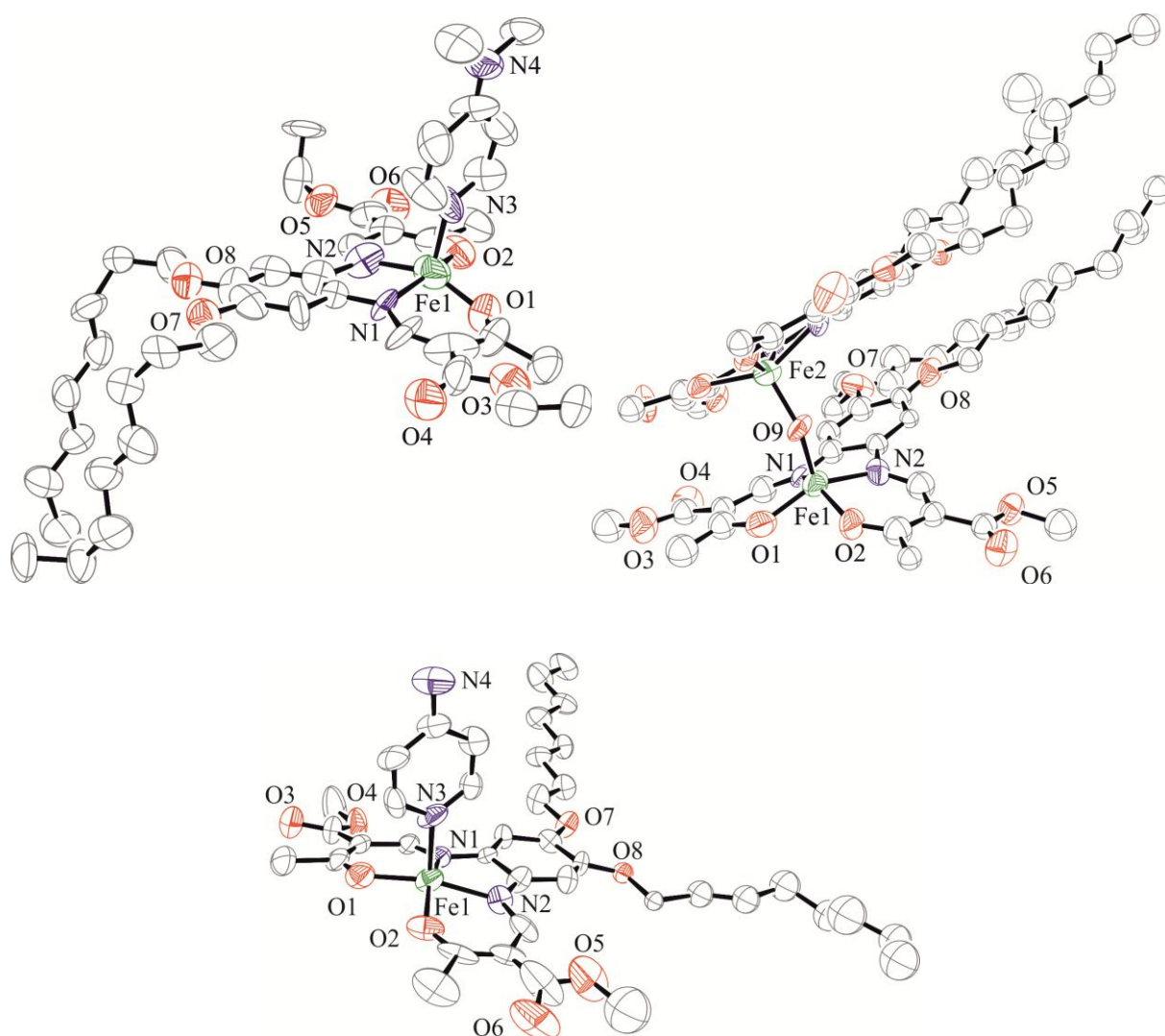
Figure 1. Molecular setups of **1** (top, left), **3** (top, right) and **5** (bottom). Hydrogen atoms are omitted for clarity. Ellipsoids for the crystal structures are drawn at the 50 % probability level.

The packing of **1** is very similar to that of **2b** (Figure 2, top). The almost planar planes of the equatorial ligand including the iron are arranged above each other, the alkyl chains are bent in the direction of the dmap of the neighbouring molecule. Like in **2b**, the dmap ligands in **1** are arranged parallel to each other and also almost parallel to the C8 alkyl chains, and the chains are also parallel to each other and form a lipid layer like arrangement. In the packing of **2b** vdW interactions between the alkyl chains and π-π-interactions between the planes of the equatorial ligand are observed.

The arrangement of the molecules of **5** in the crystal (Figure 2, bottom) is very similar to the second modification of the penta-coordinated complex **2a**. As the quality of both structures is low, no discussion about the potential vdW interactions between the alkyl chains is possible.

In the μ-oxido sample of [FeLc(C8)] (**3**) (Figure 2, middle), the only iron(III)-complex in this study, two inequivalent molecules each with two iron centres (Fe–O–Fe angles: *ca.* 154°) are stacked above each other, shifted sideways in a small angle. The chains point in the same direction. Next to these two molecules, another pair is arranged whose alkyl chains point in the opposite direction, so the molecules form a zipper-type structure in which the polar head groups are arranged next to each other as the nonpolar tail groups are.

For complexes with relatively short C8 alkyl chains the crystallization mode is quite unpredictable. The strength of the vdW interactions increases with the dimension of the hydrophobic part of the molecule. For the complexes with C8 alkyl chains they are weak and not dominating the crystal packing. They are easily surpassed by other, energetically more favourable conditions, such as hydrogen bonds or π-π-interactions.

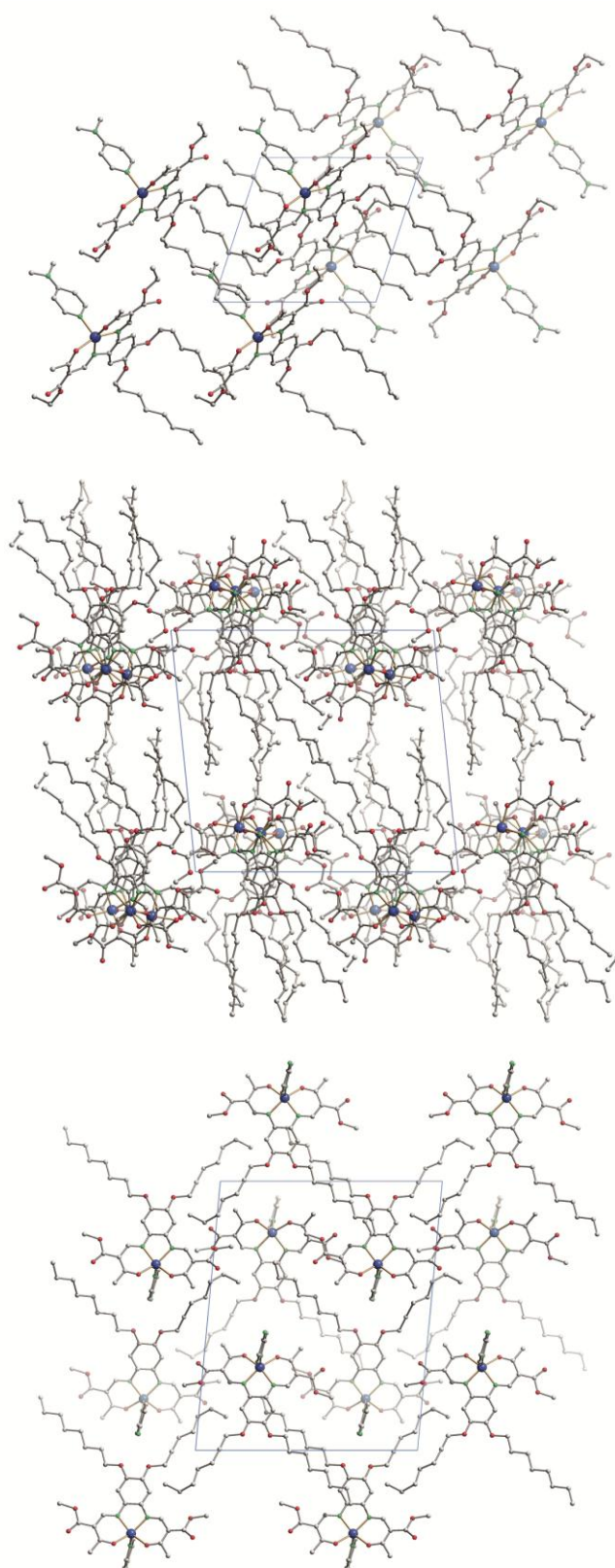**Figure 2**. Packing in the crystal of **1** along [0 0 1] (top), **3** along [1 0 0] (middle) and **5** along [0 1 0] (bottom). Hydrogen atoms are omitted.

Table 2. Selected bond lengths /Å and angles /° within the inner coordination sphere and spin state of the complexes discussed in this work.

	Fe–N$_{eq}$ /Å	Fe–O$_{eq}$ /Å	Fe–N$_{ax}$ /Å	O–Fe–O /°	spin state
1	2.1/2.0	1.9/2.0	2.1	101	HS
2a[18]	2.1/2.0	2.0/2.0	2.1	100	HS
2b[18]	2.073(4)/2.085(4)	2.002(3)/1.980(3)	2.127(4)	101.62(14)	HS
3[a]	2.0/2.0; 2.0/2.1	1.9/1.9; 1.9/2.0	Fe–O$_{ax}$: 1.8/1.8	91/94	HS
4aLS[18]	1.909(2)/1.915(2)	1.948(1)/1.957(1)	2.013(2)/2.018(2)	91.68(6)	LS
4aHS[18]	2.065(3)/2.080(3)	2.002(3)/2.012(3)	2.216(3)/2.217(3)	107.16(11)	HS
4b[18]	1.9/1.9	2.0/2.0	2.0/2.0	92	LS
5	2.0/2.1	2.0/2.0	2.1	97	HS
6[16]	2.093(2)/2.095(2)	2.009(1)/2.030(1)	Fe–O$_{ax}$: 2.203(1)/2.230(2)	108.93(5)	HS
7[16]	2.088(2)/2.094(2)	2.007(2)/2.021(2)	Fe–O$_{ax}$: 2.201(2)/2.233(2)	109.37(8)	HS
8[b]	2.077(3)/2.075(3); 2.075(3)/2.077(3)	1.997(3)/1.978(3); 1.995(3)/1.977(3)	2.130(3); 2.132(5)	103.58(10); 102.92(12)	HS
9[c]	2.107(4)/2.101(5); 2.089(5)/2.102(4)	2.026(3)/2.040(3); 2.028(3)/2.026(3)	2.227(4); 2.242(4); Fe–O$_{ax}$: 2.228(4)/2.227(4)	112.29(16); 111.60(16)	HS
10[d]	2.1/2.0; 2.1/2.0	2.0/2.0; 2.0/2.0	2.1; 2.1	107; 105	HS
11	2.089(2)/2.095(2)	2.002(2)/2.026(2)	2.181(3); Fe–O$_{ax}$: 2.267(3)	108.87(9)	HS
12LS[17]	1.897(2)/1.907(2)	1.935(2)/1.947(2)	2.021(2)/2.014(2)	88.80(7)	LS
12HS[17]	2.059(3)/2.086(2)	2.001(2)/1.999(2)	2.284(3)/2.280(4)[f]; 2.284(3)/ 2.288(7)[g]	106.10(9)	HS
13[e]	2.113(4)/2.120(4); 2.090(4)/2.134(4)	2.030(3)/2.075(3); 2.016(3)/2.062(3)	2.186(4)/2.224(4); 2.201(4)/2.235(4)	111.66(12); 112.26(13)	HS

[a] Fe1; Fe3. [b] Fe1; Fe2. [c] Fe1; Fe2. [d] Fe1; Fe2. [e] Fe1; Fe2. [f, g] disorder.

7.2.2.2 Chain length of 12 carbon atoms

Crystals suitable for X-ray structure analysis were obtained for six complexes with the chain length of 12 carbon atoms. The two precursor complexes with two methanol as axial ligands, **6** and **7**, crystallized readily out of the reaction mixture.[16] The crystal structures of two dinuclear complexes with bpea (**8, 9**), one complex with apy (**10**; motif) and one hexa-coordinated complex with one dmap and one methanol as axial ligands (**11**) were investigated and are discussed in the following. Crystallographic data and selected bond lengths and angles are summarized in Table S1 and Table 2, respectively. In all cases lipid layer like structures are observed. However, we did not succeed with the isolation of crystalline material with the desired octahedral [N_4O_2] coordination sphere which is interesting with regard to magnetic properties.

The mononuclear complex **10** crystallizes in the triclinic space group $P\bar{1}$ with four formula units in the unit cell and two inequivalent iron centres whereas **11** crystallizes in the monoclinic space group $P2_1/c$ with only one molecule in the asymmetric unit and four molecules in the unit cell. Figure 3 displays the molecular setup of the two mononuclear complexes and Figure 4 the packing of the molecules in the crystal.

The bond lengths to the equatorial coordinating N- and O-atoms are with about 2.1 and 2.0 Å very similar for both compounds and in the typical range for complexes of this ligand type, as are the O–Fe–O angles of about 105-109° that clearly indicate the high spin state in both complexes. In **11**, the bond length to the O-atom of the axially coordinating methanol is almost 0.1 Å longer than to the N-atom of the axially attached dmap. One hydrogen bond between the O-atom of the methanol and the O-atom of one of the keto groups of the equatorial ligand of the neighboured complex molecule is observed (O7—H51···O3, Table 3). One non-classical hydrogen bond between C24—H24C···O1 connects the methyl group of a dmap pointing at the O–Fe–O site with the atom O1 of the complex shifted above. For both complexes the lipid layer-like arrangement is supported by hydrogen bonds between the polar head groups.
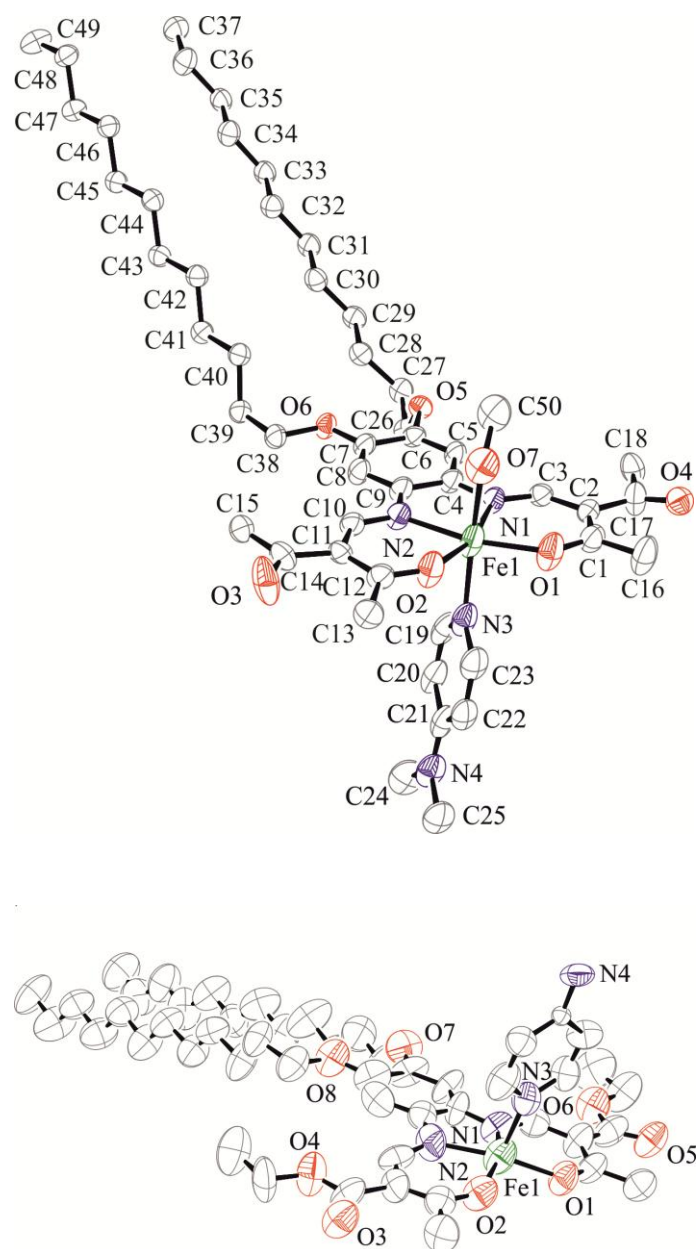
Figure 3. Molecular setups of **11** (top), and **10** (bottom). Hydrogen atoms are omitted for clarity. Ellipsoids are drawn at the 50 % probability level.

Table 3. Short contacts and hydrogen bonds and non classical hydrogen bonds /Å of the obtained crystal structures.

	D—H⋯A	D—H	H⋯A	D⋯A	D—H⋯A
11	O7—H51⋯O3[a]	0.79(4)	1.95(4)	2.730(4)	170(4)
	C24—H24⋯O1[b]	0.98	2.57	3.395(5)	142
9	O17—H17⋯O26[c]	0.82	1.87	2.686(4)	175
	O27—H27⋯O15[d]	0.82	1.90	2.689(4)	163
8	C118—H11H⋯Fe1[e]	0.98	2.90	3.491(4)	120
	C15—H15B⋯Fe2[f]	0.98	2.89	3.524(6)	123
13	C137—H13H⋯O108[g]	0.98	2.57	3.323(7)	134
	C30—H30B⋯N106[h]	0.98	2.58	3.381(11)	139
	C32—H32⋯O105[h]	0.95	2.36	3.266(6)	160
	C45—H45B⋯O8[i]	0.98	2.38	3.202(7)	141

[a] x, −1/2−y, −1/2+z; [b] x, y, 1+z; [c] 1−x, 1/2+y, 1/2−z; [d] −x, −1/2+y, 1/2−z; [e] x, y, z; [f] −1+x, y, z; [g] 1+x, y, z; [h] 2−x, 1−y, 1−z; [i] −1+x, y, z.
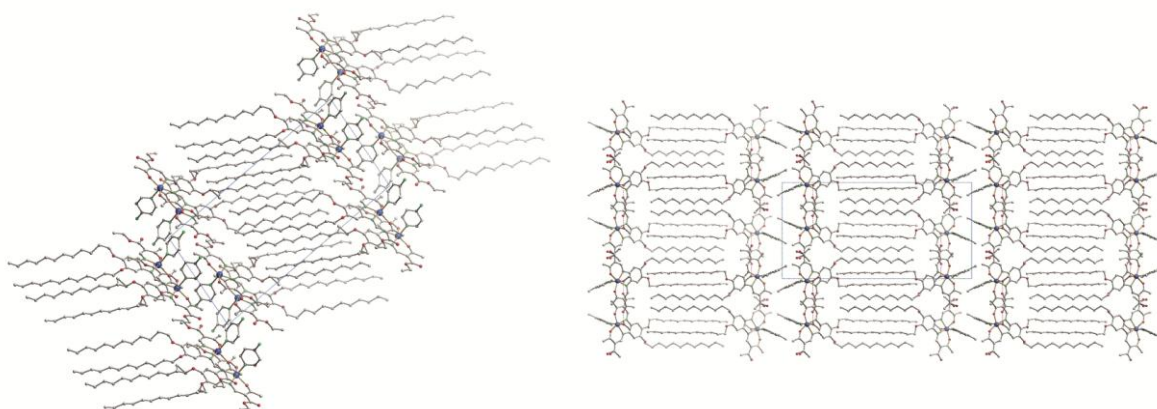

Figure 4. Packing in the crystal of **10** (left) along [1 0 0] and **11** (right) along [0 0 1]. Hydrogen atoms are omitted for clarity. Hydrogen bonds in **11** are drawn in dashed lines.

The dinuclear complexes **8** and **9** both crystallized out of the reaction mixtures of the corresponding iron-methanol complexes with the bidentade bridging bpea in an about 30 eq. excess after one day at room temperature (Scheme 2). For the corresponding parent compounds with no alkyl chains in the outer periphery those reaction conditions, even with a tenfold excess of axial ligand, always led to the corresponding coordination polymer.[20,23]
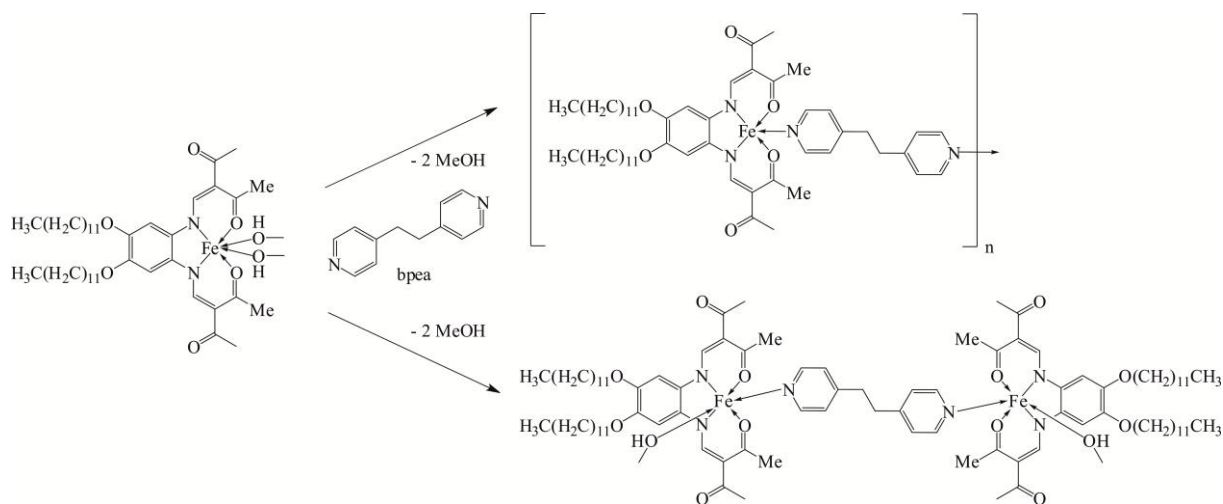
Scheme 2. Exemplary reaction pathway with the desired (top) and obtained reaction product **9** (bottom).

While **8** crystallizes in the space group $P\bar{1}$ with two molecules in the unit cell, **9** crystallizes in $P2_1/c$ with four molecules in the unit cell. Despite the comparably high excess of axial ligand, both complexes do not precipitate as coordination polymers but form dinuclear units with two iron centres per bridging ligand. For **9** the iron centre is saturated with methanol at the sixth coordination site while in **8** it is penta-coordinated. Figure 5 displays the molecular setup of **8** and **9**, and Figure 6 their packing in the crystal. The average bond lengths and angles within the first coordination sphere do not differ much from the other complexes and are listed in Table 2. Like in **11**, in **9** two hydrogen bonds are formed between the O-atoms of the coordinating methanols and the O-atoms of the keto groups of the neighboured complexes. (O17—H17···O26 and O27—H27···O15, see Table 3 and Figure 6). For **8**, no classical hydrogen bonds are possible. Surprisingly, a very short contact between atom Fe2 and H15B of atom C15 of one of the ethyl groups in the equatorial ligand surrounding the Fe1 metal centre is found that is shorter by 0.3 Å than the sum of the van der Waals radii (2.89 Å).

The angle N13 (of the bpea)–Fe2–H15B is 168.1° and the angle to the carbon atom C15 (N13–Fe2–C15) is 177.87(13)° (length Fe2–C15: 3.524(6) Å). Also for Fe1 a contact shorter by 0.2 Å than the sum of the van der Waals radii is observed to C118 (Fe1–C118: 3.491(4) Å, ∠N3–Fe1–C118: 177.89(10)°) and H11H (Fe1–H11H: 2.90 Å, ∠N3–Fe1–H11H: 168°) of one of the ethyl groups in the equatorial ligand surrounding Fe2. An intermolecular network is formed where the carbon atoms of the CH_3 of the ethylester groups are connected with the iron atoms in a nearly ideal 180° angle.
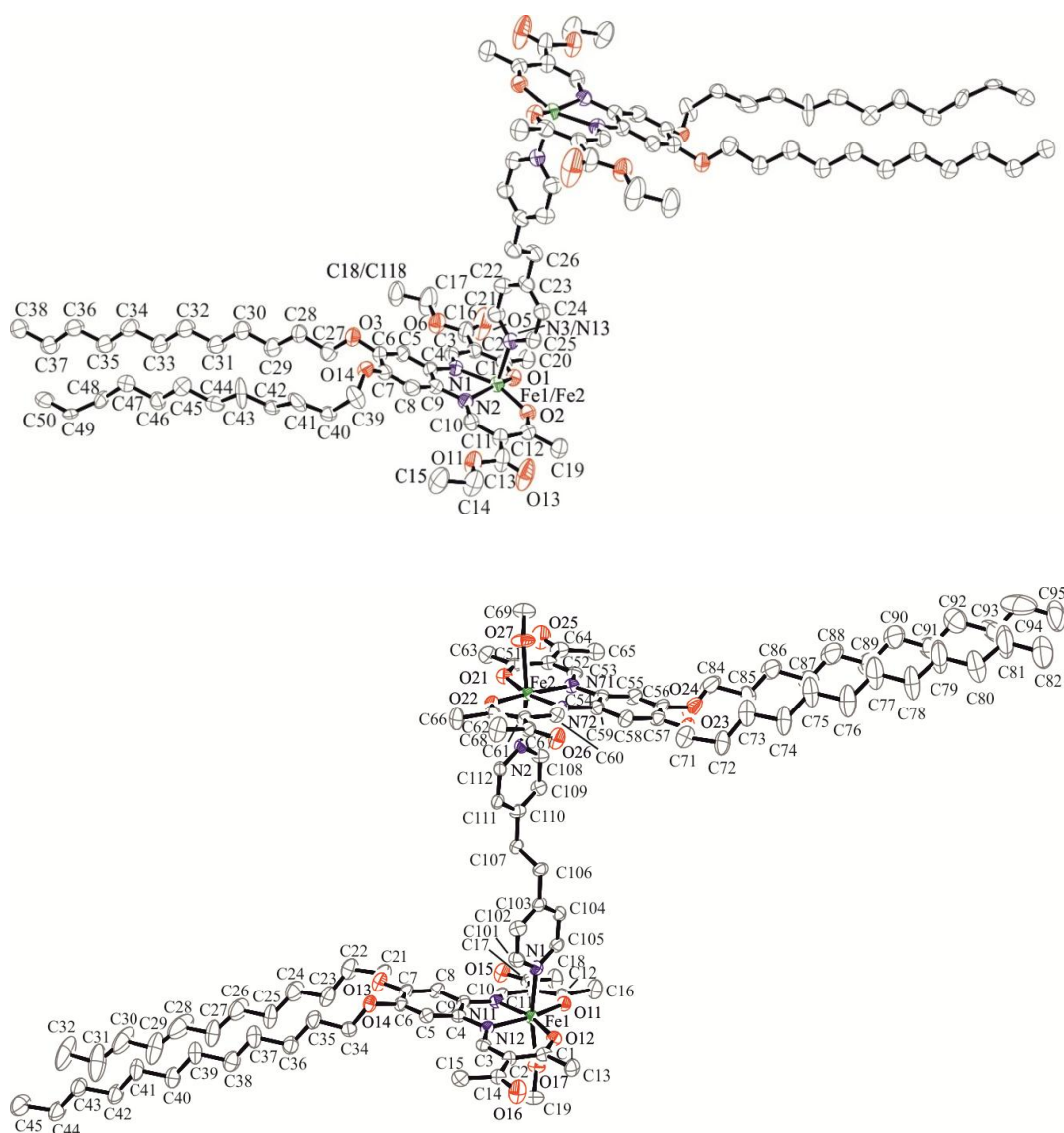

Figure 5. Molecular setups of **8** (top) and **9** (bottom). Hydrogen atoms are omitted for clarity. Ellipsoids are drawn at the 50 % probability level.

All complexes with C12 alkyl chains, the four molecules discussed in this manuscript and the two methanol complexes already described[16] crystallize in a lipid layer-like structure. The alkyl chains form layers with average layer-layer distances of about 4.8 Å (**6**), 4.8 Å (**7**), 4.1 Å (**8**), 4.4 Å (**9**), 4.2 Å (**10**) and 4.2 Å (**11**).
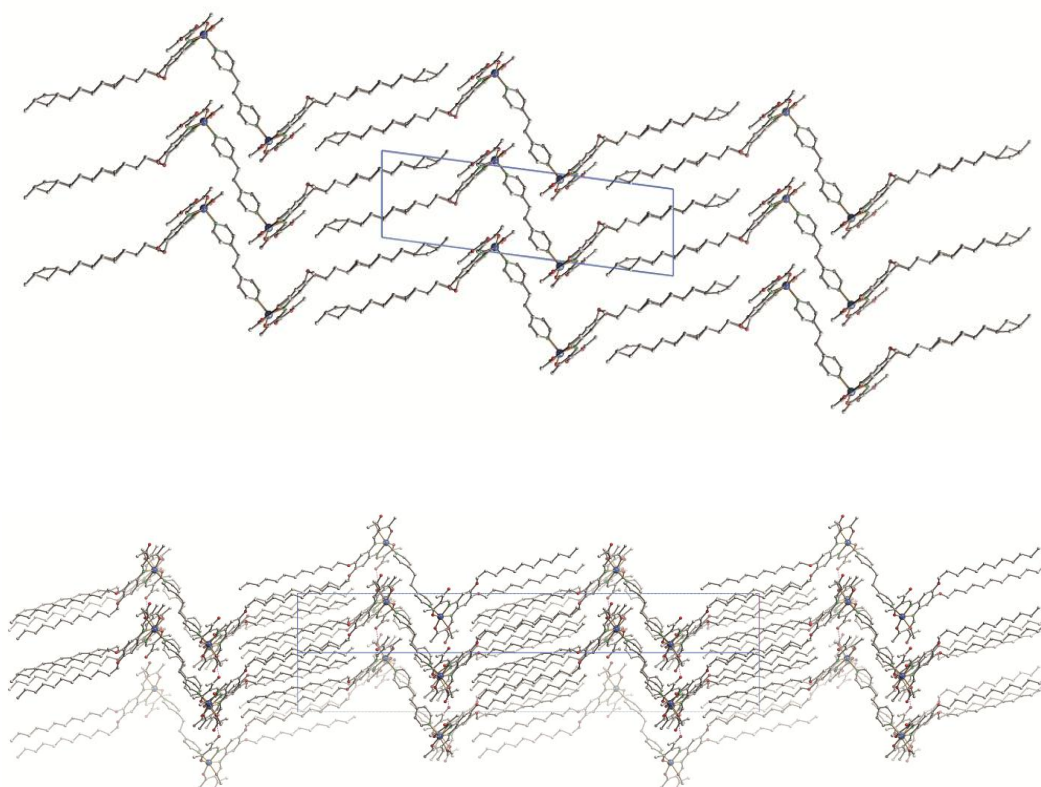

Figure 6. Packing in the crystal of **8** along [0 1 0] (top) and **9** along [1 1 0] (bottom). Hydrogen atoms are omitted for clarity. Hydrogen bonds in **9** are drawn in dashed lines.

Stabilizing van der Waals interactions between the alkyl chains (the London dispersion forces) can be considered, when the distances between the atoms are in the region of the sum of the van der Waals radii plus 0.3-0.4 Å. In the case of **8**, **10** and **11**, such stabilizing interactions are dominant. Only few destabilizing shorter contacts are observed and the average H-H-distance is about 2.7 Å. In the case of **9**, the ratio of stabilizing and destabilizing interactions is around 1:1. It can be assumed that additional strong interactions (hydrogen bonds) influence the crystal packing. In the case of the methanol complexes **6** and **7** the layer

layer-distance is comparable long. In agreement with this, fewer stabilising contacts between the alkyl chains are observed.

7.2.2.3   Chain length of sixteen carbon atoms

The structure of an octahedral spin crossover complex with two alkyl chains of 16 carbon atoms was published recently in the HS and the LS state (**12LS** and **12HS**).[17] As for the complexes with C12 alkyl chains, a lipid layer-like structure is observed in the crystal packing. The layer-layer distance between the alkyl chains is with an average of 4.3 Å (both spin states) in the same region as observed for most of the complexes with C12 alkyl chains. In agreement with this, numerous stabilising vdW contacts can be observed.

7.2.2.4   Chain length of 22 carbon atoms

We succeeded with the crystallization of an octahedral iron(II) complex with a Schiff base-like ligand with two C22 alkyl chains and two dmap as axial ligands. Single crystals of high enough quality for X-ray structure analysis were obtained and the molecular setup could be elucidated. **13** ([Fe(Ld)(C22)(dmap)$_2$]×0.5 EtOH) crystallizes in the triclinic space group $P\bar{1}$ with 4 molecules in the unit cell and two inequivalent iron centres bearing the desired octahedral [N$_4$O$_2$] coordination sphere. Selected bond lengths and angles are given in Table 2, crystallographic data in Table S1 in the Supporting Information. Similar to the hexa-coordinated complex **9**, the Fe–N$_{eq}$ and Fe–O$_{eq}$ bond lengths are with about 2.1 Å respectively 2.0 Å in the expected magnitude. The O–Fe–O angle of about 112° clearly indicates that the complex is in the HS state at 173 K. The molecular setup of **13** is displayed in Figure 7 (top). The coordination sphere around the iron(II) is a distorted octahedron. The Schiff base-like ligand can be described as saddle shaped. The chelate six rings with the delocalized π-system are bent in the direction of the phenylene substituents. The angles with the [N$_2$O$_2$] plane are 16°/23° (O1C1C2C3N1-plane and N2C10C11C12O2-plane) for Fe1 and 25°/15° for Fe2. The iron centre is slightly shifted out of the [N$_2$O$_2$] plane by 0.08 Å.
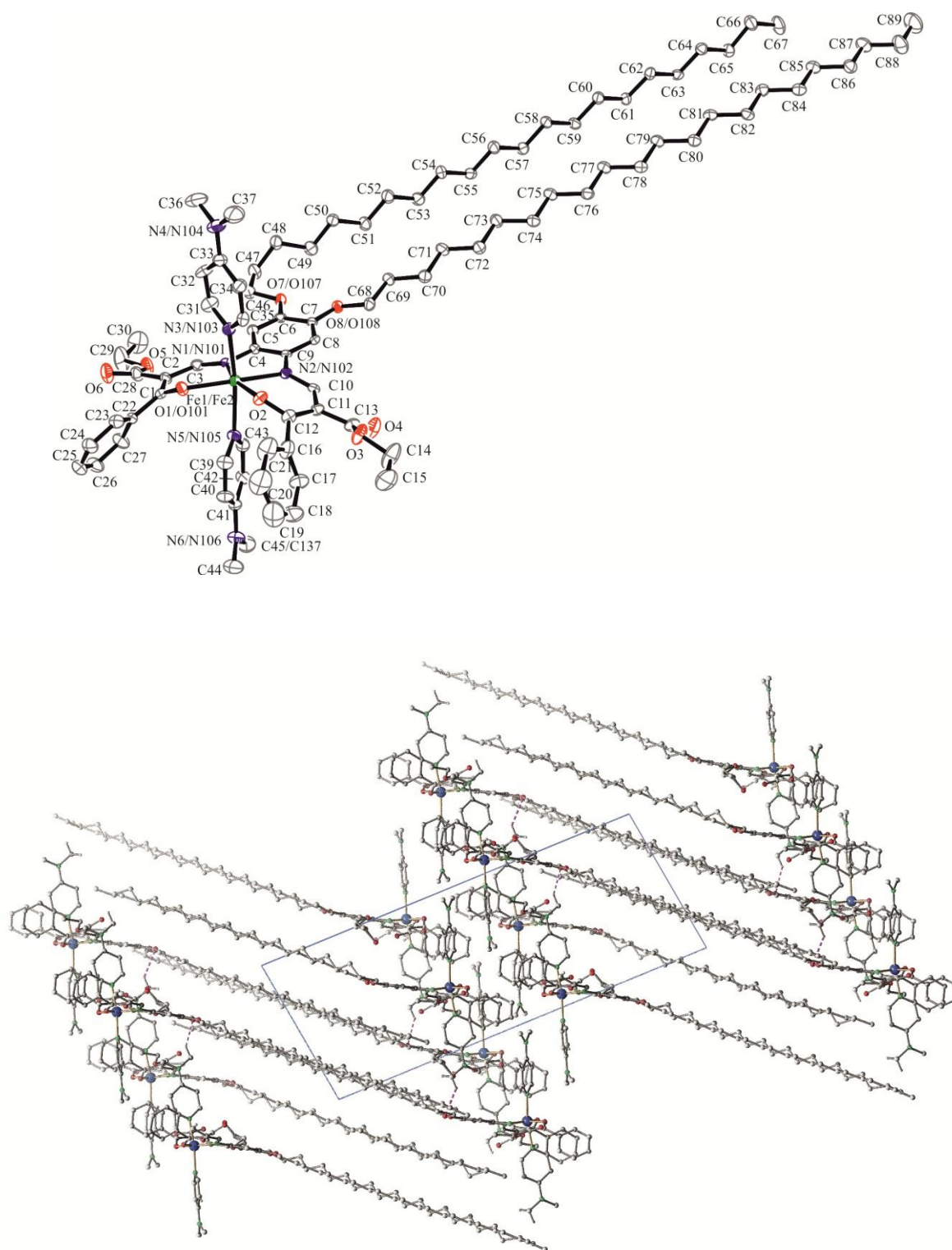
Figure 7. Molecular setup (top) and packing in the crystal (bottom) of **13**, packing along [1 0 0]. Hydrogen atoms are omitted for clarity. Ellipsoids for the crystal structures are drawn at the 50 % probability level. Non classical hydrogen bonds are drawn in dashed lines.

The bond length to the N-atom of the axial dmap ligand is slightly elongated at the more shielded site of the ligand. The planes of the dmap rings assume a staggered conformation with an angle of 74° for Fe1 and 52° for Fe2. The C22 alkyl chains are not arranged in plane with the equatorial ligand but point out of the [N_2O_2] plane with an angle of 22° at Fe1 and 28° at Fe2, bent about 45° sideward. This is different to the complexes with C12 and C16 alkyl chains.

In the crystal packing, the molecules are clearly arranged in the lipid layer-like structure with a layer-layer distance of about 4.00 Å (see Figure 7, bottom). In comparison with the layer distances of the other complexes bearing this structure motif, this is short. Several non-classical hydrogen bonds are observed between the polar head groups (C137—H13H⋯O108, C30—H30B⋯N106, C32—H32⋯O105 and C45—H45B⋯O8; see Table 3) indicating a dense packing. Most of the contacts between the alkyl chains are in the region of the sum of the van der Waals radii plus 0.3-0.4 Å. This indicates strong stabilizing vdW interactions between the alkyl chains of this complex.

Unfortunately, the amount of crystals of **13** was not enough for magnetic measurements on the single crystals. A separately prepared powder sample with the composition [Fe(Ld)(C22)(dmap)$_2$] is a low-spin complex in the entire temperature range (see Supporting Information, Figure S1). The difference to the spin state of **13** (HS at 173 K) can be explained with the missing additional ethanol molecule in the crystal packing.

7.2.2 Prediction of the molecular setup of amphiphilic complexes and their arrangement in the crystal

The results from X-ray structure analysis show clearly, that with an alkyl chain length of C12 or higher, lipid layer-like arrangements are the preferred structural motif. However, often not the desired reaction product is obtained. This implies that the formation of lipid layer-like arrangements prevents the formation of octahedral complexes. Thus the question arises, what parameters control the formation of lipid layer like arrangements. In 1976, Israelachvili *et al.* predicted how amphiphiles self-assemble in solution, depending on the geometry of the molecules.[24] For this, he introduced the critical packing parameter (cpp, equation **A**).[24]

$$cpp = V/(A \cdot L) \qquad \text{(Equation A)}$$

It correlates the volume of the hydrophobic part (V), in relation to the area of the head group (A) and the length of the hydrophobic part (L). If cpp ≈ 1, in a polar solvent the molecules bearing two alkyl chains will arrange in lipid layers. If the cpp is smaller than one, flexible micellar structures are realized, and if it is bigger than 1, in nonpolar solvents inverse micelles are formed. It should be pointed out, that for all of our reactions a polar solvent was used. On the basis of this, we tried to establish a rule for our complexes regarding how they will arrange in solution and thus in the solid. In order to obtain this rule, the broadness and the height of the polar head and the length of the whole molecule (exemplarily shown for the complex **12LS** in Figure 8) were measured. The results are listed in Table 4.

First attempts to predict the crystal packing with the help of the critical packing parameter (cpp) of Israelachvili *et al.* were not successful. It then became obvious, that the following straight forward relation (the **s**elf-**a**ssembly **p**arameter *sap*, equation **B**) can be used. When the sum of the broadness (B) and the height (H) of the polar head group, divided through the entire length of the molecule (L) is around 1, a lipid layer-like packing in the crystal can be expected.

$$sap = (H+B)/L \qquad \text{(Equation B)}$$

The complexes with alkyl chains of eight carbon atoms have an entire length, L, of about 20.4 Å, when the chains are ideally arranged. Adding for example two dmap ligands in the axial positions would cause an inappropriate relation of (H+B)/L (substituent c: B ≈ 14.4 Å, H ≈ 16.30 Å; *sap* ≈ 1.50). In agreement with this, other packing patterns are observed. Examples for this are the hexa-coordinated complexes **4a/4b**.
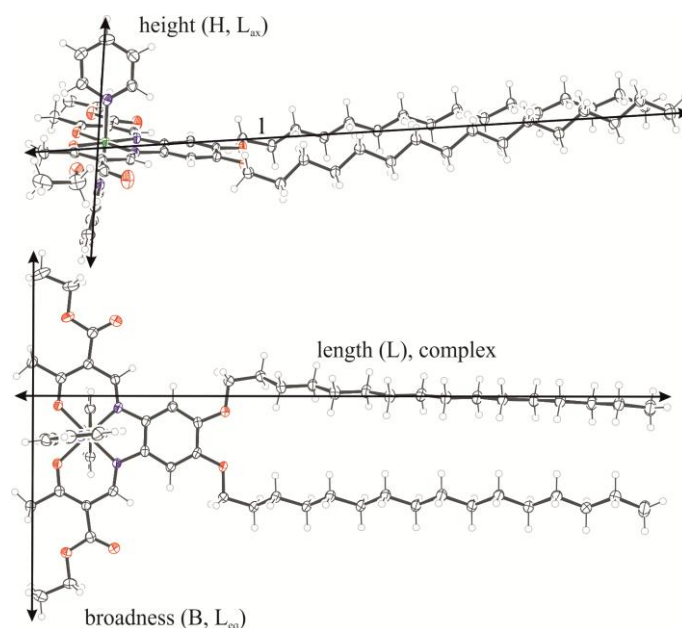
Figure 8. Dimensions of the compounds taken in account for the calculation of the *sap*. L denotes the length, H the height and B the broadness of the complex.

The values would match exactly for example for a penta-coordinated complex [FeLc(C8)(MeOH)]. Indeed, the synthesized fine crystalline powder of the methanol precursor has this composition. Additionally it is extremely air sensitive – a further indication for penta-coordination. Unfortunately, no crystals of high enough quality could be isolated. For the penta-coordinated complexes with one N-heterocyclic axial ligand (**2a/2b**, **1** and **5**) the ratio is closer to 1 compared to the octahedral systems. Thus lipid layer like structures, for example, with bent alkyl chains as for **1** and **2b**, are observed. For the μ-oxido complex **3** the ratio is smaller than 1 and again another structural motif is observed.

Table 3. Height (H /Å), broadness (B /Å) and length (L /Å) of the complexes discussed in this work.

	H /Å	B /Å	L /Å	(H+B)/L
1	8.10	17.13	16.19	1.56
2a	8.11	14.68	16.02	1.42
2b	8.12	14.24	15.90	1.41
3	1.72	14.24	19.70	0.81
4aLS	15.90	14.40	19.15	1.58
4aHS	16.29	14.28	18.32	1.67
4b	16.00	14.11	18.12	1.66
5	6.74	14.31	17.50	1.20
6	8.07	16.86	23.79	1.05
7	8.07	14.91	23.98	0.96
8	6.71	15.47	23.56	0.94
9	10.87	13.26	24.25	1.00
10	6.78	15.27	23.90	0.92
11	12.22	12.83	23.86	1.05
12LS	11.48	16.91	29.44	0.96
12HS	11.97	17.44	29.30	1.00
13	16.26	16.36	32.20	1.01

For the complexes with alkyl chain lengths of 12 carbon atoms the situation is different. Penta- and hexa-coordinated products are obtained. Due to the longer hydrophobic tails the importance of the vdW interactions as structure determining element increases and lipid layer-like structures are observed for every complex. The alkyl chains are arranged along the [N_2O_2] plane without significant differences in the angles. However, reactions with dmap, apy or the bridging bpea did not give the desired hexa-coordinated products. Only spin crossover

inactive methanol complexes **6** and **7**,[16] mixed derivatives like **11**, dinuclear complexes as **8** and **9** or penta-coordinated compounds (**10**) crystallized. Application of Equation **B** explains this behaviour. As can be seen in Table 4, for all of the crystallized complexes with C12 alkyl chains the values for (H+B)/L are almost exactly around 1. The two penta-coordinated complexes with slightly smaller values reveal both short contacts to other atoms at the empty coordination site. Adding bigger axial ligands (for example, two dmap and substituent b: B ≈ 13.0 Å, H ≈ 16.30 Å, L ≈ 23.89 Å; *sap* ≈ 1.23) would cause a loss of the ability of the complex to crystallize in the lipid layer-like structure. This is the reason why **11,** for example, crystallizes in this unusual modification bearing one methanol instead of a second dmap. It also explains the formation of dinuclear complexes instead of coordination polymers, despite the large excess of axial ligand.

For complexes with C16 alkyl chains the situation is very similar. Unfortunately, only the crystal structure of one complex **12** (HS and LS) could be obtained so far.[17] The axial pyridine ligands fit exactly in combination with substituent a and the C16 alkyl chains ((H+B)/L for the complex in HS: 1.00) to give a lipid layer-like structure in the crystal.

To add more bulky ligands like dmap, following Equation **B**, the chain length had to be elongated. Consequently, the corresponding ligand and the methanol precursor with alkyl chain lengths of 22 carbon atoms was synthesized and converted with dmap. The complex **13** is hexa-coordinated and exhibits a lipid layer-like arrangement of the molecules in the crystal.
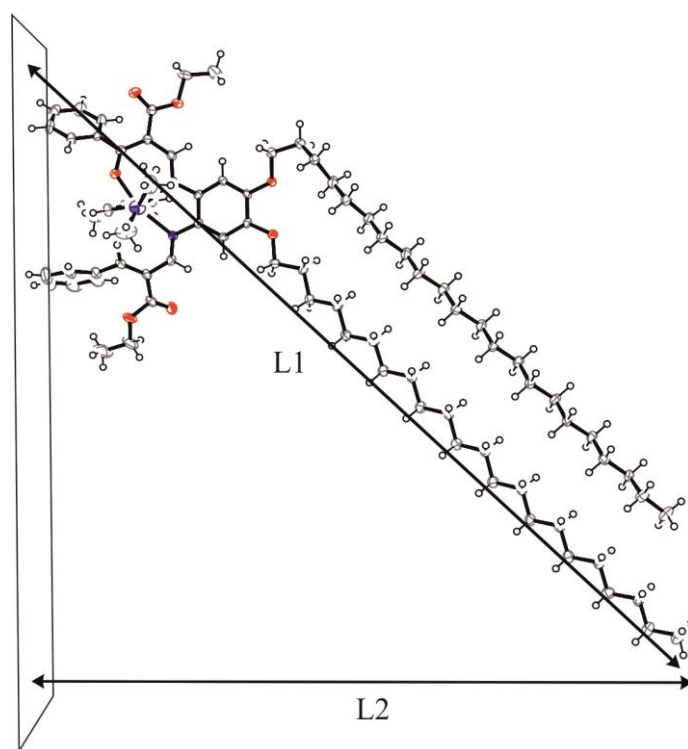
Figure 9. Measurement of the length taken in account for the calculation of (H+B)/L for complex **13**. L denotes the length of the complex. The plane on the left is spanned by the ultimate four hydrogen atoms of the complex.

The structural situation for the C22 compound is more complicated. The calculated length of **13** is 40.6 Å (Figure 9). This is too long for the dmap ligands, even if the high steric demand of the equatorial ligand is considered (calculated *sap* = 0.81). This can be the reason, why the nonpolar chains are bent quite strongly sideward. As shown in Figure 9, a plane was spanned at the outer H atoms of the two phenylene rings of the equatorial ligand. Measuring the distance between the plane and the latest H atoms of the alkyl chains leads to an average length of 32.2 Å which denotes the actual length of the complex in the crystal, and a *sap* of 1.01. Consequently, it should be possible to add more bulky axial ligands like phenylpyridine without losing the lipid layer-like arrangement.

The next question to be answered is, if this concept can be transferred to other amphiphilic complexes.[12,25] In the field of spin crossover research, amphiphilic systems are so far reported for iron(II),[8,26] cobalt(II),[9] iron(III)[11,13,14,27] and manganese(III)[10].

A few X-ray structures are available for complexes with alkyl chains ≤ C8. In contrast to our system, in all cases counter ions are involved. For manganese(III) complexes with the bapen ligand and C6 alkyl chains different orientations of the alkyl chains in the crystal packing are observed.[10] For a similar iron(III) complex with the sal$_2$trien ligand and C8 alkyl chains already a layered structure is observed with interactions between the polar heads (and the counter ions) and interactions between the nonpolar chains.[27] A similar situation is observed for an iron(II) complex of the C$_6$tren ligand with three C6 alkyl chains.[7d]

The cobalt(II) complexes investigated by Hayami and co-workers differ from our system as the two alkyl chains point in opposite directions and again counter ions are involved.[6,28] Layered structures are observed that differ, however, quite strongly from lipid layer-like arrangements.

An iron(III) complex of a Schiff base ligand with *n*-dodecyl chains showed a very similar behaviour to our complexes with C12 alkyl chains. X-ray structure analysis revealed a self-assembly to lipid layer like structures for this neutral complex in the solid state.[29] Between the polar head-groups a network of hydrogen bonds is observed. For this system, the calculated value of (H+B)/L is with 0.87 significantly smaller than 1 and a better result is obtained if only the length of the alkyl chain is considered (1.08). This illustrates the influence of the different numbers of alkyl chains on the *sap*.

7.3   Conclusion

In this work, the crystal structures of 7 published and 8 new amphiphilic iron complexes with Schiff base-like ligands and nonpolar alkyl chain groups with lengths of 8, 12, 16 and 22 carbon atoms are presented and discussed. With regard to the spin transition properties of the central metal atom, a [N$_4$O$_2$] coordination sphere and self-assembly to lipid layer-like structures is desired. This can be achieved, if the newly introduced *sap* (self-assembly parameter) is considered. The *sap* allows us to predict, which general requirements have to be fulfilled for the observation of octahedral complexes with lipid layer-like structures in the solid. For the synthesis of octahedral complexes with rather bulky axial ligands as the dmap, long alkyl chains are necessary. The synthesis of a ligand with C22 alkyl chains allowed the crystallization of a corresponding octahedral iron(II) complex with dmap. This is, to the best

of our knowledge, the complex with the longest alkyl chains in which crystallization succeeded.

This empirically derived rule to design octahedral SCO complexes can also be successfully applied to explain the crystallization behaviour of other ligand systems. Depending on the system, slight adjustments may be necessary. Additionally, we gain a further insight into the self-assembly of such complexes in solution. This is of great importance for the nanostructuring of SCO systems (e.g., micelles or inverse micelles) or the creation of thin layers (e.g., Langmuir-Blodgett films).

7.4   Experimental Section

Synthesis: The synthesis of the iron complexes and syntheses with the diamino precursor were carried out under an argon atmosphere using Schlenk tube techniques. The solvents therefore were purified as described in the literature[30] and distilled under an atmosphere of argon. The synthesis of 1,2-dioctyloxybenzene, 1,2-didodecyloxybenzene, 1,2-dihexadecyloxybenzene, 1,2-didocosyloxybenzene, 4,5-dioctyloxy-1,2-dinitrobenzene, 4,5-didodecyloxy-1,2-dinitrobenzene, 4,5-dihexadecyloxy-1,2-dinitrobenzene, 4,5-didocosyloxy-1,2-dinitrobenzene, 1,2-diamino-4,5-dioctyloxybenzene, 1,2-diamino-4,5-didodecyloxybenzene, 1,2-diamino-4,5-dihexadecyloxybenzene, 1,2-diamino-4,5-didocosyloxybenzene,[16,17] ethoxymethyleneethylacetoacetate,[31] methoxymethylenemethyl-acetoacetate,[32] ethoxymethyleneacetylacetone,[31] ethoxymethylenephenylacetoacetate,[33] $H_2La\text{-}c$, [Fe(La-c)(Cn+1)(MeOH)$_{1\text{-}2}$],[16,17] and iron(II) acetate[34] are described in the literature. Pyridine (py), 4-aminopyridine (apy) (Alfa Aesar, 98 %), 4-(dimethylamino)pyridine (dmap) (Merck, ≥99 %) and 1,2-bis(4-pyridyl)ethane (bpea) (Aldrich, 99 %) were purchased and used as received. For the complexes 5, 9 and 13 the amount of crystals was not enough to perform elemental analysis.

[Fe(La)(C8)(dmap)] (1). [Fe(La)(C8)(MeOH)$_2$] (0.40 g, 0.52 mmol) and dmap (2.1 g, 17.19 mmol, 33.1 eq.) were dissolved in methanol (17 mL) and heated to reflux for 90 min. After storing at −30°C black crystalline precipitate was filtered and washed two times with methanol (2.5 mL). In the residual solution black needle-like crystals were formed at 7°C within few days. Yield: 0.02 g (5 %); (820.84 g mol^{-1}). Elemental analysis calcd (%) for $C_{43}H_{64}FeN_4O_8$: C 62.92, H 7.86, N 6.83; found: C 62.97, H 8.09, N 7.32.

[(Fe(Lc)(C8))$_2$O] (3). [Fe(Lc)(C8)(MeOH)$_{1\text{-}2}$] (0.3 g 0.41 mmol) was dissolved in pyridine (6 mL) and heated to reflux for 15 min. After cooling to room temperature, H_2O (4 mL) was added and the mixture was shortly heated again until it boiled. After cooling to room temperature, fine crystalline brown precipitate was filtrated. Yield: 0.27 g (79 %); (828.81 g mol^{-1}). Elemental analysis calcd (%) for $C_{44}H_{60}FeN_4O_8$: C 63.76, H 7.30, N 6.76; found: C 63.66, H 7.21, N 7.27. Needle-like crystals of μ-oxido complex were formed in the remaining solution standing on air.

[Fe(Lc)(C8)(apy)] **(5)**. [Fe(Lc)(C8)(MeOH)$_{1-2}$] (0.29 g, 0.39 mmol) and apy (1.11 g, 11.79 mmol, 30.2 eq.) were dissolved in methanol (10 mL) and heated to reflux for 1 h. After storing the black solution for 4 d at 6°C, black block-like crystals were isolated. Yield: 0.08 g (25 %); (858.84 g mol^{-1}).

[{Fe(La)(C12)}$_2$(bpea)] **(8)**. [Fe(La)(C12)(MeOH)$_2$] (0.34 g, 0.39 mmol) and bpea (2.15 g, 11.67 mmol, 29.9 eq.) were dissolved in methanol (10 mL) and heated to reflux for 75 min. After 1 d at room temperature, greenish-black needles were filtrated and washed with methanol (3 mL). Yield: 0.06 g (16 %); (1806.00 g mol^{-1}). Elemental analysis calcd (%) for C$_{100}$H$_{152}$Fe$_2$N$_6$O$_{16}$: C 66.50, H 8.48, N 4.65; found: C 66.64, H 8.70, N 4.72.

[{Fe(Lb)(C12)(MeOH)}$_2$(bpea)] **(9)**. [Fe(Lb)(C12)] (0.27 g, 0.36 mmol) and bpea (1.83 g, 9.93 mmol, 27.5 eq.) were suspended in methanol (10 mL) and heated to reflux for 1 h. After 1 d at room temperature, black platelet-like crystals were filtrated. Yield: 0.02 g (3 %); (1749.98 g mol^{-1}).

[Fe(La)(C12)(apy)] **(10)**. [Fe(La)(C12)(MeOH)$_2$] (0.22 g, 0.37 mmol) and apy (1.03 g, 10.94 mmol, 29.6 eq.) were dissolved in methanol (10 mL) and heated to reflux for 1 h. After cooling to room temperature, black platelet-like crystals were isolated. Yield: 0.13 g (39 %); (904.99 g mol^{-1}). Elemental analysis calcd (%) for C$_{49}$H$_{76}$FeN$_4$O$_8$: C 65.03, H 8.46, N 6.19; found: C 65.34, H 8.55, N 6.33.

[Fe(Lb)(C12)(dmap)(MeOH)] **(11)**. [Fe(Lb)(C12)] (0.26 g, 0.35 mmol) and dmap (1.17 g, 9.58 mmol, 27.4 eq.) were dissolved in methanol (10 mL) and heated to reflux for 1 h. After 14 d at 6°C black needle-like crystals were filtrated and washed with methanol (3 mL). Yield: 0.01 g (3 %); (905.04 g mol^{-1}). Elemental analysis calcd (%) for C$_{50}$H$_{80}$FeN$_4$O$_7$: C 66.35, H 8.91, N 6.19; found: C 66.64, H 9.09, N 6.15.

H$_2$Ld(C22). 1,2-diamino-4,5-didocosyloxybenzene (1.2 g, 1.58 mmol) was suspended in ethanol (200 mL) saturated with argon and ethoxymethylenephenylacetoacetate (0.94 g, 3.80 mmol, 2.4 eq.) was added dropwise. The yellow suspension was heated to reflux for 90 min. and then stored at −30°C overnight. The precipitate was filtered and washed with eth-

anol (20 mL). The orange product was recrystallized from ethanol (30 mL). Yield: 1.42 g (77 %); (1161.72 g mol^{-1}). ^{1}H NMR (296 K, CDCl$_3$): $\delta = 0.87$ (t, 6 H, $^3J = 8$ Hz, CH_3), 1.20–1.64 (m, 80 H, CH$_3$(CH_2)$_{19}$, CH_3(Et)), 1.75–1.90 (m, 4 H, CH_2CH$_2$O), 3.95–4.11 (m, 8 H, CH_2O), 6.82 (s, 2 H, NHC$_q$CH), 7.30−7.75 (m, 10 H, Phenyl-CH), 8.30 (dd, 2 H, $^3J = 12.9$ Hz, C=CH), 12.14 ppm (dd, 2 H, $^3J = 12.9$ Hz, NH); Elemental analysis calcd (%) for C$_{74}$H$_{116}$N$_2$O$_8$: C 76.51, H 10.06, N 2.41; found C 76.76, H 9.96, N 2.71.

[Fe(Ld)(C22)(MeOH)$_2$]. H$_2$Ld(C22) (1.14 g, 0.98 mmol) and iron(II) acetate (0.36 g, 2.06 mmol, 2.1 eq.) were mixed in methanol (160 mL) and heated to reflux for 5 h. The brown precipitate was filtered, washed with methanol (2×15 mL) and dried in vacuum. Yield: 0.93 g (74 %); (1279.63 g mol^{-1}). Elemental analysis calcd (%) for C$_{76}$H$_{122}$FeN$_2$O$_{10}$: C 71.33, H 9.61, N 2.19; found: C 71.45, H 10.05, N 2.48.

[Fe(Ld)(C22)(dmap)$_2$]×0.5EtOH (13). [Fe(Ld)(C22)(MeOH)$_2$] (0.25 g, 0.20 mmol) and dmap (1.22 g, 10.02 mmol, 50.0 eq.) were dissolved in a mixture of toluene (8 mL) and ethanol (2 mL) and heated to reflux for 90 min. After cooling to −30°C ethanol (5 mL) were added and the green solution again stored at −30°C for 11 d. The brown precipitate was filtered and dried in vacuum. Yield: 0.13 g (45 %); (1482.92 g mol^{-1}). In the residual solution black needle-like crystals were formed.

[Fe(Ld)(C22)(dmap)$_2$] (powder). [Fe(Ld)(C22)(MeOH)$_2$] (0.17 g, 0.13 mmol) and dmap (0.81 g, 6.65 mmol, 50 eq.) were heated to reflux in ethanol (30 mL) for 90 min. After 3 d the brown precipitate was filtered, washed with ethanol (3 mL) and dried in vacuum. Yield: 0.19 g (98 %); (1459.89 g mol^{-1}). Elemental analysis calcd (%) for C$_{88}$H$_{134}$FeN$_6$O$_8$: C 72.40, H 9.25, N 5.76; found: C 72.20, H 9.45, N 5.97.

X-ray Diffraction: The intensity data of **1**, **2**, **3**, **9**, **10** and **11** were collected with a Stoe IPDS II diffractometer, the intensity data of **5** with a Bruker Nonius Kappa CCD diffractometer and the intensity data of **13** with a Bruker D8 Venture diffractometer using graphite-monochromated Mo-K_α radiation. The data were corrected for Lorentz and polarization effects. The structures were solved by direct methods (SIR97 (**1**, **10**, **11**)[35], SIR2004 (**3**, **5**)[36] and SHELXS-97 (**8**, **9**, **13**)[37]) and refined by full-matrix least-square tech-

niques against $F_0{}^2$ (SHELXL-97, SHELXH-97 for **3**, **10** and **13**).[37] The hydrogen atoms were included at calculated positions with fixed displacement parameters, allowed to ride on their parent atoms. If not denoted differently, for methyl and hydroxyl groups the torsion angles were allowed to be refined according to the electron density. In the structure of **11**, the proton of the methanol hydroxyl group was directly located according its electron density. If not denoted differently in the cif-file, all non-hydrogen atoms were refined anisotropically. Due to bad quality of the data of **1**, **3**, **5** and **10** only the general molecular setup could be investigated. For **3** and **5**, twin refinement was conducted based on twin law

$$
\begin{pmatrix}
-1.000 & 0.000 & 0.000 \\
0.026 & 1.000 & -0.188 \\
0.000 & 0.000 & -1.000
\end{pmatrix}
\qquad
\begin{pmatrix}
-1.000 & 0.000 & 0.000 \\
0.000 & -1.000 & 0.000 \\
0.224 & 0.000 & 1.000
\end{pmatrix}
$$

<div align="center">

(3)   **(5)**

</div>

found by PLATON.[38] ORTEP-III[39] was used for the structure representation, Schakal-99[40] and Mercury[41] for the representation of the molecule packing. The CCDC numbers corresponding to the compounds are listed in the Supporting Information (Table S1).

7.5   References

[1]   M. A. Halcrow in *Spin-Crossover Materials*; (Ed. M. A. Halcrow), John Wiley & Sons Ltd, **2013**, 147–169.

[2]   a) M. A. Halcrow, *Coord. Chem. Rev.* **2009**, *253*(21-22), 2493–2514. b) A. B. Koudriavtsev, W. Linert, *J. Struct. Chem.* . **2010**, *51*(2), 335–365. c) K. S. Murray, *Aust. J. Chem.* **2009**, *62*(9), 1081–1101. d) S. Brooker, J. A. Kitchen, *Dalton Trans.* **2009**, *36*, 7331–7340. e) A. Gaspar, M. Seredyuk, P. Gütlich, *J. Mol. Struc.* **2009**, *924-926*, 9–19. f) J.-F. Létard, *J. Mater. Chem.* **2006**, *16*(26), 2550–2559. g) P. Gütlich, H. Goodwin, Eds, *Spin Crossover in Transition Metal Compounds I-III;* Springer Berlin / Heidelberg, **2004**. h) J. A. Kitchen, S. Brooker, *Coord. Chem. Rev.* **2008**, *252*(18-20), 2072–2092. i) O. Sato, J. Tao, Y.-Z. Zhang, *Angew. Chem. Int. Ed.* **2007**, *46*(13), 2152–2187.

[3]   P. Gütlich, A. Hauser, H. Spiering, *Angew. Chem. Int. Ed.* **1994**, *33*(20), 2024–2054.

[4]   B. Weber, *Coord. Chem. Rev.* **2009**, *253*(19-20), 2432–2449.

[5]   M. A. Halcrow, *Chem. Soc. Rev.* **2011**, *40*(7), 4119–4142.

[6]   Y. Garcia, B.-L. Su, Y. Komatsu, K. Kato, Y. Yamamoto, H. Kamihata, Y. H. Lee, A. Fuyuhiro, S. Kawata, S. Hayami, *Eur. J. Inorg. Chem.* **2012**, *16*, 2769–2775.

[7]   a) S. Hayami, R. Moriyama, A. Shuto, Y. Maeda, K. Ohta, K. Inoue, *Inorg. Chem.* **2007**, *46*(19), 7692–7694. b) M. Seredyuk, A. B. Gaspar, V. Ksenofontov, Y. Galyametdinov, J. Kusz, P. Gütlich, *Adv. Funct. Mater.* **2008**, *18*(14), 2089–2101. c) Y. Bodenthin, U. Pietsch, H. Möhwald, D. G. Kurth, *J. Am. Chem. Soc.* **2005**, *127*(9), 3110–3114. d) M. Seredyuk, A. B. Gaspar, V. Ksenofontov, Y. Galyametdinov, J. Kusz, P. Gütlich, *J. Am. Chem. Soc.* **2008**, *130*(4), 1431–1439.

[8]   A. B. Gaspar, M. Seredyuk, P. Gütlich, *Coord. Chem. Rev.* **2009**, *253*(19-20), 2399–2413.

[9]   S. Hayami, Y. Komatsu, T. Shimizu, H. Kamihata, Y. H. Lee, *Coord. Chem. Rev.* **2011**, *255*(17-18), 1981–1990.

[10]   C. Gandolfi, T. Cotting, P. N. Martinho, O. Sereda, A. Neels, G. G. Morgan, M. Albrecht, *Dalton Trans.* **2011**, *40*(9), 1855–1865.

[11]   P. N. Martinho, C. J. Harding, H. Müller-Bunz, M. Albrecht, G. G. Morgan, *Eur. J. Inorg. Chem.* **2010**, *5*, 675–679.

[12]   S. Hayami in *Spin-Crossover Materials*; (Ed. M. A. Halcrow), John Wiley & Sons Ltd, **2013**, 321–345.

[13]   C. Gandolfi, G. G. Morgan, M. Albrecht, *Dalton Trans.* **2012**, *41*(13), 3726–3730.

[14]   P. N. Martinho, Y. Ortin, B. Gildea, C. Gandolfi, G. McKerr, B. O'Hagan, M. Albrecht, G. G. Morgan, *Dalton Trans.* **2012**, *41*(25), 7461–7463.

[15]   a) P. N. Martinho, C. Rajnak, M. Ruben in *Spin-Crossover Materials*; (Ed. M. A. Halcrow), John Wiley & Sons Ltd, **2013**, 375–404. b) J. A. Kitchen, N. G. White, C. Gandolfi, M. Albrecht, G. N. L. Jameson, J. L. Tallon, S. Brooker, *Chem. Commun.* **2010**, *46*(35), 6464. c) D. R. Talham, *Chem. Rev.* **2004**, *104*(11), 5479–5502.

[16]   S. Schlamp, P. Thoma, B. Weber, *Eur. J. Inorg. Chem.* **2012**, *16*, 2759–2768.

[17]   S. Schlamp, B. Weber, A. D. Naik, Y. Garcia, *Chem. Commun.* **2011**, *47*(25), 7152–7154.

[18]   S. Schlamp, K. Dankhoff, B. Weber, *New J. Chem.* **2014**, **DOI:** 10.1039/C3NJ00991B.

[19]   B. Weber, E.-G. Jäger, *Eur. J. Inorg. Chem.* **2009**, *4*, 465–477.

[20]   W. Bauer, W. Scherer, S. Altmannshofer, B. Weber, *Eur. J. Inorg. Chem.* **2011**, 2803–2818.

[21]   a) J. Larionova, L. Salmon, Y. Guari, A. Tokarev, K. Molvinger, G. Molnár, A. Bousseksou, *Angew. Chem. Int. Ed.* **2008**, *47*(43), 8236–8240. b) F. Volatron, L. Catala, E. Rivière, A. Gloter, O. Stéphan, T. Mallah, *Inorg. Chem.* **2008**, *47*(15), 6584–6586. c) E. Coronado, J. R. Galán-Mascarós, M. Monrabal-Capilla, J. García-Martínez, P. Pardo-Ibáñez, *Adv. Mater.* **2007**, *19*(10), 1359–1361. d) I. Boldog, A. B. Gaspar, V. Martínez, P. Pardo-Ibañez, V. Ksenofontov, A. Bhattacharjee, P. Gütlich, J. A. Real, *Angew. Chem.* **2008**, *120*(34), 6533–6537. e) J. R. Galán-Mascarós, E. Coronado, A. Forment-Aliaga, M. Monrabal-Capilla, E. Pinilla-Cienfuegos, M. Ceolin, *Inorg. Chem.* **2010**, *49*(12), 5706–5714. f) S. M. Neville, C. Etrillard, S. Asthana, J.-F. Létard, *Eur. J. Inorg. Chem.* **2010** (2), 282–288. g) T. Forestier, A. Kaiba, S. Pechev, D. Denux, P. Guionneau, C. Etrillard, N. Daro, E. Freysz, J.-F. Létard, *Chem. Eur. J.* **2009**, *15*(25), 6122–6130.

[22]   W. Bauer, B. Weber, *Acta Cryst. C* **2008**, *64*(6), m237.

[23]   a) W. Bauer, M. M. Dîrtu, Y. Garcia, B. Weber, *CrystEngComm* **2012**, *14*(4), 1223. b) T. M. Pfaffeneder, S. Thallmair, W. Bauer, B. Weber, *New J. Chem.* **2011**, *35*(3), 691–700.

[24]   J. N. Israelachvili, D. J. Mitchell, B. W. Ninham, *J. Chem. Soc, Faraday Trans. 2* **1976**, *72*, 1525–1568.

[25]   K. S. Murray in *Spin-Crossover Materials*; (Ed. M. A. Halcrow), John Wiley & Sons Ltd, **2013**, 1–54.

[26]   a) S. Hayami, N. Motokawa, A. Shuto, R. Moriyama, N. Masuhara, K. Inoue, Y. Maeda, *Polyhedron* **2007**, *26*(9-11), 2375–2380. b) M. Seredyuk, A. B. Gaspar, V. Ksenofontov, Y. Galyametdinov, M. Verdaguer, F. Villain, P. Gütlich, *Inorg. Chem.* **2010**, *49*(21), 10022–10031. c) M. Seredyuk, A. B. Gaspar, V. Ksenofontov, Y. Galyametdinov, M. Verdaguer, F. Villain, P. Gütlich, *Inorg. Chem.* **2008**, *47*(22), 10232–10245.

[27]   C. Gandolfi, C. Moitzi, P. Schurtenberger, G. G. Morgan, M. Albrecht, *J. Am. Chem. Soc.* **2008**, *130*(44), 14434–14435.

[28]   S. Hayami, Y. Shigeyoshi, M. Akita, K. Inoue, K. Kato, K. Osaka, M. Takata, R. Kawajiri, T. Mitani, Y. Maeda, *Angew. Chem. Int. Ed.* **2005**, *44*(31), 4899–4903.

[29]   A. M. Ako, M. S. Alam, M. Rahman, J. P. Hill, N. M. Sanchez-Ballester, K. Ariga, G. Buth, C. E. Anson, A. K. Powell, *Chem. Eur. J.* **2012**, *18*(51), 16419–16425.

[30]   H. G. O. Becker, *Organikum*, Organisch-chemisches Grundpraktikum; Johann Ambrosius Barth, Berlin, **1993**.

[31]   L. Claisen, *Justus Liebigs Ann. Chem.* **1897**, *297*(1-2), 1–98.

[32]   W. Bauer, T. Ossiander, B. Weber, *Z. Naturforsch. B* **2010**, *65b*, 323–328.

[33]   E.-G. Jäger, E. Häussler, M. Rudolph, A. Schneider, *Z. Anorg. Allg. Chem.* **1985**, *525*(6), 67–85.

[34]   B. Weber, R. Betz, W. Bauer, S. Schlamp, *Z. Anorg. Allg. Chem.* **2011**, *637*(1), 102–107.

[35]   A. Altomare, M. C. Burla, M. Camalli, G. L. Cascarano, C. Giacovazzo, A. Guagliardi, A. G. G. Moliterni, G. Polidori, R. Spagna, *J. Appl. Cryst.* **1999**, *32*(1), 115–119.

[36]   M. C. Burla, R. Caliandro, M. Camalli, B. Carrozzini, G. L. Cascarano, L. de Caro, C. Giacovazzo, G. Polidori, R. Spagna, *J. Appl. Cryst.* **2005**, *38*(2), 381–388.

[37]   G. Sheldrick, *Acta Cryst. A* **2008**, *64*(1), 112–122.

[38]   A. L. Spek, *PLATON - A Multipurpose Crystallographic Tool;* Utrecht University, Utrecht, The Netherlands, **2008**.

[39]   a) L. Farrugia, *J. Appl. Cryst.* **1997**, *30*(5), 565. b) C. K. Johnson, M. N. Burnett, *ORTEP-III;* Oak-Ridge National Laboratory, Oak-Ridge, TN, **1996**.

[40]   E. Keller, *Schakal-99;* University of Freiburg, Freiburg, Germany, **1999**.

[41]   C. F. Macrae, P. R. Edgington, P. McCabe, E. Pidcock, G. P. Shilds, R. Taylor, M. Towler, J. van de Streek, *J. Appl. Cryst.* **2006**, *39*, 453–457.

7.6   Supporting Information

Table S1. Crystallographic data for the complexes discussed in this work. (Part 1)

	1	3	5	8
net formula	$C_{43}H_{64}FeN_4O_8$	$C_{68}H_{100}Fe_2N_4O_{17}$	$C_{39}H_{56}FeN_4O_8$	$C_{100}H_{152}Fe_2N_6O_{16}$
M_r/g mol^{-1}	820.83	1357.23	764.73	1805.98
crystal size /mm	0.04×0.13×0.53	0.16×0.19×0.35	0.05×0.09×0.14	0.21×0.23×0.32
T/K	133	133	133	140
radiation	0.71073	0.71073	0.71073	0.71073
diffractometer	Stoe IPDS II	Stoe IPDS II	Bruker Nonius Kappa CCD	Stoe IPDS II
crystal system	triclinic	triclinic	monoclinic	triclinic
space group	$P\bar{1}$	$P\bar{1}$	$P2_1/c$	$P\bar{1}$
a/Å	11.937(7)	17.0266(17)	19.8908(15)	9.3120(5)
b/Å	12.691(6)	19.491(2)	8.2455(7)	16.9900(7)
c/Å	15.441(8)	21.547(2)	24.2820(19)	31.6108(15)
α/°	97.06(4)	84.173(10)	90	93.931(3)
β/°	99.48(4)	77.669(8)	95.253(3)	97.344(4)
γ/°	106.46(4)	89.375(9)	90	92.276(4)
V/Å^3	2177(2)	6949.2(12)	3965.8(5)	4942.5(4)
Z	2	2	4	2
d_{calc}/g cm^{-3}	1.252	1.297	1.281	1.214
μ/mm^{-1}	0.401	0.487	0.435	0.359
absorption correction	none	none	none	none
refls. measured	17168	54770	18860	48391
R_{int}	0.595	0.00 (0.287)*	0.00 (0.216)*	0.0852

F(000)	880	2896	1632	1948
θ range /°	1.4–21.4	1.0–21.1	3.2–23.0	1.2–23.1
hydrogen refinement	constr	constr	constr	constr
Indep. reflections	4670	14954	5456	13178
parameters	504	1606	479	1337
$R(F_{obs})$	0.0968	0.0686	0.1619	0.0558
$R_w(F^2)$	0.2505	0.1910	0.3572	0.1535
S	0.67	0.71	1.14	0.98
max electron density /e Å^{-3}	0.27	0.34	0.90	0.32
min electron density /e Å^{-3}	−0.31	−0.28	−0.89	−0.73
CCDC	952444	952445	952442	952449

* new hkl file written by PLATON; original R_{int} in brackets.

Table S1. Crystallographic data for the complexes discussed in this work. (Part 2)

	9	**10**	**11**	**13**
net formula	$C_{98}H_{152}Fe_2N_6O_{14}$	$C_{49}H_{76}FeN_4O_8$	$C_{50}H_{80}FeN_4O_7$	$C_{88}H_{134}FeN_6O_8$, 0.5 C_2H_6O
M_r /g mol^{-1}	1749.97	904.99	905.03	1428.90
crystal size /mm	0.17×0.22×0.27	0.09×0.09×0.13	0.15×0.31×0.71	0.02×0.06×0.19
T /K	133	133	133	173
radiation	0.71073	0.71073	0.71073	0.71073
diffractometer	Stoe IPDS II	Stoe IPDS II	Stoe IPDS II	Bruker D8 Venture

crystal system	monoclinic	triclinic	monoclinic	triclinic
space group	$P2_1/c$	$P\bar{1}$	$P2_1/c$	$P\bar{1}$
a/Å	8.9561(3)	12.8590(19)	34.2715(13)	12.5393(10)
b/Å	17.2696(6)	13.992(2)	17.3134(6)	21.3080(14)
c/Å	61.915(3)	28.702(5)	8.3910(3)	32.365(3)
α/°	90	92.294(13)	90	96.343(3)
β/°	90.085(3)	102.641(12)	93.345(3)	97.189(2)
γ/°	90	101.611(11)	90	92.590(2)
V /Å^3	9576.3(7)	4916.7(14)	4970.4(3)	8511.7(12)
Z	4	4	4	4
d_{calc} /g cm^{-3}	1.214	1.223	1.209	1.157
μ /mm^{-1}	0.367	0.361	0.356	0.235
absorption correction	none	none	none	multi-scan
refls. measured	31375	59374	56757	48069
R_{int}	0.076	0.345	0.145	0.080
F(000)	3784	1952	1960	3228
θ range /°	1.2– 24.6	1.5–24.7	1.2–24.6	2.2– 22.8
hydrogen refinement	constr	constr	mixed	constr
Indep. reflections	11256	16557	8347	21598
parameters	1097	1079	582	1918
$R(F_{obs})$	0.0585	0.0721	0.0616	0.0566
$R_w(F^2)$	0.1450	0.2149	0.1399	0.1861
S	0.87	0.70	1.03	1.00

max electron density /e $\mathring{A}^{-3}$	0.48	0.27	0.40	0.70
min electron density /e $\mathring{A}^{-3}$	−0.50	−0.19	−0.45	−0.44
CCDC	952446	952447	952448	952443

Figure S1. $\chi_M T$ vs. T plot of **[Fe(Ld)(C22)(dmap)₂]** (powder) displayed in the temperature range 10–350 K.
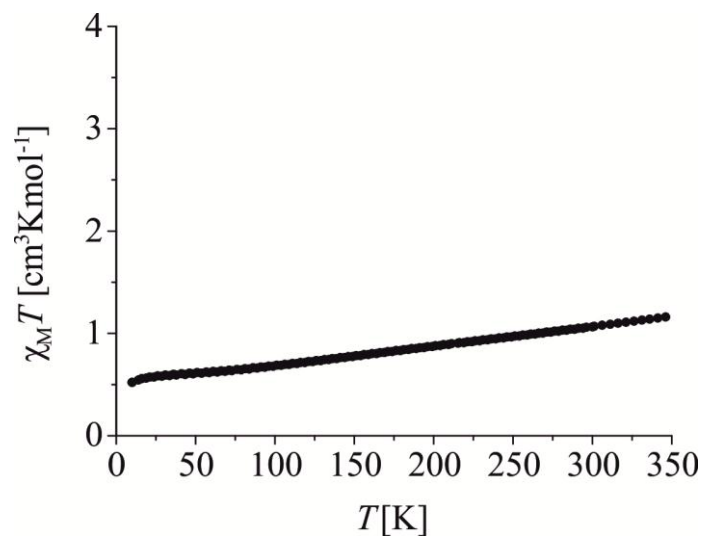
8   Amphiphilic Iron(II) Spin Crossover Coordination Polymers with C22 Alkyl Chains

Stephan Schlamp,[a] Birgit Weber*[a]

[a] Prof. Dr. Birgit Weber, Stephan Schlamp, Inorganic Chemistry II, Universität Bayreuth, Universitätsstraße 30, NW 1, 95440 Bayreuth, Germany, Fax: +49-92155-2157, E-mail: weber@uni-bayreuth.de

Manuscript in preparation.

Abstract: Novel iron(II) spin crossover coordination polymers with two C22 alkyl chains on the outer periphery of the ligand were synthesized. The hexa-coordinated complexes are composed of an equatorially coordinating amphiphilic tetradentate Schiff base-like ligand and different axially coordinating bridging ligands (1,2-bis(4-pyridyl)ethane (bpea) (**1**), 1,2-bis(4-pyridyl)ethene (bpee) (**2**) and 1,2-bis(4-pyridyl)ethyne (bpey) (**3**)) that lead to the formation of coordination polymers. The crystal structure of **1** could be obtained showing a lipid layer-like arrangement of the molecules in the crystal. Despite the extended alkyl chains, magnetic measurements reveal abrupt spin transitions above room temperature. The transition temperature of the spin crossover rises from single (bpea), towards double bond (bpee) and the abruptness from single (bpea), towards double bond (bpee) to triple bond (bpey) in the axial ligand. The organization of the three coordination polymers into spherulites could be observed between crossed polarizers in an optical microscope.

8.1   Introduction

Magnetic bistability is a property of mostly hexa-coordinated complexes that can occur within transition metals in d^4-d^7 electron configuration.[1] Through external perturbations like temperature, light or pressure changes, the spin state of the central metal can be switched between the high spin (HS) to the low spin (LS) state. This is accompanied, for example, by changes in the structure (shortening of the metal-ligand bond lengths for the HS to LS transition), of the colour and other physical properties like magnetism. In the case of a cooperative spin transition (ST), the structural changes are mediated through the material by intermolecular interactions between the molecules, like hydrogen bonds or π-π interactions.[2] Van der Waals interactions or a direct linking of the iron centres via covalent bonds resulting in the formation of coordination polymer can also enhance cooperative effects.[3] These switchable molecular materials have a high potential for applications like information storage or as sensors in temperature control or cold channel control units.[4] Combining spin crossover (SCO) with additional properties like softness (metallomesogens) or the synthesis of nanostructured composite materials leads to multifunctionality enlarging the range of potential SCO applications. Seredyuk *et al*. demonstrated that the SCO can be influenced by crystal-liquid crystal phase transitions (PTs) of metal complexes functionalized with long alkyl substituents.[5,6] But also PTs in solid state are very interesting due to the possibility to study the spin switching mechanism and therefore explain the occurring SCO curve as it was demonstrated before for a lipid layer-like arranged SCO complex of Fe(II) with an alkylated Schiff base-like ligand.[7]

The aim of this work is to design SCO complexes that are able to accumulate in a self-assembly process to higher ordering in the crystal packing. Previous work on this type of Schiff base-like ligands with long alkyl chains showed that the molecules arrange in a lipid layer-like structure in the crystal, where van der Waals interactions occur between the alkyl chains and due to this the cooperative interactions between the molecules can be increased.[7–10] Attempts with the different chain lengths of 8, 12, and 16 carbon atoms were conducted and it turned out that not only the molecular arrangement in the solid state, but also the coordination number of the metal centre strongly depends on the length of these chains. The interplay of the amount and the size of the axial ligands attached at the iron(II) centre and the chain length is now understood.[9] In order to obtain hexa-coordinated iron centres with the relatively large bridging ligands bpea/bpee/bpey leading to a lipid layer-like arrangement of

coordination polymers it is necessary to increase the chain lengths of the Schiff base-like ligand to 22 carbon atoms.

The synthesis of complex **1, 2** and **3** follows an eight step synthesis and is described in the Experimental Section, Scheme 1, exemplarily for **1**. Next to the black crystalline sample of **1**, also a brown powder sample (**1b**) and another modification (**1c**) were investigated. **2** precipitates as bluish black, and **3** as black microcrystalline powder.

All intermediate products were characterized by elemental analysis, ^{1}H NMR and IR spectroscopy as well as mass spectrometry. The final products were analyzed using elemental analysis, X-ray structure analysis, magnetic measurements, thermogravimetry (TGA) and polarizing optical microscopy (POM).

8.2   Results and Discussion

8.2.1   Discussion of the X-ray structure

Spicular crystals of **1** could be isolated. The molecular setup was determined at 200 K, corresponding to the LS state of the molecule and is shown in Figure 1. Selected bond lengths and angles of **1** are displayed in Table 1, crystallographic data in Table S1. The compound crystallizes in the triclinic space group $P\bar{1}$ and contains 2 molecules in its unit cell. The average bond lengths within the first coordination sphere of the iron(II) centres are 1.90 Å (Fe–N_{eq}) and 1.93 Å (Fe–O_{eq}) and relatively short 2.01 Å for Fe–N_{ax}. The O–Fe–O angle of 90° shows a typical value for this kind of iron(II) complexes in the LS state.[11] The planes spanned by the axially attached pyridine rings are with 88.6° nearly perpendicular to each other, the N_{ax}–Fe–N_{ax} angle of 175.9° shows only a very small deviation of the ideal octahedral coordination geometry. Parts of solvent could not be solved in the structure and were squeezed. Only one short contact shorter than 0.1 Å than the sum of the van der Waals radii connects the molecules in the nearer neighbourhood of the iron centres (O1···H18B of the methylester group: 2.61 Å). This contact connects the molecules shifted right above. Interactions between the opposed heads can be observed taking short contacts longer than at least 0.1 Å than the sum of the van der Waals radii and higher. Only very few interactions between the chain layers can be obseved taking short contacts that are bigger by 0.1 Å than the sum of the van der Waals radii (H51A–H33A (2.404), H54B–H72B (2.469)) into account.

A maximum of chain interaction is reached with short contacts longer by 0.3-0.4 Å than the sum of the van der Waals radii. This corresponds to a maximum of stabilizing van der Waals interactions within the alkyl chains. This is also expressed by the particularly high ordering of the alkyl chains without major bending in comparison to a previously described C22 alkyl chain.[9]
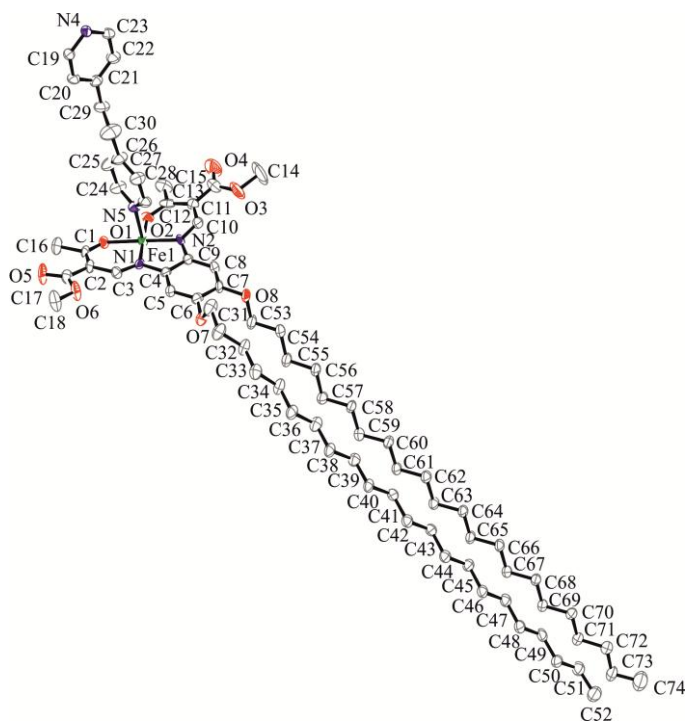

Figure 1. Crystal structure of **1**. Hydrogen atoms are omitted for clarity.

Table 1. Selected bond lengths [Å] and angles [°] of **1** within the first coordination sphere.

Complex	Fe–N$_{eq}$	Fe–O$_{eq}$	Fe–N$_{ax}$	O$_{ax}$–Fe–O$_{ax}$	L$_{ax}$–Fe–L$_{ax}$
1	1.885(4), 1.908(3)	1.917(3), 1.953(3)	2.012(3), 2.003(4)	90.05(10)	175.91(16)

As shown in Figure 2, the molecules are ordered in the crystal in a lipid layer-like arrangement, the polar "heads", synonymic with the infinite chains built by the Schiff base-like ligand and bpea directly coordinating the iron point to each other and the nonpolar C22

alkyl chains ("tails") are overlaying each other with an approximate layer-layer distance of about 4.19 Å. The nonpolar part spans an angle to the N_2O_2 plane of 49.6° and is shifted aside for around 15°. This deviation of the ideal arrangement along the equatorial ligand is made responsible for the possibility of the complex to crystallize hexa-coordinated. The movement compensates the sterical demand of the axial bpea and nevertheless provides a lipid layer-like ordering. This is not the case for ligands of the same family with shorter alkyl chains where the molecules did not crystallize octahedrally with two sterically demanding axial ligands and at the same time in the layered structure.[10] The length of the complex in the crystal is around 28.71 Å, and in relation to the height of 13.35 Å and a broadness of 14.15 Å this results in a self-assembly parameter (*sap*) of 0.96.[9]
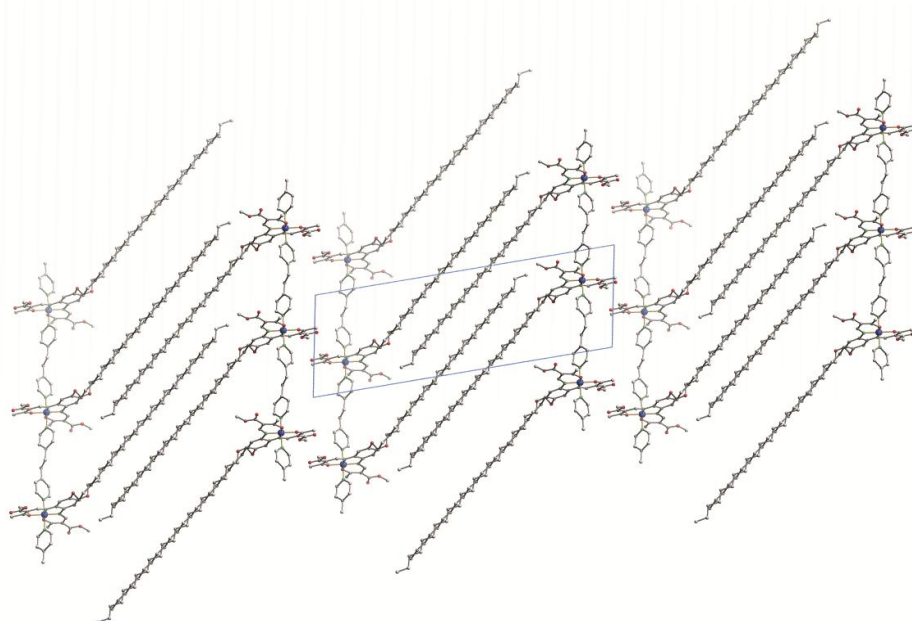
Figure 2. Packing of the molecules of **1** in the crystal projected along [1 0 0].

8.2.2   Magnetic measurements

The magnetic measurements for the crystalline sample of **1** and the microcrystalline samples of **2** and **3** are depicted in Figure 3.

At room temperature, the magnetic moment of **1** is with a $\chi_M T$ value of 0.52 cm^3 K mol^{-1} in the region for an iron(II) complex almost in the LS. Decreasing of the temperature leads to a

gradual decrease of the magnetic moment until 225 K where nearly 100 % of the complex molecules are clearly in the LS state with a $\chi_M T$ value of 0.15 cm^3 K mol^{-1}. Upon warming, the material stays at $\chi_M T = 0.52$ cm^3 K mol^{-1} until 310 K where an abrupt ST till 315 K takes place involving about 14 % of the molecules. From 335 K on, where about 40 % of the molecules are already in the HS state, again an abrupt ST occurs until $\chi_M T = 3.57$ cm^3 K mol^{-1} at 350 K, involving the remaining 60 % of the molecules.
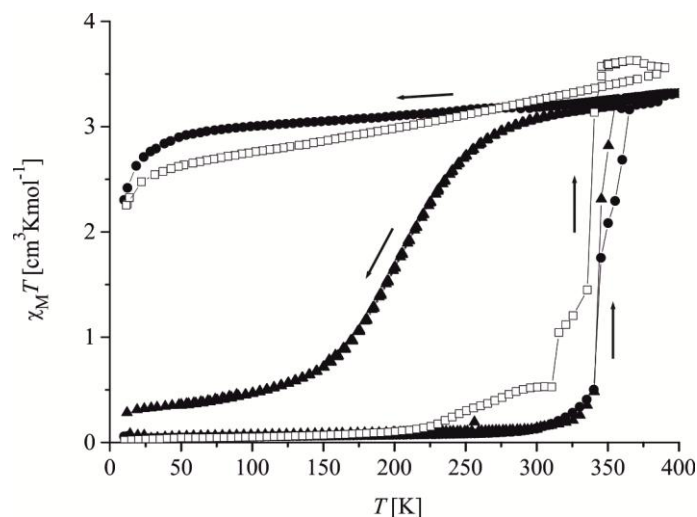
Figure 3. $\chi_M T$ vs. T plot of **1** (open squares), **2** (circles) and **3** (triagles) in the warming and first cooling mode displayed in the temperature range 10–400 K.

In contrary to **1**, the complexes **2** and **3** present only $\chi_M T$ values around 0.14 cm^3 K mol^{-1} at room temperature referring to reside in the LS state. Heating of the compounds leads to a slow increase of the magnetic moment until 340 K ($\chi_M T = 0.50$ cm^3 K mol^{-1}), where both, **2** and **3** undergo an abrupt ST. In this frame, the course of **3** is clearly more abrupt than the one of **2**. While at 345 K the magnetic moment of **2** is at 1.74 cm^3 K mol^{-1}, the one for **3** is already at 2.39 cm^3 K mol^{-1}. From then on, **2** exhibits a more gradual part and is in the HS state at around 365 K, whereas **3** features the HS state at 355 K. Comparing of the ST temperature ranges of the three compounds reveal 45 K for the complex with bpea, 25 K for the one with bpee and only 15 K for the compound with bpey as axial ligand. $T_{1/2}$ of **2** and **3** rises from 335 K to 345 K in comparison to **1**. This demonstrates the increase of cooperativity of SCO on exchanging the single bond in the bridging ligand through a more rigid double bond or a triple bond.

After heating to 400 K, the ST of **1** and **2** upon cooling is vanished, the SCO is irreversible. For **3**, the situation is different. After heating to 400 K, the shape of the curve is gradual, the SCO occurs between about 275 K and 100 K and vanishes successively after several cycles.

The complex **1** can precipitate as a brown powder (**1b**) or as a further microcrystalline sample (**1c**). Differential thermogravimetry and elemental analysis show a content of 0.3-0.8 molecules of ethanol per complex molecule for **1b**, the complex starts to decompose at about 222°C. **1c** contains about 0.2 molecules ethanol per complex molecule.

The spin transition curve is more gradual for **1b** in comparison to **1**, especially in the part below 330 K. A typical representative is shown in Figure 4. This is due to the more disordered morphology in comparison to the crystalline sample, where the cooperative effects propagate the ST easier and more consistently through the crystal. **1c** shows a complete different behaviour with regard to magnetic character (see Figure 4). A relatively abrupt ST is observed between 200 K and 250 K, exhibiting a 5 K wide hysteresis. In this SCO about 83 % of the molecules are involved and after heating above 360 K, SCO activity is again lost upon cooling. The different amount of included solvent could be the reason for the different SCO behaviour. After heating above 360 K all solvent is removed and the same HS behaviour is observed for all complexes.
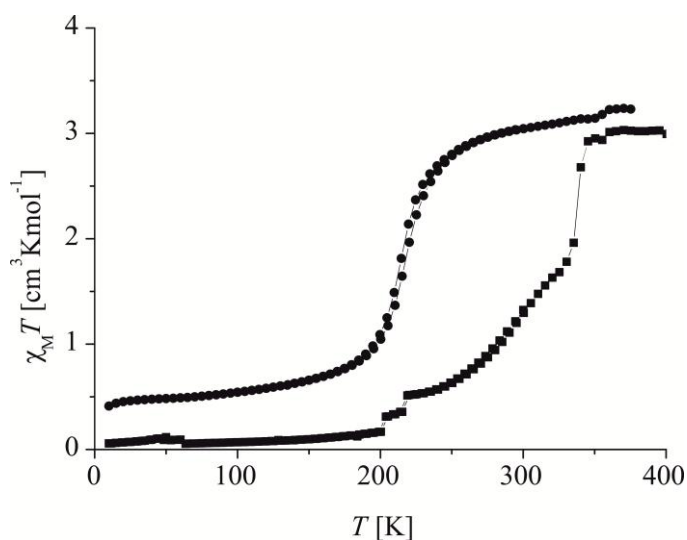

Figure 4. $\chi_M T$ vs. *T* plot of **1b** (squares) and **1c** (cycles) displayed in the temperature range 10–400 K.

The different appearances of SCO imply that, independent of the ligand field strength of the N_4O_2 coordination sphere, particularly packing effects are responsible for ST behaviour. For increased cooperativity, crystalline matter with a lipid layer-like arrangement seems to be most appropriate. The small plateaus and gradual parts can be caused by either the loss of solvent or rearrangement of the alkyl chains or molecules (PTs).

8.2.3 Polarizing optical microscopy

Polarizing optical microscopy was conducted on compounds **1b**, **2** and **3**. It revealed for all coordination polymers ordering into spherulites. Figure 5 shows the appearances of the compounds at the given temperatures.

a)

b)

c)
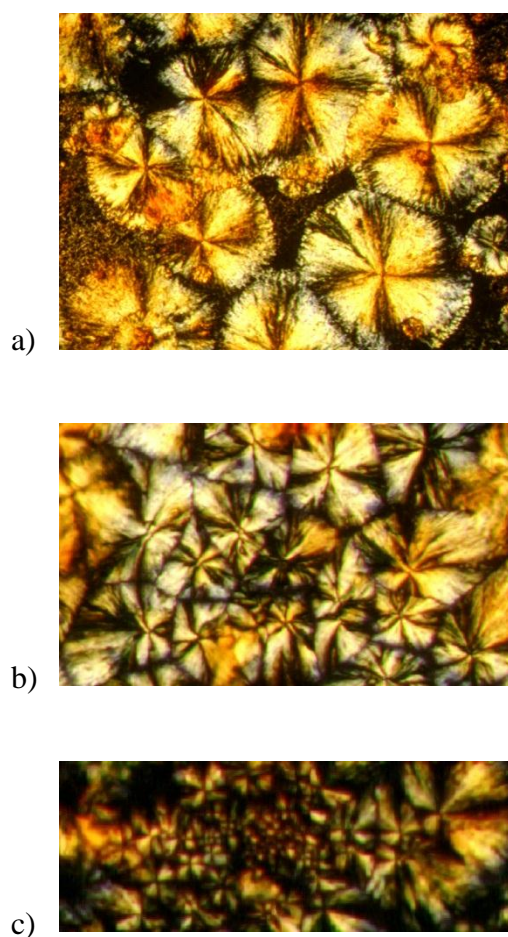
Figure 5. Appearance of a) **1b** at 333 K, b) **2** at 366 K and c) **3** at 373 K viewed between crossed polarizers.

Upon cooling from 408 K, after the irreversible SCO occurred, **1b** arranges in spherulites at about 360 K. At around 340 K, the growth of spherulites is increasing and the coordination polymer remains like this until room temperature (Figure 5a). This can be the reason for the irreversibility of the SCO of **1b**. **2** arranges, like **1b**, in spherulites that grow from 348 K until around 380 K upon the second warming, visible between crossed polarizers (Figure 5b). They are vanishing at around 381 K. The spherulites cannot be seen upon first heating and not upon cooling as well. The growth of spherulites of **3** between 345 K and 380 K (Figure 5c) can be observed in a very similar temperature region like in **2** upon second warming. An explanation why they cannot be seen also during cooling like in **1b** might be the insufficient time for the rearrangement of the rigid coordination polymer chains.

8.3   Conclusion

In this article, new octahedral amphiphilic SCO coordination polymers with two C22 alkyl chains in the outer periphery of the equatorial ligand and bpea, bpee and bpey as axial ligands are presented and the X-ray structure of the former is discussed. It shows that the molecules arrange in a lipid layer-like arrangement with the nonpolar tails forming the layers and the polar head groups pointing to each other. The transition temperature of the mostly irreversible spin crossover rises from single (bpea), towards double bond (bpee) and the abruptness from single (bpea), towards double bond (bpee) to triple bond (bpey) in the axial ligand. In comparison to **1**, which precipitates in two modifications containing different amounts of solvent that show different SCO behaviour, solvent influence in **2** and **3** seems less pronounced. All coordination polymers arrange in spherulites after warming.

8.4 Experimental Section

General: The synthesis of the iron complexes was carried out under an argon atmosphere (argon 5.0) using Schlenk techniques. The solvents were purified as described in the literature[12] and distilled under an atmosphere of argon or saturated with argon over one hour. When argon is used for the synthesis of the intermediate products, it is described in the text. The alkylbromide, bpea and bpee were a commercial product (Sigma-Aldrich) and used as received. The synthesis of methoxymethylenemethylacetoacetate (**F**)[13], 1,2-bis(4-pyridyl)ethyne (bpey)[14] and iron(II) acetate[15] are described elsewhere.

The synthesis of complex **1** and **2** follows an eight step synthesis starting with the alkylation of 1,2-dihydroxybenzene. The product **A** is nitrated with fuming nitric acid in acetic acid to give **B** in good yields, and **B** is again reduced with hydrazine and a Pd/C catalyst to give **C** as an air sensitive white powder. Conversion with **D** what was synthesised according to Claisen[16] gave the desired ligand **H$_2$L**. Further reaction with iron(II) acetate synthesized according to literature[17] yielded in the compound **[Fe(L)(MeOH)$_2$]** with two methanol as axial ligands. Final replacement of the methanol by bpea/bpee/bpey with two N-donor ligands shifts the iron in the resulting product **1/2/3** into the right energy region for thermal induced spin crossover activity.
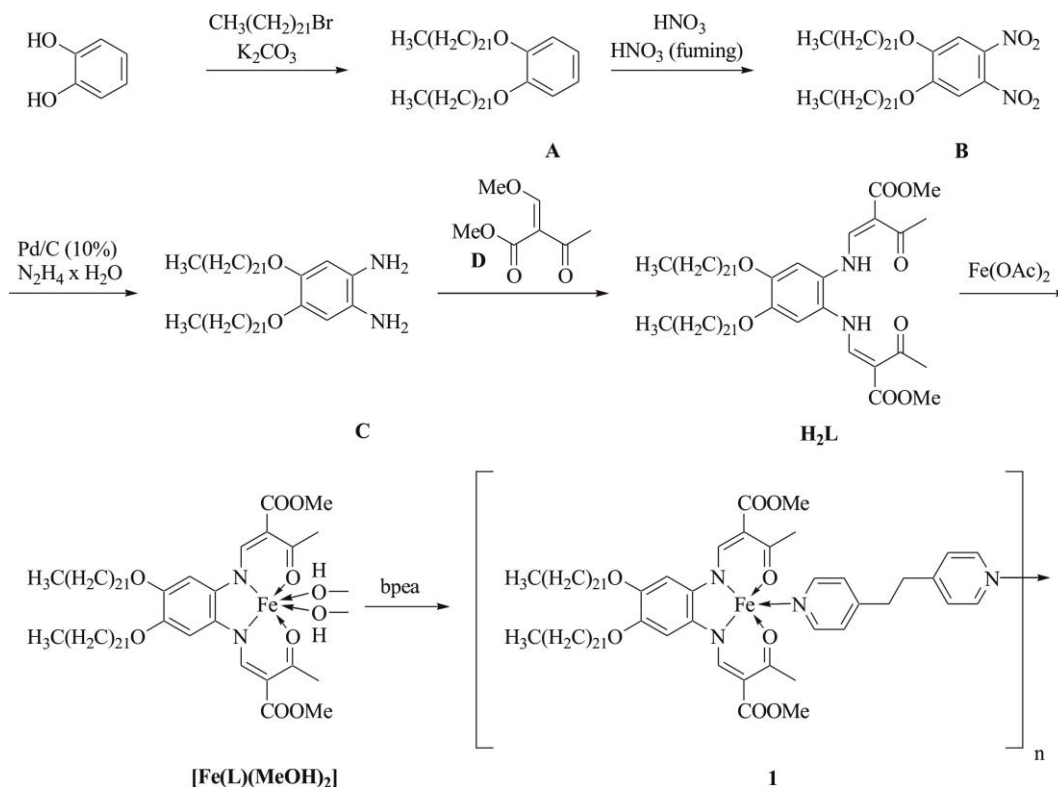
Scheme 1. General synthesis of compound **1**. Compound **2** and **3** were synthesized accordingly.

1,2-Didocosyloxybenzene (A). 1,2-dihydroxybenzene (10 g, 0.09 mol) were mixed with K_2CO_3 (31.21 g, 0.226 mol, 2.5 eq.) in 650 mL DMF and the turquoise suspension was stirred at room temperature for 1 h. 1-bromodocosane (70.75 g, 0.182 mol, 2 eq.) were added in portions and suspension was heated to 80 °C for 17 h. The mixture was poured into 6 L H_2O and stirred for 4 days at room temperature. After filtrating and washing the white precipitate with 100 mL H_2O and 200 mL EtOH, it was recrystallized 4 times from each time 500 mL EtOH to obtain white fine crystalline **A**. Yield: 38.6 g (58.9 %). $C_{50}H_{94}O_2$ (727.28): calcd. C 82.57, H 13.03; found C 82.68, H 13.58. MS (DEI+): m/z (%) = 727 (100) $[M]^+$, 419 (14), 110 (47). ^{1}H NMR (299.83 MHz, CDCl$_3$, 296 K): δ = 0.86 (t, J = 6.3 Hz, 6H, CH$_3$), 1.21–1.30 (m, 72 H, CH$_2$), 1.41–1.47 (m, 4H, CH$_2$), 1.74–1.83 (m, 4H, CH$_2$), 3.97 (t, 4H, J = 6.0 Hz CH$_2$O) 6.81–6.85 (m, 4 H, H$_{ar}$) ppm.

1,2-Dinitro-4,5-didocosyloxybenzene (B). **A** (25.02 g, 0.03 mol) were suspended in 300 mL acetic acid for 1 h. 70 mL nitric acid were added dropwise and heated shortly to 60 °C to ob-

tain a yellow suspension. Over 1.5 h, 250 mL fuming nitric acid were added dropwise and the mixture was stirred for 2 d. It was poured into 2.5 L of ice water and stirred for 15 min. It was filtered off, washed neutral and dried on air. Recrystallization from 700 mL EtOH gave **B** as a yellow powder. Yield: 24.1 g (85.0 %). $C_{50}H_{92}N_2O_6$ (817.28): calcd. C 73.48, H 11.35, N 3.43; found C 72.85, H 11.80, N 3.95. MS (DEI+): m/z (%) = 817 (100) $[M]^+$, 476 (10). ^{1}H NMR (299.83 MHz, CDCl$_3$, 296 K,): δ = 0.81 (t, J = 7.0 Hz, 6 H, CH$_3$), 1.05–1.51 (m, 80 H, CH$_2$), 1.80 (quint, J = 7.0 Hz, 4 H, CH$_2$), 4.02 (t, J = 7.0 Hz, 4 H, CH$_2$O), 7.3 (s, 2 H, H$_{ar}$).

1,2-Diamino-4,5-didocosyloxybenzene (C). B (23.75 g, 0.03 mol) and palladium on activated charcoal Pd/C (10%) (2.5 g) were suspended in 700 mL in EtOH saturated with argon for 30 min. Hydrazine monohydrate (70.34 mL, 1.34 mol, 50 eq.) was added dropwise and the mixture was heated to reflux for 3.5 h. The Pd/C was removed by hot filtration through Celite® 545. After storage for 1 d at −30°C, the yellow-white precipitate was filtrated, washed twice with 20 mL EtOH and dried in vacuum. Yield: 15.4 g (70 %). $C_{50}H_{96}N_2O_2$ (757.31): calcd. C 79.30, H 12.78, N 3.70; found C 79.56, H 13.29, N 4.42.

Dimethyl (2E,2ʻE)-2,2ʻ-{[4,5-Bis(docosyloxy)-1,2-phenylene]bis[imino-(E)-methylidene]} bis(3-oxobutanoate) (D). C (2.5 g, 3.30 mmol) and methoxymethylenemethylaceto-acetate[13] **(F)** (1.25 g, 7.90 mmol, 2.4 eq.) were heated to reflux in 250 mL EtOH saturated with argon for 1 h. The mixture was stored at room temperature for one day and the product filtrated and washed with EtOH (50 mL). Recrystallization from EtOH gave **D** as a yellow powder. Yield: 2.86 g (85 %). $C_{62}H_{108}N_2O_8$ (1009.53): calcd. C 73.76, H 10.78, N 2.77; found C 74.04, H 11.60, N 3.01. MS (DEI+) m/z (%) = 978 (5) $[M−2\,CH_3]^+$, 785 (55) $[M−2\,C_8H_{16}]^+$, 767 (59) $[M−2\,C_8H_{16}−CH_3]^+$, 566 (74), 43 (100) $[C_3H_7]^+$. ^{1}H NMR (299.83 MHz, CDCl$_3$, 296 K,): δ = 0.85 (t, J = 9.0 Hz, 6 H, CH$_3$), 1.21–1.38 (m, 72 H, CH$_2$), 1.40–1.49 (m, 4 H, CH$_2$), 1.76–1.83 (m, 4 H, CH$_2$), 2.53 (s, 6 H, CH$_3$), 3.76 (s, 6 H, CH$_3$), 3.99 (t, J = 6.3 Hz, 4 H, CH$_2$O), 6.72 (s, 2 H, H$_{ar}$), 8.24 (d, J = 12.0 Hz, 2 H, CH), 12.87 (d, J = 12.0 Hz, 2 H, NH) ppm. **IR:** $\tilde{\nu}$ = 2916 vs, 2849 s, 1709 m, 1619 m, 1566 m, 1413 m, 1250 s, 1200 s, 1074 m, 718 m.

Iron(II)-(D)×2(MeOH) (E). D (2.54 g, 2.52 mmol) and iron(II) acetate[14] **(G)** (1.02 g, 5.86 mmol, 2.37 eq.) were heated to reflux in 140 mL MeOH for 6 h. The solution was stored at room temperature for 1 d and the product, a brown powder was then filtrated and washed

with 20 mL MeOH and dried in vacuum. Yield: 2.37 g (85 %). $C_{64}H_{114}FeN_2O_{10}$ (1127.44): calcd. C 68.18, H 10.19, N 2.48; found C 68.06, H 10.47, N 2.67.

1. **E** (0.18 g, 0.16 mmol) and 1,2-bis(4-pyridyl)ethane (bpea, 0.35 g, 1.92 mmol, 12 eq.) were dissolved in 8.5 mL toluene and heated to reflux for 1.5 h. After cooling to room temperature, black needle like crystals were filtrated and dried in vacuum. The crystals obtained were suitable for single crystal X-ray diffraction. Yield: 0.12 g (60 %). $C_{74}H_{118}FeN_4O_8 \times 0.3$ Tol (1278.31): calcd. C 71.24, H 9.53, N 4.48; found C 71.72, H 9.51, N 4.38.

1b. **E** (0.21 g, 0.17 mmol) and bpea (0.17 g, 0.93 mmol, 5 eq.) were heated to reflux in a mixture of 5 mL toluene and 2 mL ethanol for 1.5 h. After storing the solution at 6°C, the brown precipitate was filtered and dried und reduced pressure. Yield: 0.13 g (56 %). $C_{74}H_{118}FeN_4O_8 \times 0.8$ EtOH (1284.45): calcd. C 70.69, H 9.64, N 4.36; found C 70.88, H 10.55, N 4.67.

1c. **E** (0.32 g, 0.28 mmol) and bpea (0.02 g, 3.40 mmol, 12 eq.) were heated to reflux in 8.5 mL toluene for 1.5 h. 2 mL ethanol were added and the mixture was again heated to reflux for 0.5 h. After storing at 6°C, black fine crystalline powder was filtrated and dried under reduced pressure. Yield: 0.14 g (40 %). $C_{74}H_{118}FeN_4O_8 \times 0.2$ EtOH (1256.81): calcd. C 71.10, H 9.56, N 4.46; found C 70.17, H 10.02, N 4.97.

2. **E** (0.21 g, 0.19 mmol) and 1,2-bis(4-pyridyl)ethene (bpee, 0.34 g, 1.86 mmol, 10 eq.) were heated to reflux in a mixture of 5 mL toluene and 2.5 mL ethanol for 1 h. After 1 d at room temperature, the dark blue fine crystalline precipitate was filtered out of the dark brown solution, washed with 1.5 mL ethanol and dried in vacuum. Yield: 0.17 g (73 %). $C_{74}H_{116}FeN_4O_8$ (1245.58): calcd. C 71.36, H 9.39, N 4.50; found C 71.32, H 9.75, N 4.25.

3. **E** (0.16 g, 0.14 mmol) and 1,2-bis(4-pyridyl)ethyne (bpey, 0.05 g, 0.28 mmol, 2 eq.) were heated to reflux in a mixture of 5 mL toluene and 2.5 mL ethanol for 1 h. After 4 d, the dark blue fine crystalline powder was filtered, washed twice with 2 mL ethanol and dried in vacuum. Yield: 0.11 g (62 %). $C_{74}H_{114}FeN_4O_8 \times 4$ EtOH (1427.84): calcd. C 68.98, H 9.74, N 3.92; found C 68.84, H 9.73, N 4.10.

Magnetic Susceptibilities: Data for **1**, **2** and **3** were collected with a Quantum Design MPMS XL-5 SQUID magnetometer under an applied field of 0.1 and 0.5 T over 10–400 K in the settle mode. All samples were placed in gelatine capsules held within plastic straws. The data were corrected for the diamagnetic magnetization of the ligands, which were estimated using Pascal's constants, and for the sample holder.

X-ray diffraction: The intensity data of **1** was collected with a Bruker D8 Quest diffractometer using graphite-monochromated Mo-K_α radiation (Table S1). The data were corrected for Lorentz and polarisation effects. The structure was solved by direct methods (SHELXS-97)[18] and refined by full-matrix least-square techniques against F_0^2 (SHELXL-97).[18] The hydrogen atoms were included at calculated positions with fixed displacement parameters. All non-hydrogen atoms were refined anisotropically. ORTEP-III[19] was used for the structure representation, Schakal- 99[20] and Mercury[21] for the representation of the molecule packing.

Thermal decomposition results were monitored in a thermogravimetric analysis (TGA) employing TGA 2050 (TA instruments) at a heating rate of 10 K min^{-1} from 300 to 870 K under a nitrogen flow.

Microscopy images (POM) were recorded on a polarization optical microscope Nikon Diaphot 300 with a Mettler FP 90 temperature-controlled hot stage. The sample was placed between two glasses and was measured under a nitrogen atmosphere.

Elemental analysis was performed with a VarioEL III CHN instrument using tin boats purchased from Elementar and Acetanilid (Merck) as a standard.

Mass spectrometry: Mass spectra were recorded with a Varian MAT CH7 instrument (direct inlet system, electron impact ionization 70 eV).

8.5   References

[1]   a) M. A. Halcrow (Ed.) *Spin-Crossover Materials*, John Wiley & Sons Ltd, **2013**. b) P. Gütlich, H. Goodwin (Eds.) *Topics in Current Chemistry*, *233-235*, Springer, Berlin, Heidelberg, **2004**.

[2]   a) B. Weber, W. Bauer, T. Pfaffeneder, M. M. Dîrtu, A. D. Naik, A. Rotaru, Y. Garcia, *Eur. J. Inorg. Chem.* **2011**, 3193–3206. b) Z. J. Zhong, J.-Q. Tao, Z. Yu, C.-Y. Dun, Y.-J. Liu, X.-Z. You, *J. Chem. Soc., Dalton Trans.* **1998**, 327–328. c) J.-F. Létard, P. Guionneau, E. Codjovi, O. Lavastre, G. Bravic, D. Chasseau, O. Kahn, *J. Am. Chem. Soc.* **1997**, *119*, 10861–10862.

[3]   a) J. A. Real, A. B. Gaspar, V. Niel, M. C. Muñoz, *Coord. Chem. Rev.* **2003**, *236*, 121–141. b) J. Krober, E. Codjovi, O. Kahn, F. Groliere, C. Jay, *J. Am. Chem. Soc.* **1993**, *115*, 9810–9811.

[4]   J. Linares, E. Codjovi, Y. Garcia, *Sensors* **2012**, *12*, 4479–4492.

[5]   M. Seredyuk, A. B. Gaspar, V. Ksenofontov, Y. Galyametdinov, J. Kusz, P. Gütlich, *J. Am. Chem. Soc.* **2008**, *130*, 1431–1439.

[6]   A. B. Gaspar, M. Seredyuk, P. Gütlich, *Coord. Chem. Rev.* **2009**, *253*, 2399–2413.

[7]   S. Schlamp, B. Weber, A. D. Naik, Y. Garcia, *Chem. Commun.* **2011**, *47*, 7152–7154.

[8]   S. Schlamp, P. Thoma, B. Weber, *Eur. J. Inorg. Chem.* **2012**, 2759–2768.

[9]   S. Schlamp, P. Thoma, B. Weber, *Chem. Eur. J.* **2014**, DOI: 10.1002/chem.201304653.

[10]   S. Schlamp, K. Dankhoff, B. Weber, *New J. Chem.* **2014**, DOI: 10.1039/C3NJ00991B.

[11]   a) B. Weber, E.-G. Jäger, *Eur. J. Inorg. Chem.* **2009**, 465–477. b) T. M. Pfaffeneder, S. Thallmair, W. Bauer, B. Weber, *New J. Chem.* **2011**, *35*, 691–700. c) B. Weber, E. Kaps, *Heteroatom Chem.* **2005**, *16*, 391–397.

[12]   H. G. O. Becker, *Organikum, Organisch-Chemisches Grundpraktikum*, Johann Ambrosius Barth, Berlin, **1993**.

[13]   M. Tanner, A. Ludi, *Chimia* **1980**, *34*, 22–24.

[14]   W. Bauer, T. Ossiander, B. Weber, *Z. Naturforsch. B* **2010**, *65*, 323–328.

[15]   B. Weber, R. Betz, W. Bauer, S. Schlamp, *Z. Anorg. Allg. Chem.* **2011**, *637*, 102–107.

[16]   L. Claisen, *Justus Liebigs Ann. Chem.* **1897**, *297*, 1– 98.

[17]   B. Weber, R. Betz, W. Bauer, S. Schlamp, *Z. Anorg. Allg. Chem.* **2011**, *637*, 102–107.

[18]   G. Sheldrick, *Acta Cryst. A* **2008**, *64*(1), 112–122.

[19]   a) C. K. Johnson, M. N. Burnett, *ORTEP-III;* Oak-Ridge National Laboratory, Oak-Ridge, TN, **1996**; b) L. Farrugia, *J. Appl. Cryst.* **1997**, *30*(5), 565.

[20]   E. Keller, *Schakal-99,* University of Freiburg, Freiburg, Germany, **1999**.

[21]   C. F. Macrae, P. R. Edgington, P. McCabe, E. Pidcock, G. P. Shilds, R. Taylor, M. Towler, J. van de Streek, *J. Appl. Cryst.* **2006**, *39*, 453–457.

8.6   Supporting Information

Table S1. Parameters for crystal structure determination of 1.

sum formula	C74 H118 Fe N4 O8
formula weight	1247.58
crystal system	triclinic
space group	$P\bar{1}$
a /Å	8.8292(5)
b /Å	13.3483(8)
c /Å	38.144(2)
α /°	100.300(3)
β /°	90.396(3)
γ /°	104.379(3)
V /Å^3	4278.2(4)
Z	2
$\rho_{calcd.}$ /g cm^{-3}	0.969
μ /mm^{-1}	0.222
F(000)	1360
crystal size /mm	0.303×0.139×0.024
temperature /K	200
radiation /Å	Mo-K$_\alpha$, 0.71073
θ-min, θ-max /°	2.2, 23.4
hkl	−9: 9; −14: 14; −40: 42
measured reflections	56143
independent reflections	11638

R_{int}	0.097
reflections with $I \geq 2\sigma(I)$	11638
reflections	14173
parameters	790
R	0.0757
$wR2$	0.1952
S	1.00
shift/*error*$_{max}$	0.00
$\Delta\rho_{max}$	0.45
$\Delta\rho_{min}$	−0.54

9   List of Publications

[1]   B. Weber, R. Betz, W. Bauer, <u>S. Schlamp</u>, *Z. Anorg. Allg. Chem.* **2011**, *637*, 103–107.
"Crystal Structure of Iron(II) Acetate"

[2]   C. Lochenie, W. Bauer, <u>S. Schlamp</u>, P. Thoma, B. Weber, *Z. Anorg. Allg. Chem.* **2012**, *638*, 98–102.
"Synthesis and Characterisation of Schiff Base-like Iron(II) Complexes with Imidazole as Axial Ligand"

[3]   <u>S. Schlamp</u>, J. Schulten, R. Betz, T. Bauch, A. V. Mudring, B. Weber, *Z. Anorg. Allg. Chem.* **2012**, *638* (7-8), 1093–1102.
"Synthesis of Anionic Spin Crossover Complexes with Schiff Base-like Ligands"

[4]   W. Bauer, <u>S. Schlamp</u>, B. Weber, *Chem. Commun.* **2012**, *48*, 10222–10224.
"A ladder type iron(II) coordination polymer with cooperative spin transition"

[5]   S. Heider, H. Petzold, G. Chastanet, <u>S. Schlamp</u>, T. Rüffer, B. Weber, J-F. Létard, *Dalton Trans.* **2013**, *42*, 8575–8584.
"Biphenyl bridged hexadentate N6-Ligands – a rigid ligand backbone for Fe(II) Spin Crossover Complexes"

[6]   <u>S. Schlamp</u>, P. Thoma, B. Weber, *Eur. J. Inorg. Chem.* **2012**, 2759–2768.
"New Octahedral, Head–Tail Iron(II) Complexes with Spin Crossover Properties"

[7]   <u>S. Schlamp</u>, B. Weber, A. D. Naik, Y. Garcia, *Chem. Commun.* **2011**, *47*, 7152–7154.
"Cooperative spin transition in a lipid layer like system"

[8]   <u>S. Schlamp</u>, P. Thoma, T. Bauer, R. Kempe, B. Weber, *Z. Anorg. Allg. Chem.* **2013**, *639* (10), 1763–1767.
"A New Iron(II) Complex with Strongly Saddle Shaped Schiff Base-like Ligand"

[9]   S. Schlamp, K. Dankhoff, B. Weber, *New J. Chem.* **2014**, *38*, 1965–1972.

"Amphiphilic iron(II) complexes with short alkyl chains – crystal packing and spin transition properties"

[10]   S. Schlamp, P. Thoma, B. Weber, *Chem. Eur. J.* **2014**, *20*, 6462–6473.

"Influence of the Alkyl Chain Length on the Self-Assembly of Amphiphilic Iron Complexes – An Analysis of X-ray Structures"

[11]   S. Schlamp, B. Weber, to be submitted.

"Amphiphilic Spin Crossover Compounds with C22 Alkyl Chains"

[12]   C. Lochenie, S. Schlamp, A. P. Railliet, K. Robeyns, B. Weber, Y. Garcia, *CrystEngComm* **2014**, *16*, 6213–6218.

"Water channels and zipper structures in Schiff base-like Cu(II) and Ni(II) mononuclear complexes"

Contributions to national and international conferences

<u>S. Schlamp</u>, P. Thoma, B. Weber: **Poster** "On the way to multifunctional spin crossover complexes", Advanced Complex Inorganic Nanomaterials, Namur, Belgien, 11.-14.09.2011.

<u>S. Schlamp</u>, B. Weber: **Poster** "Spin Crossover-Komplexe mit lipidähnlicher Struktur"
and
<u>S. Schlamp</u>, P. Thoma, B. Weber: **Poster** "Spin Crossover Komplexe - Design und Strukturierung", 8. Koordinationschemietagung, Dortmund, Germany, 26.-28.02.2012.

S. Heider, H. Petzold, <u>S. Schlamp</u>, B. Weber: **Poster** "New Fe(II) complexes with anion dependent spin crossover", JCF Frühjahrssymposium, Rostock, Germany, 18.-21.03.2012.

<u>S. Schlamp</u>: **Oral Presentation** "Spin-Crossover Komplexe mit lipidähnlicher Struktur"
and
C. Lochenie, A. P. Railliet, W. Bauer, <u>S. Schlamp</u>, B. Weber, Y. Garcia: **Poster** "Iron(II) Spin Crossover Coordination Polymer: Crystal Structure, Mößbauer Spectrometry and Solvent Influence." 9. Koordinationschemietagung, Bayreuth, Germany, 24.-26.02.2013.

<u>S. Schlamp</u>: **Poster** and **Oral Presentation** "Spin Crossover Complexes with Amphiphilic Ligands", Advanced Complex Inorganic Nanomaterials, Namur, Belgien, 15.-19.07.2013.

10 Acknowledgements/Danksagung

11   Declaration/(Eidesstattliche) Versicherungen und Erklärungen

(§ 5 Nr. 4 PromO)

Hiermit erkläre ich, dass keine Tatsachen vorliegen, die mich nach den gesetzlichen Bestimmungen über die Führung akademischer Grade zur Führung eines Doktorgrades unwürdig erscheinen lassen.

(§ 8 S. 2 Nr. 5 PromO)

Hiermit erkläre ich mich damit einverstanden, dass die elektronische Fassung meiner Dissertation unter Wahrung meiner Urheberrechte und des Datenschutzes einer gesonderten Überprüfung hinsichtlich der eigenständigen Anfertigung der Dissertation unterzogen werden kann.

(§ 8 S. 2 Nr. 7 PromO)

Hiermit erkläre ich eidesstattlich, dass ich die Dissertation selbständig verfasst und keine anderen als die von mir angegebenen Hilfsmittel benutzt habe.
Ich habe die Dissertation nicht bereits zur Erlangung eines akademischen Grades anderweitig eingereicht und habe auch nicht bereits diese oder eine gleichartige Doktorprüfung endgültig nicht bestanden.

(§ 8 S. 2 Nr. 9 PromO)

Hiermit erkläre ich, dass ich keine Hilfe von gewerblichen Promotionsberatern bzw. –vermittlern in Anspruch genommen habe und auch künftig nicht nehmen werde.

_____

Ort, Datum, Unterschrift